AN ABSTRACT OF THE DISSERTATION OF

Guido Corno for the degree of Doctor of Philosophy in Oceanography presented on June 23, 2006.

Title: Primary Production Dynamics in the North Pacific Subtropical Gyre

Abstract approved:

_____

Mark R. Abbott, Ricardo M. Letelier

The North Pacific subtropical gyre (NPSG), once considered to be a biological desert due to low primary production (PP) and its associated variability, has been found more productive and variable than previously thought. The environmental conditions controlling this relatively high PP variability are yet to be elucidated, despite important implications regarding the role of this large oceanic region in the global C- cycle and marine trophic dynamics. In this context, the present investigation is aimed to further elucidate PP patterns and their underlying causes of variability in the NPSG, across different vertical (meters) and temporal (decadal to monthly) scales. Physical and biogeochemical data collected at Station ALOHA (Sta. ALOHA, 22º 45' N 158º 00' W), as part of the on-going Hawaii Ocean Time-Series (HOT) program, were used to address these research topics. Over the last two decades, PP, based on *in situ* $^{14}C$ measurements, has increased by approximately 50 %. This increase has not been linear, but punctuated by sudden temporal changes in relation to variations in the physical stability of the upper water column. These physical changes are related to large scale, ocean-atmosphere interactions occurring during the El Niño/ Southern Oscillation (ENSO) and the Pacific Decadal Oscillation (PDO).

Concomitant with these bio-physical variations, a significant change in community structure was also observed; *Prochlorococcus* spp. cell abundance declined, while picoeukaryote and prymnesiophyte concentrations increased.

In order to understand the seasonal efficiency and variability of the energy flow in the NPSG, the relationship between gross vs. net primary production (GPP vs. NPP, respectively) was determined by comparing *in situ* Fast Repetition Rate Fluorometry (FRRF) derived PP and $^{14}C$ measurements. The GPP and NPP were significantly related across vertical (10-20 m) and temporal (months) scales, but the GPP:NPP ratio decreased as a function of depth and peaked during fall. Monthly and vertical PP variability was assessed by photosynthetic efficiency as determined by *in situ* FRRF. Photosynthetic efficiency was low at the surface, but increased with depth peaking in the Deep Chlorophyll Maximum Layer (DCML). Chronic nutrient limitation seemed to control photosynthetic processes in surface layers, while community structure changes appeared to contribute to the observed variability in photosynthetic efficiency in the lower euphotic zone.

This investigation supports the current view of NPSG as a more productive and variable ecosystem than previously thought. It also provides some insights regarding the controlling mechanisms of the biological (i.e. PP) variability in the NPSG. Over decadal scales, the ecosystem PP and variability appear sensitive to large-scale, atmosphere-ocean interactions in relation to ENSO and PDO events. However, a predictive relationship was not found between PP and ENSO-PDO in the NPSG. In addition, the efficiency of the ecosystem in storing fixed C seems to vary in relation to season's development. Finally, nutrients availability and community

structure could control the observed vertical variability in photosynthetic efficiency, and in turn in PP, in the NPSG.

# Primary Production Dynamics in the North Pacific Subtropical Gyre

by

Guido Corno

A DISSERTATION

submitted to

Oregon State University

in partial fulfillment of
the requirements for the
degree of

Doctor of Philosophy

Presented June 23, 2006
Commencement June 2007

Doctor of Philosophy dissertation of Guido Corno presented on June 23, 2006.

APPROVED:

_____

Major Professor, representing Oceanography

_____

Dean of the College of Oceanic and Atmospheric Sciences

_____

Dean of the Graduate School

I understand that my dissertation will become part of the permanent collection of Oregon State University libraries. My signature below authorizes release of my dissertation to any reader upon request.

_____

Guido Corno, Author

# ACKNOWLEDGMENTS

There are many people I need to thank for their support and encouragement during my graduate studies: foremost my two major advisors Dr. Mark Abbott and Dr Ricardo Letelier, who gave me the opportunity to study and to pursue a scientific research. Mark has been a great mentor, taught me to be clear and focused. Ricardo was a great source of ideas and taught me to expand my scientific boundaries. I really appreciate their endless availability and patience to discuss ideas.

I am greatly indebted to Dr. Dave M. Karl for its insightful advice, collaboration and discussion. I feel fortunate to have had the opportunity to interact with him. His questions and comments represented a continuous challenge to my scientific endeavor.

I am also grateful to Dr. Fred Prahl and Dr. Stanley V. Gregory for being part of my committee. Fred was also open to discussion and he was of great support during difficult moments. In addition, I thank Dr. Matthew Church, Dr. Roger Lukas and Dr. Yvette Spitz for their collaboration and insightful scientific exchanges.

Thanks to my office and laboratory mates Angel White and Samuel Laney, with whom I shared the everyday problems and aspirations of a graduate student. Angel was great for sharing scientific discussion and challenging my views at all times. Thanks to Samuel for his help, discussion and availability at all times, without which I would not been able to proceed in my analysis.

This research would not have been possible without the dedication and skilled efforts of scientists, technicians and students of the HOT program. In particular, I am greatly indebted to Lance Fujieki who was essential in collecting and providing the

data. In addition, Amanda Ashe was critical for her organization skills and help during my trips.

Thanks to all my friends for their encouragement and friendship during my graduate studies. In particular, Julian Licata, Jorge Ramirez, Eben Haase and Martin Saraceno were true friends constantly reminding me of the broader life prospective.

I would like to thank my girlfriend Sandra for her support, enthusiasm and love especially during the last stages of my research. She was essential for keeping me alive.

I would not have been able to complete my research without the unconditional support and love of my family. Claudio, Pinuccia and Carolina are always present in every moment of my endeavors. Finally, I am indebted to Pablo N., Giuseppe U. and Eugenio M. for everyday inspiration.

This research would not have been possible without the funding support of NSF and NOAA.

# CONTRIBUTION OF AUTHORS

Dr. David M. Karl was involved with the design, writing and data interpretation of Chapter 2, 3 and 4.

Dr. Matthew J. Church and Dr. Roger Lukas assisted in the interpretation of the data in Chapter 2.

TABLE OF CONTENTS

LIST OF FIGURES

LIST OF TABLES

# Chapter 1. Research background and motivation

## 1.1 Introduction

The oligotrophic realm constitutes more than 75% of the surface waters of the world's ocean (Jones *et al.* 1996). Therefore, due to this extensive area, oligotrophic regions may play a significant role in the oceanic biogeochemical budgets and, subsequently, in global elemental cycling. Their vast surface extension also affects ocean-atmosphere interactions by influencing atmospheric heat distribution in the subtropical regions and gas exchange and recycling, with consequences for global climate (Graham 1994, Duarte and Agusti 1998, McGowan *et al.* 1998).

In the oligotrophic subtropical gyres of the open ocean, the strong vertical stratification of the water column limits the supply of nutrients from below the thermocline to the euphotic zone. In addition, the large scale anticyclonic circulation which defines the physical boundaries of these gyres, leads to a persistent downwelling and isolation of the upper water column from large volume water exchange with bordering current systems (Karl and Lukas 1996). Due to (i) this relative spatial and temporal stability of the physical environment and (ii) consequent chronic nutrient limitation, carbon fixation by primary producers in these oligotrophic regions has been found low and fairly constant (on average below 0.35 g C $m^{-2}$ $d^{-1}$ with annual variations below 15%, Eppley *et al.* (1973) , Berger (1989), Longhurst *et al.* (1995)). These historical measurements have led to the idea of oligotrophic regions as oceanic biological deserts.

This view of oligotrophic regions has, however, been challenged and, to a large extent, refuted by the increasing number of primary productivity measurements in these areas (Karl *et al.* 1996, Letelier *et al.* 1996, Karl 1999, Karl *et al.* 2002, Steinberg *et al.* 2001, Maranon *et al.* 2003), which found higher (average around 0.50 g C $m^{-2}$ $d^{-1}$) and more variable (deviation of 0.30-0.40 g C $m^{-2}$ $d^{-1}$ from the mean) PP rates than earlier estimates. Oligotrophic regions are now considered as more productive and dynamic systems than previously thought, with a high degree of biological variability. This new view is also supported by (i) the appearance of extensive (400,000 $km^2$) blooms (Wilson 2003) and (ii) large aperiodic variations in PP inside the subtropical gyres (DiTullio and Laws 1991, Karl *et al.* 2002). These phenomena dramatically increase the primary production (PP) and the spatial heterogeneity of oligotrophic gyres, with significant implications for biogeochemical cycles and food-web dynamics. Given the relative physical and chemical stability but high biological variability across scales, a new paradigm regarding these ecosystems has been evolving. The emerging paradigm for subtropical gyre ecosystems consists of understanding the causes and controls of this high biological variability across different spatial and temporal scales.

Understanding the mechanism controlling this biological variability represents the main motivation of the present research. In particular, this investigation focused on further elucidating PP patterns and variability in an oligotrophic system, the North Pacific Subtropical Gyre (NPSG), across vertical and temporal scales not yet fully considered. Main goals were (i) to test the validity of this new paradigm, (ii) to determine principal abiotic and biotic causes for this high biological variability and

(iii) to present some potential ecological implications of such variations for oceanic oligotrophic systems and global biogeochemical cycles.

## 1.2 Scientific background of the NPSG

### 1.2.1 Physical Oceanography

The NPSG extends from approximately 10º N to 45-50° N latitude and 125° E to 120° W longitude (Fig.1.1). The physical boundaries are represented by the North Pacific Current in the north, the California Current in the eastern part, the North Equatorial Current in the south and the Kuroshio Current in the west. The NPSG is characterized by warm (higher than 24° C) surface waters and seasonally variable surface mixed layer depths (40-100 m) (Bingham and Lukas 1996). Large-scale characterization of the NPSG based on surface dynamic height relative to 1000m places the center of the gyre at 20° N.

Surface circulation (above 50m) is the result of local wind forcing. The anticyclonic circulation indicates convergence of surface waters in the NPSG. This characteristic has been observed to restrict exchanges with adjacent current systems (Ledwell *et al.* 1993). Horizontal currents are less than 4 cm $s^{-1}$. These velocities are used to estimate vertical downwelling by Ekman convergence, of approximately 2-3 cm $d^{-1}$ through the main thermocline (Bingham and Lukas 1996).

The NPSG is considered a semi-enclosed, stable and homogenous habitat due to low gradients in most physical characteristics when compared to other marine systems (Karl 1999). However, this homogeneity is influenced by a series of mesoscale physical processes. This influence has caused to reconsider the common

picture of the relative stability of the NPSG to a more dynamic system. One such physical process is represented by winter cyclones, which cross the North Pacific from west to east every 5-7 d (Bingham and Lukas 1996). These cyclones directly affect the upper ocean by deepening the mixed layer and cooling the surface waters due to increased evaporation and mixing of cool water from below. The forcing of these cyclones is relevant in determining the annual cycle in the surface waters of the NPSG.

In addition to this annual variability, a significant influence of mesoscale variability has been recognized in the NPSG (Bingham and Lukas 1996). This variability includes discrete eddies, near-inertial motions and internal tides; all of which influence the physical characteristics of the upper ocean. During winter, lateral heterogeneity has also been observed (Venrick 1990); mixed layer depths varied consistently over a few kilometers (from 110 m to 10m within 5 km). Variations in horizontal current velocities within 1-200 km also contrast with the supposed homogeneity of the NPSG. These currents greatly influence the vertical circulation; they can increase vertical transport by two orders of magnitude (Venrick 1990). Although the general features (i.e. surface circulations, boundaries, water mass composition) of the NPSG appear to be fully understood, mesoscale variability still remains poorly resolved.

### 1.2.2 Biological Oceanography

#### 1.2.2.1 Photoautotrophic biomass and community composition

The NPSG is characterized by low photoautotrophic biomass (average surface chlorophyll of 0.10 mg Chl *a* $m^{-3}$) and a persistent deep-water (100-125m) Chl *a* maximum layer (DCML) (Fig 1.2). The photoautotrophic community is dominated (approximately 50% of total Chl *a*) by *Prochlorococcus* like micro-organisms with divinyl Chl *a*, Chl *b* and zeaxanthin as key pigments (Campbell and Vaulot 1993). Other cyanobacteria (including *Synechococcus* spp. and *Trichodesmium* spp.) and two picoeukaryotic algal groups, prymnesiophytes and pelagophytes, together account for the most of the remainder of the standing stock of photoautotrophic cells (Andersen *et al.* 1996). A quantitative analysis utilizing HPLC pigment data indicates that in the DCML the mean phytoplankton community consists of *Prochlorococcus* spp. (39%), cyanobacteria (24%), prymnesiophytes (22%), and chrysophytes (13%) (Letelier *et al.* 1993).

The NPSG photoautotrophic community is dominated by prokaryotes, while larger cells are rare. This prokaryote dominance has been suggested to be the result of a decadal shift in photoautotrophic community due to climate variations in the NPSG, which would have selected for such organisms (Karl *et al.* 2001). The relative abundances of diatoms and dinoflagellates, once thought to dominate the NPSG photoautotrophic assemblage, are low (Venrick 1982). Monads and flagellates and non-thecate dinoflagellates are the most recurrent nanoplanktoners (Beers *et al.* 1982). Distinct diatom assemblages can be found in the mixed layer and in the DCML (Scharek *et al.* 1999). In the DCML, diatom abundances and export are low

throughout the year, with the exception of one genus (*Pseudonitzschia* spp.) which increases in spring.

Although the mean standing stock of diatoms is low, it can significantly increase to the point of producing blooms (Karl *et al.* 2001, Wilson 2003). These blooms are principally characterized by species containing endosymbiotic $N_2$-fixing cyanobacteria, such as *Richelia intracellularis*. *Trichodesmium* spp. can also become the dominant species in surface waters of the NPSG during summer blooms, as result of increased $N_2$ fixation activity by these organisms (Letelier and Karl 1996).

1.2.2.2 Primary productivity patterns

The current view of NPSG as a more productive system than previously thought has been confirmed by a number of on-going and past $^{14}C$ measurements (Laws *et al.* 1987, Laws *et al.* 1989, Letelier *et al.* 1996, Karl *et al.* 2001). $^{14}C$ measurements during summer at a site in the CLIMAX region averaged 456 mg C $m^{-2}$ $d^{-1}$, a value greater than twice the historical mean for the same location (Marra and Heinemann 1987). At a nearby location, photosynthetic rates were found to be 727 mg C $m^{-2}$ $day^{-1}$ (Jones *et al.* 1996). These high rates of photoautotrophic growth were also found in another site of the NPSG (Laws *et al.* 1987). At Station ALOHA (22° 45′ N 158° 00′ W, Sta. ALOHA, Fig. 1), PP based on a 15 year time-series $^{14}C$ incubations have yielded a mean production of 484 mg C $m^{-2}$ $d^{-1}$, approximately two- to threefold higher from the period 1965-1980 in the nearby region.

PP displays predictable temporal patterns in the NPSG. At Sta. ALOHA, PP shows maxima in summer and minima in winter. Such a seasonal pattern is mostly

related to light intensity and day length (Karl *et al.* 2001). In this area, the seasonal pattern of PP is directly out of phase with the concentrations of Chl *a* (i.e. high summertime rate of $^{14}C$ incorporation during low ambient Chl *a* concentrations); this pattern is explained by photo-adaptation processes that would control Chl *a* concentrations as a function of seasonal light variations. Aperiodic PP maxima (> 900 mg C $m^{-2}$ $d^{-1}$) concomitant with Chl *a* maxima can also occur in the NPSG; large blooms of *Trichodesmium* spp. and diatoms containing $N_2$-fixing bacteria have been observed during spring and summer periods.

As stated previously, PP variability in the NPSG appears to be greater than previously estimated across different temporal and vertical scales. During 18-month period at the VERTEX site (Knauer et al. 1990), primary production varied approximately 2.5-fold, ranging from 220 to 550 mg C $m^{-2}$ $d^{-1}$, compared to the low variability (within one standard deviation) indicated by historical measurements. At Sta. ALOHA, large aperiodic variations from long-term mean production rate (< 200 to > 900 mg C $m^{-2}$ $d^{-1}$) have also been observed. Furthermore in this region, the combined effect of near-inertial oscillations and solar irradiance variations can result in an eightfold variation in the light field at the DCML on consecutive days (Letelier *et al.* 1996). Such significant light variation can lead to similar variations in PP in this area of the water column.

In addition, PP patterns in the NPSG appear to be influenced by large-scale climate-ocean interactions, such as those occurring during the El-Niño Southern Oscillation (ENSO) and the Pacific Decadal Oscillations (PDO). A significant ENSO event during 1991-1992 has been suggested to be responsible for the increase in

primary productivity at Sta. ALOHA (Karl *et al.* 1995), by influencing mixed layer dynamics and $N_2$-fixation. However, how PP variations in the NPSG are related to the ocean-atmosphere interaction during ENSO and PDO changes is yet to be assessed.

The PP variability in the NPSG appears also to possibly influence the spatial and temporal variations between new and recycled production. New production measurements in the NPSG, based on particulate organic carbon and nitrogen fluxes coupled with $^{14}C$ primary production and $^{15}N$ uptake at the VERTEX time-series site, showed no clear relationship between new production and primary productivity (Knauer *et al.* 1990). These measurements showed that the *f*-ratio was inversely related to primary production. Values of annual new production ranged from 13-17 g C $m^{-2}$ $yr^{-1}$, while the average annual *f*-ratio ranged from 0.11 to 0.14. Variability in the *f*-ratio was found in relation of a cyclonic mesoscale eddy in the North Pacific subtropical gyre (Colleen *et al.* 1996); the *f*-ratio varied between 0.20 to 0.81 from outside to inside the eddy. PP also varied from 399 (outside the eddy) to 662 (inside the eddy) mg C $m^{-2}$ $day^{-1}$. The temporal variability observed at the VERTEX site was not reflected spatially, as indicated by free-floating particle traps (Martin *et al.* 1990). These measurements indicated that there was relatively little variability in open ocean export fluxes.

1.2.2.3 Two-layer system

The NPSG has been viewed as a two-layer system with (i) an upper mixed layer (0-40m) of relatively high PP, low chlorophyll concentration, and low zooplankton biomass, and (ii) a lower layer (40-100m) containing the chlorophyll

maximum, higher zooplankton biomass, and relatively low PP (Knauer *et al.* 1990) (Fig 1.2). The two-layer system of the oligotrophic NPSG was first elucidated by $^{234}Th$:$^{238}U$ disequilibria that showed long and short dissolved $^{234}Th$ residence times for the upper and lower euphotic zone, respectively (Coale and Bruland 1987). Sediment trap measurements also provided evidence for a two-layer system. At the VERTEX II oligotrophic sediment trap station (18° N 108′ W), particulate traps at 30m yielded no particulate carbon flux, while traps at 120m registered 38 mg C $m^{-2}$ $d^{-1}$, with many visible fecal pellets (Small *et al.* 1987). Zooplankton in the upper layer apparently produced small pellets, which were recycled *in situ*, while in the lower layer fecal pellets were larger and could escape the recycling loop accounting for 30% of trap-measured C flux.

An additional difference between the upper and the lower layer in the NPSG is the extent of new vs. recycled production. The upper layer is a region where recycling processes dominate and they are fundamental to supply the needed substrate for primary production. Most of the time, recycled production is the prevailing method of production in this region. In the upper layer, enhancement of $N_2$-fixation can increase the amount of new production by supplying new N. In the lower layer, new production is the main mode of autotrophic production. The increase in N concentrations in this region (due to the nitracline) provides a constant source of new N to the local photoautotroph population. Evidence for this difference in production modes has been found by analysis of nitrogen dynamics at the VERTEX time-series site (Harrison *et al.* 1992). Ammonium concentrations were greater in the surface than deep layers, suggesting a greater recycling rate in the upper region of the water

column. Furthermore, ammonium uptake displayed similar patterns indicating that recycled production was dominant in the upper layer. Finally, estimated values for the *f*-ratio were greater at depth.

The upper and lower layer also differ for temporal variations in Chl *a* concentrations. Seasonal patterns of photoautrophic biomass show a Chl *a* increase in winter and a decrease in summer in the upper euphotic zone (0-50 m), while in the lower euphotic zone (100-175m) Chl *a* increases in spring and decreases in fall (Letelier *et al.* 1993, Winn *et al.* 1995). The winter increase in Chl *a* concentration in the upper 50 m of the water column appears to be a consequence of photo-adaptation, as a response to decreased average mixed-layer light intensity (Winn *et al*. 1995). In the lower euphotic zone, the seasonal cycle in Chl *a* reflects a change in the rate of PP and in phytoplankton biomass as a consequence of increased light intensity in summer. These seasonal variations are a result of photoadaptation and the balance between net growth and accumulation of biomass, respectively.

According to spatial and temporal patterns in PP, Chl *a* concentrations, new and recycled production, the MLD represents the vertical limit of the two-layer system. However, if photoautotrophs species distribution is considered, the vertical limit of this idealized system becomes the DCML. The vertical distribution of key phytoplankton species indicates that a significant distinction between shallow and deep flora occurs around the DCML (Venrick 1982, 1988, 1990, 1992, 1993, 1999). These two distinct floral associations are separated by a region of rapid transition near or below 100m (Venrick 1982). Recent recurrent group analysis also clearly shows the dichotomy between shallow and deep associations (Venrick 1999). A new

finding is that the deep flora consists of two related groups of species, whose abundance centers are vertically displaced from one another. This analysis also revealed that the DCML is compromised of species characteristic of the deep assemblage, with only insignificant numbers of shallow species (Venrick 1988, 1992). The vertical distributions of these key species suggest that the increase in abundance of deep species closely resembles the increase in chlorophyll *a* at the top of the DCML. Analysis of bio-physical interactions indicates that the winter mixing can be deep enough to mix species from the deep phytoplankton association to the surface (Venrick 1993). This mixing has been found to stimulate growth of these species. Interestingly, no difference in species composition and dominance was found between locations in the center and at the edge of the gyre, indicating spatial homogeneity in vertical species composition (Venrick 1988).

**1.3 Aims and motivation of this research**

The goal of the present investigation is to elucidate environmental mechanism controlling biological variability in the NPSG across different scales. In particular, this study strives to elucidate PP patterns and associated variability in the NPSG across temporal (inter-decadal), vertical (meters) and physiological (PSII to intracellular metabolic pathways) scales not fully considered by previous investigations. These new temporal, spatial and physiological patterns in organic matter production have important implications for biogeochemical cycling and food-webs dynamics in the NPSG, and in turn for oceanic oligotrophic regions. From an ecological to a physiological prospective, this research also aims to understand how

the physiological variability in utilizing the available intracellular energy can affect vertical and temporal PP patterns in photoautrophs. This information can provide an indication of the efficiency of the NPSG in transferring energy to other trophic levels. Finally, the present study seeks to establish the role of abiotic and biotic factors in controlling photosynthetic efficiency in the NPSG. This analysis will help predicting changes in PP due to biological and physical forcing.

### 1.3.1 Scientific questions

In relation to the general aims described above, the specific scientific questions addressed by the present research are:

1) What is the relationship between large-scale climate phenomena and PP patterns at Sta. ALOHA?

i) Do physical changes induced by ENSO events enhance PP in a predictable way?

ii) How does the interaction between physical changes occurring during ENSO and other large-scale climate events influence PP changes at Sta. ALOHA?

2) What is the relationship between gross and net PP at Sta. ALOHA?

i) How do such relationships vary through vertical (meters) and temporal (months) scales?

ii) What abiotic and biotic factors control this relationship?

3) What is the photosynthetic activity and efficiency at Sta. ALOHA?

i) How do they vary across vertical (meters) and temporal (months) scales?

ii) What are the environmental factors controlling these variations?

All these questions have not been fully answered by this research. This task would require a great effort of field, laboratory and theoretical studies. However, parts of them have been appropriately undertaken and elucidated.

### 1.3.2 Scientific Relevance

The scientific relevance of this research is related to biogeochemical cycles, ecological and physiological processes, and methodological considerations for marine studies. In particular, the scientific relevance can be summarized by the following arguments:

- biogeochemical cycles:

1. the NPSG is one of the largest biomes on earth (Karl 1999). It is therefore crucial investigating its role in controlling global elemental fluxes and recycling by analyzing the magnitude of PP and associated variability in this environment;
2. due to its large dimensions, the NPSG is likely to be influenced by the atmosphere-ocean climate forcing differently in its sub-regions. Furthermore, oligotrophic regions play a significant role in the ocean-atmosphere interactions with clear implications for global climate. The elucidation of vertical and temporal PP patterns in relation to large scale physical perturbations would help clarify the present role of NPSG in the $CO_2$ atmospheric budget and its response to large-scale climate events;
3. marine PP plays a central role in controlling the production of particulate and dissolved organic matter. The analysis of PP variability across

different temporal scales will help determine the role of the NPSG in the global C-cycle in terms of absolute C-fixation rates;

-ecological processes:

1. the emerging paradigm regarding the environmental controls of biological variability in oceanic gyres needs to be further investigated. This research strives to improve such understanding by assessing PP dynamics at different vertical and temporal scales and their relative forcing mechanism;
2. ecosystem variability needs to be considered when trying to understand the natural behavior of ecosystems. Analysis of PP variability can further enhance our knowledge of this ecosystem variability and behavior in relation to environmental perturbations;
3. the flow of energy within and through organisms influences the efficiency of an ecosystem. The current analysis of the relationship between gross and net PP is aimed to understand the efficiency of primary producers in transferring energy to other trophic levels. Such information is needed to determine the efficiency of oceanic gyres;

-physiological processes:

1. aquatic (in particular oceanic) photosynthesis still remains under-sampled compared to its terrestrial counterpart. This research provides further insights about the physiological adaptations of marine photosynthetic organisms in relation to their surrounding environment and, in particular, in relation to a chronic nutrient limitation condition;

2. the photosynthetic characteristics of *in situ* photoautotrophs could be used to understand the evolutionary adaptations of marine photosynthesis to this particular enviroment. In particular, information regarding cyanobacterial photosynthetic processes, as those organisms dominate the NPSG, will be obtained by this research;

- methodological considerations for marine studies:

1. information regarding *in situ* photoautotrophic activity, gathered by this research, will be included in the parameterization of current and future primary productivity models. In particular, previous modeling efforts for the NPSG (Ondrusek *et al.* 2001) have highlighted the critical need to characterize short term (days) and vertical variations of the maximum quantum yield of photosynthesis in the NPSG. This investigation presents some of this information;
2. the feasibility of new techniques (fluorescence methods) in low chlorophyll areas for oceanographic research in oceanic gyres is being explored by the present study. In addition, the comparison of two *in situ* methodologies for estimating marine PP is also performed here so to better constrain our PP estimates and variations.

**1.4 Methods**

*In situ* measurements were made at Sta. ALOHA (22º 45' N, 158º 00' W, Fig. 1.1) as part of the ongoing Hawaii Ocean Time-Series (HOT) (Karl and Lukas 1996). In addition to the core biogeochemical measurements routinely done at Sta. ALOHA

(for a complete list refer to Karl and Lukas 1996), photosynthetic parameters such the quantum yield of photosynthesis, the absorption cross section of PSII, P vs. E characteristics, PP rates by Fast Rate Repetition Fluorometry (FRRF) (Kolber and Falkowski 1993) have been obtained since August 2002 at relatively high vertical resolution (~ 1m) for standard *in situ* measurements.

Chlorophyll *a* fluorescence by photoautotrophs was used as a proxy to derive photosynthetic properties and activity in the NPSG. Reviews of fluorescence and photosynthesis can be found in Falkowski *et al.* (1986), Krause and Weis (1991), Kiefer and Reynolds (1992), Kolber and Falkowski (1993). Both active and passive fluorescence methodologies have been proven to be promising tools to determine photoautotrophs activity in the ocean. In this study, only active fluorescence was considered. Fluorescence also represents an ideal technique for photoautotroph investigations, as it is non-invasive, fast, *in situ*, sensitive and it allows high spatial and temporal resolution measurements, typical of some photoautotrophs ecological and physiological processes. However, a major limitation of the fluorescence technique used here is its specificity to Chl *a* activity. The photosynthetic activity of photoautotrophs, whose major light absorbing pigment is not Chl *a* (cyanobacteria), may be not fully characterized by these fluorescence measurements. This limitation is particularly relevant for the NPSG, where the photoautotrophic cyanobacteria are dominant (in particular *Prochlorococcus* spp.) (Campbell and Vaulot 1993, Campbell *et al.* 1994). Alternative approaches to determine phototosynthetic activity of these organisms include (i) flow cytometer sorted samples from $C^{14}$ incubations and (ii)

fluorescence measurements at different excitation wavelengths. Such methodological constrains have been taken into account in this research.

### 1.5 Dissertation structure

This dissertation consists of five chapters. After an introduction and motivation of the research (this chapter), chapter 2 analyzes changes in PP patterns at Sta. ALOHA in relation to the ENSO and PDO during the last 17 years. Chapter 3 explores the relationship between gross and net PP in the NPSG by comparing time-series *in situ* measurements of FRRF and $^{14}C$ at ALOHA. A novel analysis to determine light-driven photoautotrophic respiration is given in this chapter. Chapter 4 addresses the question of determining the photosynthetic activity in the NPSG by time-series FRRF measurements at Sta. ALOHA. An analysis of the environmental parameters controlling such activity and variability is presented. Finally, chapter 5 summaries main findings of this research, presenting implications for this ecosystem and suggesting recommendations for future research in the NPSG.

### 1.6 Reference

Andersen, R.A., Bidigare, R.R., Keller, M.D. and Latasa, M. 1996. A comparison of HPLC pigment signatures and electron microscopic observations for oligotrophic waters of the North Atlantic and Pacific Oceans. *Deep-Sea Res. II* **43**: 517-537.

Beers, J.R., Reid, F.M.H. and Stewart, G.L. 1982. Seasonal abundance of the microplankton population in the North Pacific central gyre. *Deep-Sea Res. I* **29**: 227-245.

Berger, W.H. 1989. Global maps of ocean productivity. In : *Productivity of the ocean: Present and past*, Berger, W.H., Smetacek, V.S. and Wefer, G., editors, John Wiley and Sons, New York, 429-455.

Bingham, F.M. and Lukas, R. 1996. Seasonal cycles of temperature, salinity and dissolved oxygen observed in the Hawaii Ocean Time-series. *Deep-Sea Res. II* **43**: 199-213.

Campbell, L. and Vaulot, D. 1993. Photosynthetic picoplankton community structure in the subtropical North Pacific Ocean near Hawaii (station ALOHA). *Deep-Sea Res. I*. **40:** 2043-2060.

Campbell, L., Nolla, H.A. and Vaulot, D. 1994. The importance of *Prochlorococcus* to community structure in the central North Pacific Ocean. *Limnol. Oceanogr.* **39:** 954-961.

Coale, K.H. and Bruland, K.W. 1987. Oceanic stratified euphotic zone as elucidated by $^{234}$Th:$^{238}$U disequilibria. *Limnol. Oceanogr.* **32:** 189-200

Colleen, B.A., Kanda, J. and Laws, E.A. 1996. New production and photosynthetic rates within and outside cyclonic mesoscale eddy in the North Pacific subtropical gyre. *Deep-Sea Res. I* **43**: 917-936.

DiTullio, G.R. and Laws, E.A. 1991. Impact of atmospheric-oceanic disturbance on phytoplankton community dynamics in the North Pacific Central Gyre. *Deep-Sea Res. I* **38**: 305-329.

Duarte, C.M. and Agusti, S. 1998. The $CO_2$ balance of unproductive aquatic systems. *Science* **281**: 234-236.

Eppley, R.W., Renger, E.H., Venrick, E.L. and Mullin, M.M. 1973. A study of plankton dynamics and nutrient cycling in the central gyre of the North Pacific Ocean. *Limnol. Oceanogr.* **18**: 534-551.

Falkowski, P.G., Wyman, K., Ley, A.C. and Mauzerall, D. 1986. Relationship of steady state photosynthesis to fluorescence in eukaryotic algae. *Biochim. Biophys. Acta* **849**: 183-192.

Graham, N.E. 1994. Decadal-scale variability in the tropical and North Pacific during the 1970s and 1980s: observations and model results. *Clymate Dyn.* **10**: 135-162.

Harrison, W.G., Harris, L.R., Karl, D.M., Knauer, G.A. and Redalje, D.G. 1992. Nitrogen dynamics at the VERTEX time-series site. *Deep-Sea Res. I* **39**: 1535-1552.

Jones, D.R., Karl, D.M. and Laws, E.A. 1996. Growth rates and production of heterotrophic bacteria and phytoplankton in the North Pacific subtropical gyre. *Deep-Sea Res. I* **43**: 1567-1580.

Karl, D.M. 1999. A sea of Change: Biogeochemical Variability in the North Pacific Subtropical Gyre. *Ecosystems* **2**: 181-214.

Karl, D.M., Bidigare, R.R. and Letelier, R.M. 2001. Long-term changes in plankton community structure and productivity in the North Pacific Subtropical Gyre: the domain shift hypothesis. *Deep-Sea Res. II* **48**: 1449-1470.

Karl, D.M., Bidigare, R.R. and Letelier, R.M. 2002. Sustained and Aperiodic

Variability in Organic Matter Production and Phototrophic Microbial Community Structure in the North Pacific Subtropical Gyre. In: P. J. le B. Williams, D. R. Thomas and C. S. Reynolds, Eds., Phytoplankton Productivity and Carbon Assimilation in Marine and Freshwater Ecosystems, Blackwell Publishers, London, 222-264.

Karl, D.M., Dore, D.V., Hebel, R.M. , Letelier, R.M. and Tupas, L.M. 1996. Seasonal and interannual variability in primary productivity and particle flux at Station ALOHA. *Dee- Sea Res. II* **43**: 539-568.

Karl, D.M., Letelier, R.M., Hebel, D., Tupas, L., Dore, J., Christian, J. and Winn, C. 1995. Ecosystem changes in the North Pacific subtropical gyre attributed to the 1991-92 El-Niño. *Nature* **373**: 230-4.

Karl, D.M. and Lukas, R. 1996. The Hawaii Ocean Time-series (HOT) program: Background, rationale and field implementation. *Deep-Sea Res. II* **43**: 129-156.

Kiefer, D.A. and Reynolds, R.A. 1992. Advances in understanding phytoplankton fluorescence and photosynthesis. *In* Falkowski, P.G. & Woodhead, A.D. [Eds] *Primary Productivity and Biogeochemical Cycles in the Sea.* Plenum Press, New York, pp 155-174.

Knauer, G.A., Redalje, D.G., Harrison, W.G. and Karl, D.M. 1990. New production at the VERTEX time-series site. *Deep-Sea Res. I* **37**: 1121-1134.

Kolber, Z.S. and Falkowski, P.G. 1993. Use of active fluorescence to estimate phytoplankton photosynthesis *in situ*. *Limnol. Oceanogr.* **38**: 1646-1665.

Krause, G.H. and Weis, E. 1991. Chlorophyll fluorescence and photosynthesis: the basics. *Ann. Rev. Plant Physiol. Plant Mol. Biol.* **42**: 31-349.

Laws, E.A., DiTullio, G.R. and Redalje, D.G. 1987. High phytoplankton growth and production rates in the North Pacific subtropical gyre. *Limnol. Oceanogr.* **32**: 905-918.

Ledwell, J.R., Watson, A.J. and Law, C.S. 1993. Evidence for slow mixing across the pycnocline from an open tracer-release experiment. *Nature* **364**: 701-703.

Letelier, R.M., Dore, J.E., Winn, C.D. and Karl, D.M. 1993. Temporal variability of phytoplankton community structure based on pigment analysis. *Limnol. Oceanogr.* **38**: 1420-1437.

Letelier, R.M., Dore, J.E., Winn, C.D. and Karl, D.M., 1996. Seasonal and interannual variations in autotrophic carbon assimilation at Station ALOHA. *Deep-Sea Res. II* **43:** 467-490.

Letelier, R.M., and Karl, D.M. 1996. The role of *Trichodesmium* spp. in the productivity of the subtropical North Pacific Ocean. *Mar. Ecol. Prog. Ser.* **133**: 263-273.

Longhurst, A.R., Sathyendranath, S., Platt, T. and Caverhill, C. 1995. An estimate of global primary production in the ocean from satellite radiometer data. *J. Plankton Res.* **17**:1245-1271

Maranon, E., Behrenfeld, M.J., Gonzalez, N., Mourino, B. and Zubkov, M.V. 2003. High variability of primary production in oligotrophic waters of the Atlantic Ocean: uncoupling from phytoplankton biomass and size structure. *Mar. Ecol. Prog. Ser.* **257**: 1-11.

Marra, J. and Heinemann, K.R. 1987. Primary productivity in the North Pacific Central Gyre: some new measurements based on $^{14}C$. *Deep-Sea Res. I* **34**: 1821-1829.

Martin, J.H., Knauer, G.A., Karl, D.M. and Broenkow, W.W. VERTEX: carbon cycling in the northeast Pacific. *Deep-Sea Res. I* **34**: 267-285.

McGowan, J.A. 1974. The nature of oceanic ecosystems. In: Miller, C.B. editor. The biology of the oceanic Pacific. Corvallis: Oregon State University Press, pp 9-28.

McGowan, J.A., Cayan, D.R. and Dorman, L.M. 1998. Climate-ocean variability and ecosystem response in the Northeast Pacific. *Science* **281**: 210-217.

Ondrusek, M. E., Bidigare, R., Waters, K. and Karl, D.M. 2001. A predictive model for estimating rates of primary production in the subtropical North Pacific Ocean. *Deep-sea Res. II* **48:** 1837-1863.

Scharek, R., Latasa, M., Karl, D.M. and Bidigare, R.R. 1999. Temporal variations in diatom abundance and downward vertical flux in the oligotrophic North Pacific gyre. *Deep-Sea Res. I* **46**: 1051-1075

Small, L.F., Knauer, G.A. and Tuel, M.D. 1987. The role of sinking fecal pellets in stratified euphotic zone. *Deep-Sea Res. I* **34**: 1705-1712.

Steinberg, D.K., Carlson, C.A., Bates, N.R., Johnson, R.J., Micheals, A.F. and Knap, A.H. 2001. Overview of the US JGOFS Bermuda Atlantic time-series study (BATS): a decade-scale look at ocean biology and biogeochemistry. *Deep-Sea Res. II* **48**: 1405-1447.

Sverdrup, H.U., Johnson, M.W. and Fleming, R.H. 1946. The oceans, their physics, chemistry and general biology. New York : Prentice-Hall, 230-245.

Venrick, E.L. 1982. Phytoplankton in an Oligotrophic Ocean: Observations and Questions. *Ecol. Monogr.* **52**: 129-154.

Venrick, E.L. 1988. The vertical distributions of chlorophyll and phytoplankton species in the North Pacific central environment. *J. of Plankton Res.* **10**: 987-998

Venrick, E.L. 1990. Phytoplankton in an oligotrophic ocean: species structure and interannual variability. *Ecology* **71**: 547-563.

Venrick, E.L. 1992. Phytoplankton species structure in the central North Pacific: Is the edge like the center? *J. of Plankton Res.* **14**: 665-680.

Venrick, E.L. 1993. Phytoplankton seasonality in the central North Pacific: the endless summer reconsidered. *Limnol. Oceanogr.* **38**: 1135-1149.

Venrick, E.L. 1999. Phytoplankton species structure in the central North Pacific, 1973-1996: variability and persistence. *J. of Plankton Res.* **21**: 1029-1042.

Wilson, C. 2003. Late Summer chlorophyll blooms in the oligotrophic North Pacific Subtropical Gyre. *Geophys. Res. Lett.* **30**: 1942-1946.

Winn, C.D., Campbell, L., Christian, J.R., Letelier, R.M., Hebel, D.V., Dore, J.E., Fujieki, L. and Karl, D.M. 1995. Seasonal variability in the phytoplankton community in the North Pacific Subtropical Gyre. *Global Biogeochem. Cycles* **9**: 605-620.

Wyrtki, K. 1975. Fluctuation of the dynamic topography in the Pacific Ocean. *J. Phys. Oceanogr.* **5**: 450-459.

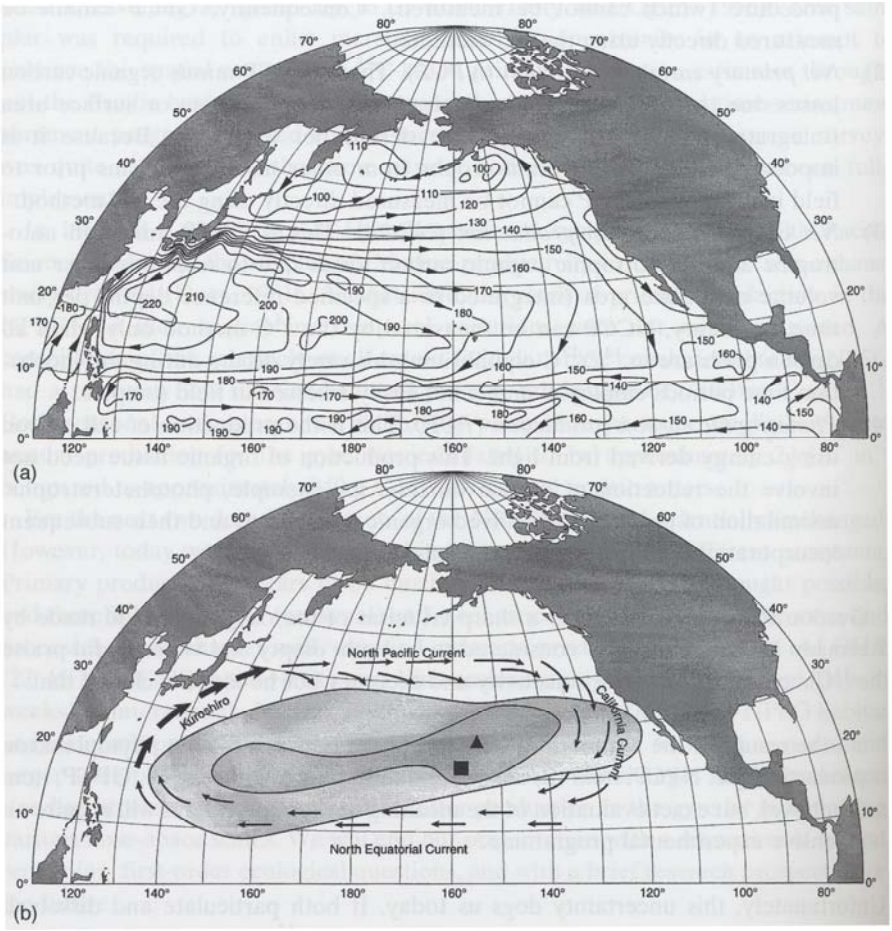


Figure 1.1 Map of the North Pacific Ocean. (a) The dynamic topography of the sea surface in dyn-cm relative to 100 dbar based on historical hydrographic observations. Arrows show the direction of geostrophic flow. Figure taken from Karl (1999) and redrawn from Wyrtki (1975). (b) Major circulation features in the North Pacific, showing the approximated physical boundaries of the NPSG. The dark area is the core of the Central Pacific fauna (100% fidelity) and the lighter shade defines the 60% fidelity boundary. Figure taken from Karl (1999) and redrawn from McGowan (1974). Sta. ALOHA (■) and CLIMAX (▲) are also shown.

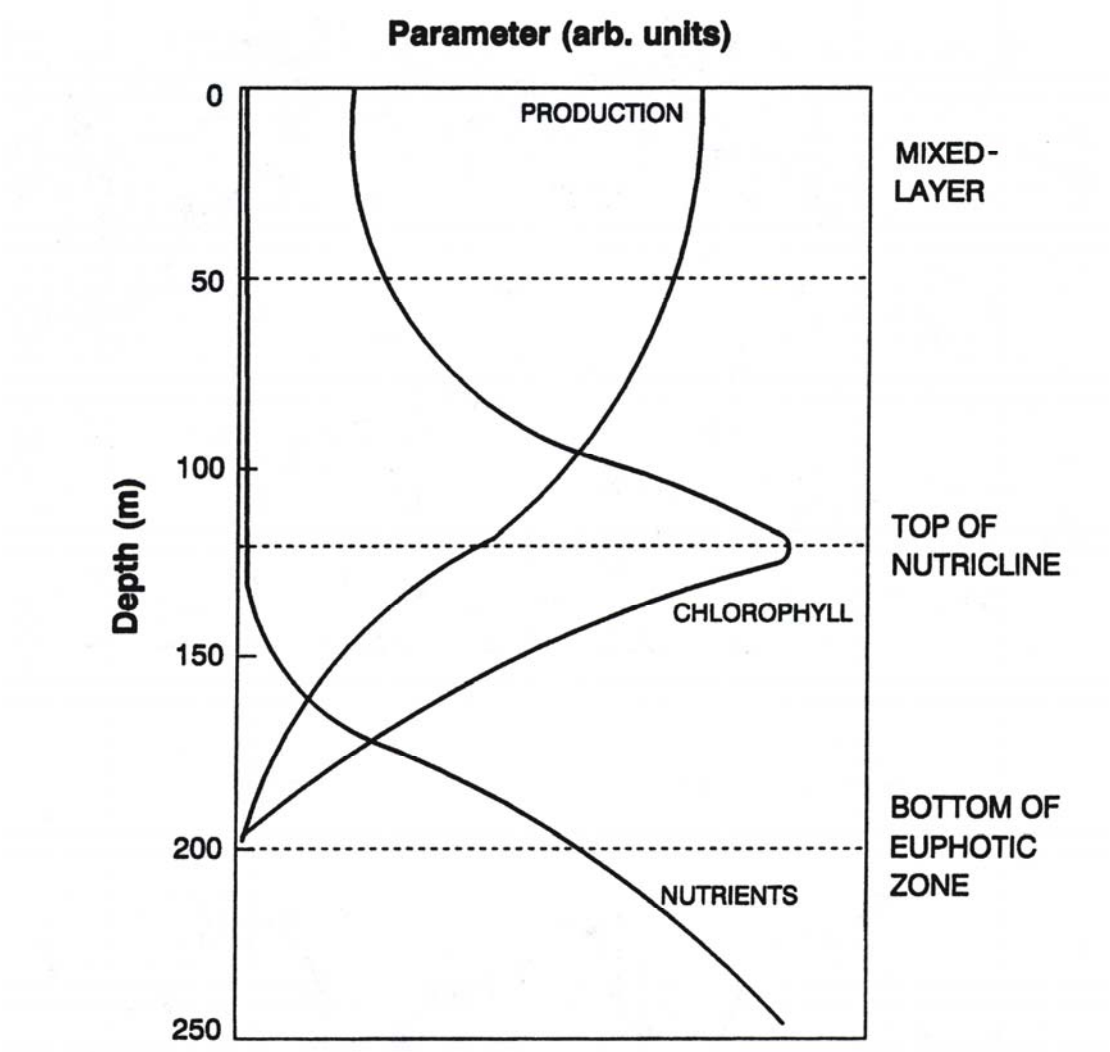


Figure 1.2 Idealized vertical variations for primary production, chlorophyll *a* and major nutrients at Sta. ALOHA. Picture taken from Karl (1999).

## 2. The impact of climate forcing on ecosystem processes in the North Pacific Subtropical Gyre

Corno, Guido, Karl, David M., Church, Matthew J., Letelier, Ricardo M., Lukas, Roger and Abbott, Mark R.

Manuscript submitted to *Journal of Geophysical Research-Oceans*

## 2.1 Abstract

Measurements at the Hawaii Ocean Time-series (HOT) Station ALOHA (22°45'N, 158°W) since October 1988 have revealed a significant, approximately 50% increase in euphotic zone depth-integrated rates of primary production (PP; mol C fixed $m^{-2}$ $d^{-1}$) based on *in situ* $^{14}C$ experiments. The character of the nearly two-decade increasing trend in PP was punctuated by several abrupt episodes that coincided with changes in the El Niño / Southern Oscillation (ENSO) or Pacific Decadal Oscillation (PDO) climate indices, or both. In contrast to the observed increase in rates of PP, the PP per unit chlorophyll *a* (mol C fixed mol chl $a^{-1}$ $d^{-1}$), a measure of the biomass-normalized production, was relatively constant, whereas PP per unit solar radiation (mol C fixed mol $quanta^{-1}$), a measure of the efficiency of light utilization, varied in synchrony with the temporal trend in PP. The HOT program core data sets also revealed changes in mixed-layer depth, upper ocean stratification, inorganic nutrients and in the taxonomic structure of the phototrophic microbial assemblage, the latter determined by flow cytometry and pigment inventories. These time-series data suggest that ENSO/PDO induced large-scale physical interaction between the atmosphere and the ocean may control upper ocean stratification and vertical nutrient delivery into the euphotic zone at Sta. ALOHA and, in turn, may influence the composition of the plankton assemblage resulting in changes in rates of PP, export and, therefore, carbon sequestration in the NPSG.

## 2.2 Introduction

Oligotrophic gyres represent approximately 75% of the total world oceans. Due to their vast surface area, these gyres play a significant role in solar energy capture, bio-elemental cycling and carbon export (Martin et al. 1987). Although rates of primary production (PP) in these areas are typically lower than in coastal or upwelling zones (Longhurst *et al.* 1995), even small variations in PP can have a significant impact on the global oceanic carbon cycle. Recent evidence suggests that oligotrophic regions, once considered biological deserts with low ecosystem variability, demonstrate relatively high spatial and temporal variability in PP and chlorophyll *a* (Karl *et al.* 2002, Maranon *et al*. 2003, Wilson 2003). Such variations may be related to different physical forcing depending on the temporal and spatial scales over which the observations are considered (Karl *et al.* 1995, Letelier *et al.* 2000, Sakamoto *et al.* 2004). Of particular interest to constrain ocean ecosystem and geochemical models are ocean-basin scale events that appear linked to climate variability events such as the El Niño/Southern Oscillation (ENSO) and the Pacific Decadal Oscillation (PDO).

Despite chronic nutrient limitation in the upper portion (0-100 m) of the North Pacific Subtropical Gyre (NPSG), both plankton biomass and rates of PP demonstrate considerable temporal variability (variance range 20-400%) (Laws *et al.* 1987, Karl *et al.* 1996, Letelier *et al.* 1996, Karl 1999, Karl *et al.* 2002). Interannual variability in plankton biomass and PP has been attributed to alterations in upper ocean nutrient supply stemming from physical variations due to ENSO and the PDO (Karl *et al.* 2001, 2002). Karl *et al.* (1995) hypothesized that ENSO events enhanced $N_2$-fixation

by stabilizing the upper ocean and shoaling mixed layer depths (MLD) due to anomalously light winds and increased insolation (due to reduced clouds) (Karl *et al.* 1995). On longer time scales, variations in the phase of the PDO may also be responsible for observed decadal changes in PP in the NPSG, as inferred by a significant increase in total chlorophyll *a* (Chl *a*) during summer months over nearly three decades (Venrick *et al.* 1987). The extended positive phase of the PDO during this period (1965-1977) led to a concomitant increase in winter winds, decrease in sea surface temperature (SST) and an apparent shift in the carrying capacity of the NPSG (Venrick *et al.* 1987). Ocean-climate related temporal variability in PP may also influence the composition of the plankton assemblages. During the PDO positive phase (1965-1977) the plankton assemblage of the NPSG appears to have shifted toward an ecosystem dominated by prokaryotes and this transition altered food web dynamics, new and export production, nutrient supply, and fishery yields (Karl 1999, Karl *et al.* 2001).

A formal assessment of the coherence of the NPSG response to changes in ENSO and PDO events (i.e. magnitude and synchrony) has not been presented, despite the potential significance of such coherence to elemental cycling and trophic dynamics in the ocean. Furthermore, such an analysis could provide a framework for the assessment of the resilience of the NPSG ecosystem to perturbation, and in turn, the level of self-organization for that habitat (Laws 2003). ENSO and PDO fluctuate on different time-scales, with ENSO demonstrating higher frequency ocean-climate variability (1-3 years), while the PDO is dominated by lower frequency variability (10-30 years) (Mantua *et al.* 1997). Because these two climate phenomena can vary

independently, and exhibit variable strength in either a "warm" or "cold" phase (Mantua *et al.* 1997, Wolter and Timlin 1998), it is possible for phase transitions to either coincide or not, possibly resulting in a variety of fundamentally different ecosystem forcing modes. It appears that most phase transitions coincide with ENSO warm event termination, but most ENSO warm event terminations do not coincide with PDO transitions (Graham 1994, Barnett *et al.* 1999). To date, the large-scale physical interactions in the upper ocean of the NPSG occurring during these two conditions remains largely unknown. Long-term, time-series measurements of biogeochemical processes are crucial for observing and eventually interpreting the relationships between these climate variations and ocean ecosystem responses. In this respect, the Hawaii Ocean Time-series (HOT) program provides the only datatset that can be used to assess temporal variability in PP in the NPSG over time scales ranging from intra-annual to sub-decadal (Karl and Lukas 1996). In this study we analyze 17 years of monthly measurements on PP (based on *in situ* $^{14}C$ incorporation into particulate matter), picoplankton abundances (derived from flow cytometric and pigments analyses), particulate matter fluxes, nutrient concentrations, and hydrographic conditions to evaluate the response of the NPSG ecosystem to large-scale climate perturbation events.

## 2.3 Methods

*Biological and Chemical data*

PP, particulate material export (at the 150 m reference depth), nutrient concentration, flow cytometry and pigment data sets were collected at Station ALOHA (A Long-term Oligotrophic Habitat Assessment; 22°45'N, 158°W) as part of the ongoing HOT program (data available at http://hahana.soest.hawaii.edu/hot/hot-dogs/interface.html). Protocols used for sampling, experimentation and analysis were consistent throughout the study; they are documented elsewhere (Letelier *et al.* 1996, Karl *et al*. 2001).

*Climate Data*

Temporal variability in ENSO was assessed using the Multivariate ENSO Index (MEI) (data obtained from the NOAA climate Diagnostics Center at http://www.cdc.noaa.gov/people/klaus.wolter/MEI/table.html). Briefly, the MEI is calculated as the first unrotated Principal Component (PC) of six observed fields combined (sea-level pressure, zonal and meridional components of the surface wind, sea surface temperature, surface air temperature, and total cloud cover). These observations are confined to the tropical Pacific. In order to keep the MEI consistent, all seasonal values are standardized by the seasonal variance during the 1950-93 reference period; a positive and negative MEI refer to El-Niño and La-Niña favorable conditions, respectively (Wolter and Timlin 1998).

The index of the PDO was obtained from the Joint Institute for the Study of the Atmosphere and Ocean (http://jisao.washington.edu/pdo/PDO.latest). Standardized values for the PDO index were derived as the leading principal

component of monthly SST anomalies in the North Pacific Ocean poleward of 20° N (Mantua *et al.* 1997). The monthly mean global average SST anomalies are removed to separate this pattern of variability from any large-scale warming signal that may be present in the time-series data.

In order to determine regional effects of ENSO and PDO at Sta. ALOHA, average sea surface heights (SSH) between the NOAA Hilo and the Honolulu tide gauges ($SSH_{Hi-Ho}$) were calculated. $SSH_{Hi-Ho}$ data were obtained from the NOAA National Data Buoy Center (http://www.ndbc.noaa.gov/Maps/Hawaii.shtml). Variability of this regional sea level index is due to a combination of local Ekman pumping and remote forcing via Rossby waves.

Time-series of the mixed layer depth (MLD) were calculated from the HOT CTD data archive as the depth where (i) an offset of 0.125 in potential density ($\sigma_\theta$) from the surface value, and (ii) a gradient of 0.005 in $\sigma_\theta$ $m^{-1}$occured. Finally, time-series of the buoyancy frequency in the upper 200 m was also calculated for Sta. ALOHA, which quantifies the detailed variability of upper ocean stratification.

*Statistical Analysis*

Normalized anomalies (defined here as the z-score) for each variable were obtained to determine possible trends in relation to changes in ENSO, PDO and local SSH. The z-score was calculated as $z_i = (x_i - \mu) / \sigma$, where $x_i$ is the measured value, and $\mu$ and $\sigma$ are the 17-year monthly mean and standard deviation values, respectively, for all observations $x_1, x_2 \ldots x_i$.

In order to compare differences in biogeochemical parameters to variability in ENSO and PDO indices, the 17-year record of biogeochemical measurements was divided into 5 periods based on changes in the ENSO, PDO and SSH. After testing for normal distribution within the five periods, significant differences between periods were then tested using Analysis of Variance (ANOVA), changing the significance level for each comparison according to the refined Bonferroni method (Hochberg 1988), and t-test at 0.05 significance level.

## 2.4 Results

*Physical forcing and habitat response*

During the HOT program observation period (1989-present), the NPSG has had two relatively strong positive (warm) ENSO forcings events. The first event occurred between 1991-1994, and the second event, which was larger in magnitude, occurred during 1997-1998 (Fig 2.1A). The PDO index exhibited similar variability as the MEI during 1991-1994 and 1997-1998 events, but the PDO index was in a positive phase during 1995-1996, while the MEI index was negative (Fig. 2.1A). Three negative (cold) events also occurred during 1988, 1996 and 1998-2001.

Monthly anomalies of the SSH averages between Hilo and Honolulu ($SSH_{av}$) displayed temporal trends in accordance with the 1997-1998 ENSO changes (Fig. 2.1B). High $SSH_{av}$ (strongly positive anomalies) occurred during the 1991-1994 ENSO ($SSH_{diff}$ anomalies >1). $SSH_{av}$ anomalies became negative between 1995-1996 in phase with the ENSO cold event, but they became positive during the 1997-1998 strong ENSO event. Another transition to negative $SSH_{av}$ occurred following this latter event as the strong ENSO cold event developed. Based on these results, the HOT program biogeochemical data were subsequently divided into five periods: (i) 1989-1990 (ENSO, PDO anomalies weak and variable between –1 and +1), (ii) 1991-1994 (ENSO, PDO anomalies > +1), (iii) 1995-1996 ( ENSO strongly negative, PDO anomaly positive), (iv) 1997-1998 (ENSO and PDO anomalies both strongly positive) and (v) 1999-2004 (ENSO and PDO anomalies weak and variable between –1 and 1).

At Sta. ALOHA, the monthly MLD anomalies significantly decreased during the initial two years of the 1991-1994 ENSO, switching phase in the latter part of 1993 (Fig. 1C). During the stronger ENSO event, MLD were significantly greater ($p < 0.005$, $n = 23$) than during the 1991-1994 ENSO event (Table 2.1). Following the 1997-1998 ENSO event, the average MLD increased significantly and became more variable (50 m vs. 66 m, Table 2.1). The potential density difference ($\sigma_{\theta\ diff\ MLD-MLD+20m}$) across the base of the mixed layer, calculated as the difference between the mean $\sigma_\theta$ in the MLD and the mean $\sigma_\theta$ in the MLD + 20 m layer became significantly positive ($p<0.005$, $n = 45$) during both the 1991-1994 and the 1997-1998 ENSO warm events (Fig. 2.1D). This indicates a weaker resistance to ML deepening (and entrainment of deeper waters) for a given increase in wind speed. A significant

decrease ($p<0.005$, $n= 23$) in $\sigma_{\theta\ diff\ MLD\text{-}MLD+20m}$ was also observed in the period between the two ENSO warm events. To further understand the stability dynamics of the water column and the link between upper and lower euphotic zone processes, the potential density difference ($\sigma_{\theta\ diff\ MLD+20m\text{-}140:160m}$) between the MLD+20m layer and the 140-160 m was calculated. The $\sigma_{\theta\ diff\ MLD+20m\text{-}140:160m}$ remained negative during the 1991-1994 ENSO but displayed a significant ($p<0.005$, $n= 45$) transition to positive anomaly during and following the 1997-1998 ENSO (Fig. 2.1E). The 140-160 m reference layer was chosen because, based on climatological data at Sta. ALOHA, it is deeper than the mean depth of the top of the nutricline (Karl *et al.* 2002). This latter difference ($\sigma_{\theta\ diff\ MLD+20m\text{-}140:160m}$) can then be used as a measure of the lower euphotic zone stratification and as a proxy for the probability of nutrient injection from the lower into the upper euphotic zone (i.e. positive $\sigma_{\theta\ diff\ MLD+20m\text{-}140:160m}$ indicates a greater probability of an injection event occurring than during negative anomalous $\sigma_{\theta\ diff\ MLD+20m\text{-}140:160m}$).

A clear transition in water column stability at Sta. ALOHA occurred following the 1997-1998 ENSO, as indicated by the mixed layer density anomalies, the scaled mixed layer temperature and salinity variations (Fig. 2.2 and 2.3). The Brunt-Väisälä frequency (a measure of the ocean buoyancy damping of turbulence) for the upper 100 m increased significantly during the 1991-1994 ENSO, while it significantly decreased during and after the 1997-1998 ENSO (Table 1). Furthermore, a clear decrease in the buoyancy frequency below the mixed layer occurred during the 1997-1998 ENSO (Fig. 2.3)**.** Buoyancy frequency time-series revealed a deepening of MLD during the 1997-1998 ENSO. Interannual variability in MLD also demonstrated

a clear transition from positive to negative values with the onset of the 1997-1998 ENSO and continuing into 1999 (Fig. 2.4). In particular, the winter and fall anomalies for MLD switched sign following the 1997-1998 ENSO (Fig. 2.4A and D).

Concomitant with the shift in water column stability, salinity values at Sta. ALOHA also displayed a clear transition following the 1997-1998 ENSO. Near-surface (5 m) salinity anomalies revealed a progressive increase in salinity with the onset of the 1997-1998 ENSO (Fig 2.5A), with salinity remaining significantly greater ($p<0.005$ $n= 65$) than average following this event. The increase in salinity at the onset of the 1997-1998 ENSO was not confined to surface layers of the euphotic zone, as salinities increased ($p < 0.005$, $n=65$) throughout most of the euphotic zone (Fig. 2.6). These higher values persisted following the 1997-1998 ENSO.

The shift to higher salinity following the 1997-1998 ENSO was temporally associated with a significant decrease in sea surface temperatures at Sta, ALOHA starting in late 1996 and lasting through 1998 (Fig. 2.5B, Table 2.1). However, this temperature change was not associated with a significant change in surface heating, as indicated by sea surface PAR anomalies. Surface PAR displayed no significant temporal variations (Fig. 2.5C), although strong positive and negative anomalies (i.e. >1 and <-1) were measured in 1992 and 1995, respectively.

*Nutrient inventories*

Nitrate + nitrite (N+N) and soluble reactive phosphorus (SRP) concentrations displayed different vertical and temporal trends between each other. In the upper euphotic zone, $N+N_{0\text{-}45m}$ anomalies decreased from the beginning of the time-series

through the 1997-1998 ENSO (Fig. 2.7A). This decreasing trend was interrupted in 1995 by a large positive anomaly. Following the 1997-1998 ENSO event, $N+N_{0\text{-}45m}$ anomalies increased significantly (Fig. 2.7A, $p<0.005$, $n= 74$). These trends were also confirmed by temporal variations in absolute N+N concentrations between the different ENSO-PDO periods previously defined (Table 2.1). $N+N_{0\text{-}45m}$ concentrations were significantly lower during the 1997-1998 ENSO than at the beginning of the time-series; a small (30 μmol $m^{-2}$), but significant, increase in $N+N_{0\text{-}45m}$ concentrations occurred after the 1997-1998 ENSO (Table 2.1). In the lower euphotic zone, $N+N_{75\text{-}125m}$ anomalies remained relatively unchanged, (Fig. 2.7B); however, following the 1997-1998 ENSO event the lower euphotic zone $N+N_{75\text{-}125m}$ anomalies were more variable than previously (i.e. greater number of spikes). In relation to this variability increase, absolute $N+N_{75\text{-}125m}$ concentrations were significantly higher following the 1997-1998 ENSO than previously.

Unlike the $N+N_{0\text{-}45m}$ anomalies, $SRP_{0\text{-}45m}$ anomalies did not significantly show a significant decrease with time for all the time-series, but they remained relatively unchanged (Fig. 2.7C). However, absolute $SRP_{0\text{-}45m}$ concentrations were significantly lower through the 1997-1998 ENSO than at the beginning of the time-series (Table1). In the lower euphotic zone, $SRP_{75\text{-}125m}$ anomalies decreased through the time-series (Fig. 2.7D). Similarly, absolute $SRP_{75\text{-}125m}$ concentrations significantly decreased between each consecutive ENSO-PDO period (Table 2.1).

*Primary Productivity*

Rates of primary production (PP) increased significantly throughout the entire 17-year observation period (1989-2004), as shown by significant increases in the monthly anomalies (Fig. 2.8A, $p<0.005$, $n=166$). However, during 2002-2003, PP displayed a weak decreasing trend. The overall PP increase is also apparent from the difference in the absolute rates of PP measured between 1989-1990 and 1999-2004 ($0.033 \pm 0.004$ vs. $0.052 \pm 0.002$ mol C $m^{-2}$ $d^{-1}$, respectively) (Table 2.1). Interannual dynamics in PP appear characterized by a step function, with stepwise increases observed between 1990-1991 and again between 1997-1998 (Fig. 2.8A) Following both these step increases, PP remained higher than previously (Table 2.1). PP increased by ~0.008 mol C $m^{-2}$ $d^{-1}$ (equivalent to approximately 25%) with the onset of the 1991-1994 ENSO, but remained relatively constant during the onset of the 1997-1998 ENSO event. PP further increased significantly (approximately 0.010 mol C $m^{-2}$ $d^{-1}$or 30%) after the 1997-1998 ENSO event, in particular from mid-1999 to beginning of 2002.

The monthly anomalies in PP normalized to Chl *a* (PP/Chl *a*) did not show a significant temporal trend (Fig. 2.8B, $p<0.005$ $n= 166$). This pattern was also reflected in the grouped PP/Chl *a* values (Table 2.1), where no significant differences were observed between the different time periods. Anomalies for PP normalized to incident light flux (PP/Light, a proxy for the photosynthetic quantum yield) displayed a significant increase throughout the observation period (Fig. 2.8C, $p<0.005$ $n=166$). In addition, PP/Light increased significantly during the 1997-1998 ENSO event (0.020 vs. 0.027 mol C mol quanta $^{-1}$, respectively) (Table 2.1).

The observed temporal changes in PP varied between the upper ($PP_{0\text{-}45m}$) and the lower ($PP_{75\text{-}125m}$) euphotic zone, as indicated by season PP anomalies and changes in the depth-integrated rates of PP (Fig. 2.9 and Table 2.1, respectively). Depth-integrated $PP_{0\text{-}45m}$ was higher by ~50% coincident with the 1991-1994 ENSO (Fig. 2.9B, or approximately 0.007 mol C $m^{-2}$ $d^{-1}$, $p<0.005$, $n$=48), but was lower by ~15% during the 1997-1998 ENSO (approximately 0.004 mol C $m^{-2}$ $d^{-1}$, $p<0.005$, $n$=23). Conversely, $PP_{75\text{-}125m}$ remained constant during the 1991-1994 ENSO, but higher by ~30 % (an increase of approximately 0.016 mol C $m^{-2}$ $d^{-1}$) following the 1997-1998 ENSO (Fig. 2.9C and Table 1). In particular, the $PP_{75\text{-}125m}$ increased during the 1997-1998 year (1998) of the 1997-1998 ENSO event (Fig. 2.9C).

Increases in PP were further demonstrated by comparing seasonal variations in PP (Fig. 2.10 and Table 2.1). Seasons were defined by the latitudinal light field variations for Sta. ALOHA. Winter, summer and fall anomalies in PP showed a clear and significant increase (Table 2.1) during the 1997-1998 ENSO (Fig 2.10A, C and D), while spring PP increased during the first half (1991-92) of the 1991-1994 ENSO (Fig 2.10B). In addition, following the 1997-1998 ENSO, rates of PP during the summer and fall significantly increased (Table 2.1). The step function increase in PP was also apparent in the winter and summer seasonally binned data (Table 2.1). Rates of PP in the spring increased by ~50% during the 1991-1994 ENSO, but did not show any other significant variations for the remaining periods examined. During the fall months, PP increased during the 1991-1994 and 1997-1998 ENSO by ~30 %.

*Planktonic community structure and pigments*

Flow cytometric analyses revealed temporal variability in the abundances of the major photoautotrophic groups at Sta. ALOHA following the 1997-1998 ENSO event (Fig. 2.11). The flow cytometric analyses are not available for the initial phase of HOT, including the 1991-1994 ENSO event. In the upper euphotic zone, *Prochlorococcus* spp. concentrations decreased significantly ($p<0.005$, $n=83$) following the 1997-1998 ENSO (Fig. 2.11A, Table 2.1). *Synechococcus* spp. did not display any coherent temporal dynamics (Fig. 2.11C); however, abundances of *Synechococcus* spp. increased during the 1997-1998 ENSO (Table 2.1). In contrast, picoeukaryote abundances increased during the initial part of the 1997-1998 ENSO (Fig. 2.11E, Table 2.1), and continued to significantly increase (Table 2.1).

In the lower euphotic zone, *Prochlorococcus* spp. cell abundances were temporally variable (Fig. 2.11B), but overall the abundance of *Prochlorococcus* spp. decreased significantly following the 1997-1998 ENSO (Table 2.1). Similar patterns were found for *Synechococcus* spp. (Fig. 2.11D). On the other hand, picoeukaryote abundances increased by 50% with the onset of the 1997-1998 ENSO (Table 2.1).

Selected pigments, including chlorophyll *b* (Chl *b*, a biomarker for prochlorophytes), 19′ -hexanoyloxyfucoxanthin (19′ -Hex, a biomarker for prymnesiophyes) and zeaxanthin (Zea, a biomarker for cyanobacteria) (Mackey ***et al.*** 1996), were also used to further asses the variability of the planktonic community structure. With the exception of Chl *b* in the lower euphotic zone (Fig. 2.12 B), all the pigments concentrations significantly ($p<0.005$, $n=850$) increased following the 1997-1998 ENSO, while they unchanged during the 1991-1994 (Fig. 2.12). In

particular, the increase in pigment concentrations following the 1997-1998 ENSO was very clear in the upper euphotic zone (Fig. 2.12 A, C, and E).

**2.5 Discussion**

The connectivity between marine ecosystems and climate variability is thought to depend in part on the intensity, duration and frequency of atmospheric forcing of upper ocean physics, including variables such as ocean circulation and stratification. To date, however, we lack a clear understanding of the specific relationships that link ocean biota, chemistry, and physics, partly because of the complexity and nonlinearity of marine ecosystems and partly due to the paucity of long-term (decadal scale) data on the time-dependent nature of biogeochemical processes in the sea. The present study confirms that impacts of large-scale, ocean-climate forcing on subsequent ecosystem changes are not exclusive and that they can be variable. This information is of interest when trying to predict future or hindcast past ecosystem changes in relation to climate variability. The different time scales of ENSO and PDO likely confound direct relationships and in the case of decade-scale phenomena like the PDO, our time-series is much too short. However, the statistical correlation between these two climate drivers of ocean variability may be useful to predict NPSG ecosystem changes. An idealized summary of the variation in ecosystem response for the NPSG is given in Table 2.2.

Based on analyses of more than 17 years of data on physical, chemical, and biological variability at Sta. ALOHA, the ecosystem's response to two ENSO events did not appear to be consistent, which may be due to a phase reversal in the PDO.

When the statistical correlation between the PDO and ENSO events was weakly positive (i.e., they were out of phase, during the 1991-1994 ENSO, $r^2_{ENSO\text{-}PDO} = 0.15$, $p < 0.005$, n= 48), rates of PP increased, and the ecosystem appeared to have returned to pre-perturbation conditions. When the statistical correlation between the two indices was strongly positive (i.e. they were in phase, during the 1997-1998 ENSO, $r^2_{ENSO\text{-}PDO} = 0.70$, $p < 0.005$, n= 24), both rates of PP and export increased, and the amount of time required for the system to return to initial conditions following perturbation was prolonged. The unique responses of the NPSG ecosystem to combined variability in PDO and ENSO suggest that the response of the upper ocean may be sensitive to competing physical perturbations from both of these ocean-climate processes. The large-scale physical interaction during these two climate signals appears to influence the wind forcing, heat and fresh water fluxes at the local scale and the ocean-basin scale, and they in turn determine the variation of upper ocean physical properties. During ENSO warm events, when ENSO and PDO signals are not in phase, the trade winds weaken, increasing the stratification of the upper ocean (Karl *et al.* 1995). On the other hand, when ENSO and PDO are highly correlated, subsurface water mass changes appear to decrease the upper water column stability.

The issue of delayed ENSO subsurface forcing (via Rossby waves) should also be considered when trying to understand the complexity of the ecosystem-climate relationship. The ecosystem response at ALOHA to direct surface forcing from one ENSO warm event may depend critically on its phasing relative to the delayed subsurface remote forcing from a previous event It may take 2-3 years for the

ENSO Rossby waves to reach Sta. ALOHA after a warm ENSO event gets underway. The mature phase surface forcing will be about 6-9 months after the very beginning of the event onset, so the maximum Rossby wave influence will lag the peak surface forcing by 1.5-2.5 years. In addition to the intensity differences among ENSO warm (and cold) events, there are anomaly pattern differences as well that should be considered. While there is a "canonical" ENSO warm (and cold) event, the actual anomalous atmospheric forcing around Hawaii differs from one event to another (Ropelewski and Halpert 1987, 1996). Some, but certainly not all, of these event-to-event differences are due to the PDO (Lukas, 2001; Chu and Chen, 2005).

*Relation of local physical forcing at Sta. ALOHA to ENSO and PDO*

Changes in MLD and in the stratification of the lower euphotic zone were critical in influencing PP at Sta. ALOHA, likely as a consequence of altering the light experienced by the exposed populations and the nutrient availability in the euphotic zone. These variations can be linked to large-scale physical interactions occurring during ENSO and PDO variations. The shoaling of the MLD and stabilization of the upper water column (decrease in $N^2$) between 1991-1992 appear driven by overall weakening of the trade winds during this period (Karl *et al.* 1995). The decrease in upper euphotic zone stability in 1997-1998, when the ENSO index began to increase and, simultaneously, the PDO index displays a sign reversal, could be related to the large-scale shift in surface forcing in the North Pacific occurring at the same time (Lukas 2001, Keeling *et al.* 2004). Sta. ALOHA was within a region of reduced SST (as indicated by the decrease in SST at Sta. ALOHA, Fig. 2.5) and increased

northerly and northeasterly winds, resulting in larger variability and increases in the absolute depth of the MLD at Sta. ALOHA. Subduction of anomalous midlatitude surface water masses and advection by the mean flow of the gyre can also qualitatively account for the upper pycnocline water mass changes (Lukas 2001). Together, these processes could explain the reduced stability of the upper ocean at Sta. ALOHA leading to the observed changes in ecosystem structure and function.

The stability decrease of the euphotic zone at Sta. ALOHA following the 1997-1998 ENSO and PDO reversal was clearly indicated by the transition to positive $\sigma_{\theta\ diff}$ anomalies and smaller $N^2$ absolute values. In particular, the stability of the lower euphotic zone showed a well-defined reduction during and following the 1997-1998 ENSO and PDO reversal (Fig. 2.1E and 2.3). During this period, the concomitant decreased stability in the higher and lower euphotic zone most likely increased the probability of surface waters being mixed deeper. During the 1991-1994 ENSO, this simultaneous reduction in stability of the higher and lower euphotic zone did not occur. The reduced stability following the 1997-1998 ENSO stemmed from both increased surface salinities and decreased temperatures, causing an increase in surface density, thus increasing the average MLD. The surface salinity change largely resulted from temporal imbalances in precipitation and evaporation across this region (Lukas 2001, Dore *et al*. 2003). The salinity increase observed below the mixed layer and throughout the euphotic zone almost certainly reflects waters that were remotely affected by anomalous surface freshwater fluxes and subsequently subducted and advected to Sta. ALOHA (Lukas 2001, Keeling *et al.* 2004). In any case, these physical processes resulted in greater MLD and reduced water column stability at Sta.

ALOHA (Table 2.1). Deep mixed-layers result in lower mean irradiances for the planktonic assemblages in the near surface, and hence lower energy fluxes.

*Variations in PP and ecosystem states*

Similar to changes in the physical stability of the upper ocean, unique responses in measured rates of PP developed during the two ENSO events and PDO phase reversals. The increase in PP during the 1991-1994 ENSO (when the PDO index was in positive phase) has previously been related to an enhancement of $N_2$-fixation, caused by a shoaling of the MLD and increased upper ocean stability (Karl *et al.* 1995). The increase in PP following the 1997-1998 ENSO and coincident reversal in the PDO likely reflects introduction of new nutrients from across the base of the nutricline due to reduced stratification (decrease in $\sigma_{\theta\ diff}$, lower $N^2$) of the upper-ocean and increased mixing. The small but significant increase observed in N+N in the upper euphotic zone (Table 2.1) and the increase in N+N spikes in the lower euphotic zone (Fig. 2.7B) after the 1997-1998 ENSO supports this hypothesis. The increased frequency in N+N spikes also highlights the role of aperiodic high concentration N+N bursts in alleviating surface nutrient limitation for this ecosystem. Conversely, the observed decrease in soluble reactive phosphorous through the time-series, despite the hypothesized increase in nutrient diffusion following the 1997-1998 ENSO and PDO reversal, may reflect a condition of microbial biomass being perturbed enough to alter the net uptake rates (i.e. uptake >> regeneration). During the first half of the 1997-1998 ENSO event (spring to fall 1997) PP remained relatively stable despite increasing frequency of N+N spikes. The apparent reasons in

the biogeochemical responses to physical forcing during the ENSO and PDO reversals are unknown. However, these upper ocean transitions were accompanied by changes in both the integrated mean light regime and accompanying decrease in the average temperature of the upper ocean, either of which may have decreased phytoplankton growth rates and, therefore, PP.

The observed depth-dependent changes in PP during the two ENSO events supports the hypothesis that $N_2$ fixation supports a larger fraction of the total production during the 1991-1994 ENSO event, with $NO_3^-$ based production accounting for a larger fraction of PP during the 1997-1998 ENSO. Conversely, in the lower euphotic zone, PP increased only during the 1997-1998 ENSO and coincident reversal in the PDO. This observation is consistent with the hypothesis that the source of the new nutrients to the upper ocean derived from increased entrainment across the top of the nitracline.

The variable response in particulate matter flux during the two ENSO events also provides insight into the different biogeochemical responses of climate forcing. Particulate carbon (PC) export decreased during the 1991-1994 ENSO, and increased during the 1997-1998 event (Table 2.1). The decrease in export could reflect increased retention of organic matter and enhanced re-mineralization in the upper euphotic zone stemming from increased stratification between the mixed-layer and the lower euphotic zone. During the 1997-1998 ENSO event and coincident with the PDO reversal, the disruption of water column stability and subsequent increase in mixing may have enhanced organic material export and provided a mechanism for a greater fraction of the organic matter produced in the euphotic zone to escape re-

mineralization and sink deeper in the water column. Biological mechanisms should also be considered as potential explanations for the difference in export during the two ENSO events. Changes in photoautotrophic community structure (as found here with increasing picoeukaryotes numbers) towards large cells (therefore more susceptible to sinking) and variations in grazing rates could have lead to increase export during the 1997-1998 ENSO.

Despite the observed variations in PP, the overall nutrient status of photoautotrophic assemblage, as indicated by PP/Chl *a*, appeared temporally stable. PP/Chl *a* can be related to the photosynthetic assimilation number, or productivity index, which represents a proxy for the physiological status of photoautotrophic community under *in situ* conditions. If the PP/Chl *a* is interpreted as evidence for nutrient (usually N) limitation (Karl *et al.* 2001), then the overall increase in PP and increased nutrient entrainment with the onset of the 1997-1998 ENSO and reversal of the PDO, did not appear to alter the underlying physiological nutrient condition of photoautotrophs. Even though some limitations exist regarding the validity of using PP/Chl *a* as a nutrient proxy (Cullen 1995), this result suggests that (i) greater concentrations of nutrients over longer time are needed to significantly affect photoautotrophs physiology in the NPSG, (ii) light limitation, due to increasing mixing, is the main factor influencing the PP/Chl *a* or (iii) the observed changes in plankton assemblage composition or nutrient uptake rates may have masked apparent changes due to nutrient enrichment.

The change in PP/Light (a proxy for the photosynthetic quantum yield) after the 1997-1998 ENSO suggests an overall increase in the efficiency of light utilization

by upper ocean photoautotrophic assemblages. Increases in PP/Light may have derived from a response by the photoautotrophic community to lower light availability stemming from increased mixing. The combination of various factors, including (i) increased nutrient injection, (ii) variations in light utilization efficiency and (iii) alteration of plankton assemblage composition, all may have contributed to the observed changes in PP following the 1997-1998 ENSO and PDO reversal in 1998.

*Community structure changes*

The observed variations in physical stability in the euphotic zone of the NPSG also appear to have led to a change in the composition of the photoautotrophic plankton assemblage. Changes in concentrations of *Prochlorococcus* spp., picoeukaryotes and prymnesiophytes (as indicated by 19′-Hex concentrations) during and after the 1997-1998 ENSO agree with the hypothesized increase in $NO_3^-$ fluxes from the lower euphotic zone. The recently completed genome sequences of three strains of *Prochlorococcus* spp. highlight that these strains lack the nitrate reductase operon required for $NO_3^-$ utilization (Moore *et al.* 2002, Dufrense *et al.* 2003). Even though $NH_4^+$ will still represent the main source of chemical substrate for photosynthesis at Sta. ALOHA, decreasing concentrations of surface *Prochlorococcus* spp. abundances following the 1997-1998 ENSO and coincident phase reversal of the PDO may reflect the inability of surface *Prochlorococcus* spp. to compete with other groups of photoautotrophic plankton capable of nitrate utilization, including *Synechococcus* spp. and various groups of picoeukaryotes. In

addition, the growth of various strains of *Prochlorococcus* spp. appear sensitive to changes in temperature (Moore *et al*. 1995), suggesting that cooling of the upper ocean following the 1997-1998 ENSO and PDO phase reversal may have allowed photoautotrophic organisms less sensitive to temperature to out-compete *Prochlorococcus* spp.

In the upper euphotic zone, the concomitant increase in Chl *b* and decrease in *Prochlorococcus* spp. are in agreement with the hypothesized increase in mixing and consequent decrease in light integrated availability following the 1997-1998 ENSO. The increase in the ratio Chl *b*: *Prochlorococcus* spp. can be interpreted as a photo-adaptation response to lower light availability resulting in a high Chl *b* cell quota. As Chl *b* is the primary accessory pigment in prochlorophytes, a higher Chl *b* concentration per cell would enhance the capture of light and energy transfer towards Chl *a* molecules in order to maintain the photosynthetic processes balanced as a response to reduced light availability. Likewise, the increase in zeaxanthin in the lower euphotic zone following the 1997-1998 ENSO could be related to changes in water column stability and light availability. In this context, cyanobacteria populations in the lower euphotic zone would have been subjected to higher light availability (due to increased mixing) following the 1997-1998 ENSO. The relative increase of zeaxanthin per cyanobacterial cell can then be interpreted as a photo-protective process. A higher concentration of zeaxanthin per cell would have protected the photosynthetic apparatus from the increased light availability by dissipating the excess energy in the form of heat and fluorescence through increase rates in the xanthophylls cycle (i.e. increase in zeaxanthin concentrations). Because

light availability scales as an exponential of depth, small changes in MLD can lead to large changes in average light. If light is a major influence on plankton rate processes, then standard $^{14}C$ *in situ* (fixed depth) incubations may not accurately estimate primary production. In the upper euphotic zone, the increase in zeaxanthin concentrations following the 1997-1998 ENSO is, however, not yet well understood. In this case, a photo-protective process could not be invoked to explain such change in pigment concentration. Rather than to be related to a photo-physiological process, this zeaxanthin increase may well indicate an increase in cyanobacteria species, other than *Prochlorococcus* and *Synechococcus* spp., able to exploit the changed physical and chemical environment following the 1997-1998 ENSO.

The observed increases in the abundances of picoeukaryotes and prymnesiophytes may reflect the ability of these broadly defined groups of pigmented picoplankton to grow on $NO_3^-$. *Synechococcus* spp. concentrations did not show any particular temporal variations. However, the significant increase in concentration in the upper euphotic zone during the 1997-1998 ENSO, indicates that this organism may well be suited for the hypothesized increase in $NO_3^-$ fluxes in this environment, as shown by the genetic capacity of *Synechococcus* spp. for $NO_3^-$-based growth (Glover *et al.* 2002; Moore *et al.* 2002). Together, these observations suggest picoeukaryotes and prymnesiophytes may be better adapted to a physically dynamic environment, where temperatures are lower and $NO_3^-$ more readily available. In contrast, during periods of prolonged stability, *Prochlorococcus* spp. abundances increased, likely reflecting the adaptation of these cells to stratified, oligotrophic

environments. This is consistent with long-term changes in the composition and the domain shift hypothesis (Karl *et al.* 2001).

## 2.6 Conclusion

Following nearly two decades of monthly observations at Sta. ALOHA, rates of $^{14}$C-derived PP in the NPSG have increased ~50 % (Table 2.1). The observed increases in PP appear to coincide with changes in upper ocean stratification including alteration to the MLD. Changes in euphotic zone water stability have the potential to influence light availability (by decreasing the daily integrated light in the mixed layer due to increasing mixing) and nutrient dynamics in the upper ocean. These local physical changes may demonstrate larger-scale linkages to ocean-basin climate forcing, such as through atmospheric-oceanic interactions occurring during ENSO and PDO. Throughout the latter seven years of time-series observations (1997-2004) rates of PP and export of carbon from the base of the euphotic zone have increased. Coincident in time with changes in the rates of production and export, the upper ocean appeared to undergo a shift in plankton assemblage composition with the abundance of *Prochlorococcus* spp. decreasing, while picoeukaryotes and prymnesiophytes becoming more abundant.

The observed variations in PP in the NPSG can significantly affect oceanic nutrient cycling, trophic interactions, and global elemental fluxes. Based on time-series analyses of biogeochemical variability at Sta. ALOHA, we suggest that both PP and carbon export may be influenced by large-scale interactions between the atmosphere and the ocean, e.g., ENSO and PDO. The nature of the ecosystem

response depends on both magnitude and duration of the perturbations, the coherence of multiple independent forcings and the interval between major events. It is then important to determine not only possible ecosystem response but also the ecosystem behavior following perturbation. At Sta. ALOHA based on PP dynamics, vertical variations in ecosystem response (upper vs. lower euphotic zone) add a new perspective of this ecosystem behavior. Future analyses are required to relate these temporal PP changes in the NPSG to resilience and resistance dynamics following perturbation. Such endeavor will help understanding if ecosystems tend to evolve to the state most resilient to perturbation (Laws 2003). Another important issue to be considered is to separate the notion of perturbations from shifts. This distinction depends in part on the intensity and scale of the event and the ecological response. In the context of photoautotrophic ecosystems, what might be a climate perturbation (like the observed PP change following the ENSO-PDO variations) might be perceived as a shift. In order to understand these ecosystems characteristics, long-term ecological research, such as the HOT program, is crucial and should be further encouraged (Magnuson 1990). Long-term research is required because ecosystems behaviors occur at different time-scales and in a "hidden present" due to their relative slow response and lag following perturbation.

## 2.7 References

Barnett, T. P., Pierce, D.W., Latif, M., Dommenget, D. and Saravanan, R. 1999. Interdecadal interactions between the tropics and midlatitudes in the Pacific basin. *Geophys. Res. Lett.* **26**: 615-618.

Bidigare, R.R., Schofield, O. and Prezelin, B.B. 1989. Influence of zeaxanthin on quantum yield of photosynthesis of *Synechoccocus* clone WH7803(DC2). *Mar. Ecol. Prog. Ser.* **56**: 177-188.

Bond, N. A., Overland, J. E., Spillane, M. and Stabeno, P. 2003. Recent shifts in the state of the North Pacific. *Geophys. Res. Lett.* **30**: 2183-7.

Chu, P.-S., and H. Chen, 2005: Interannual and interdecadal rainfall variations in the Hawaiian Islands. J. Climate, 18, 4796-4813.

Cullen, J. J. 1995. Status of the iron hypothesis after the open-ocean enrichment experiment. *Limn. Oceanogr.* **40**: 1336-43.

Dore, J. E., Brum, J. R., Tupas, L. M. and Karl, D. M. 2002. Seasonal and interannual variability in sources of nitrogen supporting export in the oligotrophic subtropical North Pacific Ocean. *Limnol. Oceanogr.* **424**: 754-7.

Dore, J. E., Lukas, R., Sadler, D. W. and Karl, D. M. 2003. Climate-driven changes to the atmospheric $CO_2$ sink in the subtropical North Pacific Ocean. *Nature* **424**: 754-7.

Dufrense, A., Salanoubat, M., Partensky, F., Artiguenave, F., Axmann, I.M., Barbe, V., Duprat, S., Galperin, M.Y., Koonin, E.V., LeGall, F., Makarova, K.S., Ostrowski, M., Oztas, S., Robert, C., Rogozin, I.B., Scanla, D.J., Tandeau de Marsac, N., Weissenbach, J., Wincker, P., Wolf, Y.I. and Hess, W.R. 2003.

Genome sequence of the cyanobacterium *Prochlorococcus marinus* SS120, a nearly minimal oxyphototrophic genome. *Proc. Natl. Acad. Sci.* **105**: 10020-5.

Glover H.E., B.B. Prézelin, L. Campbell, M. Wyman and C. Garside (1988). A nitrate-dependent Synechococcus bloom in surface Sargasso Sea water. *Nature* **331**: 161-163.

Graham, N.E. 1994: Decadal-scale climate variability in the tropical and North Pacific during the 1970s and 1980s: Observations and model results. *Clim. Dyn.* **10**: 135-162

Hochberg, Y. 1988. A sharper Bonferroni procedure for multiple tests of significance. *Biometrika* **75**: 800-803.

Karl, D. M. 1999. A sea of change: Biogeochemical variability in the North Pacific subtropical gyre. *Ecosystems* **2**: 181-214.

Karl, D. M., Letelier, R. M., Hebel, D., Tupas, L., Dore, J., Christian, J. and Winn, C. 1995. Ecosystem changes in the North Pacific subtropical gyre attributed to the 1991-92 El-Niño. *Nature* **373**: 230-4.

Karl, D. M., Dore, D. V., Hebel, R. M. , Letelier, R. M. and Tupas, L. M. 1996. Seasonal and interannual variability in primary productivity and particle flux at Station ALOHA. *Deep-Sea Res. II* **43**: 539-68.

Karl, D. M. and Lukas, R. 1996. The Hawaii Ocean Time-series (HOT) program: Background, rationale and field implementation. *Deep-Sea Res. II* **43**: 129-56.

Karl, D. M., Bidigare, R. R. and Letelier, R. M. 2001. Long-term changes in plankton community structure and productivity in the North Pacific Subtropical Gyre: the domain shift hypothesis. *Deep-Sea Res. II* **48**: 1449-70.

Karl, D. M., Bidigare, R. R. and Letelier, R. M. 2002. Sustained and aperiodic variability in organic matter production and phototrophic microbial community structure in the North Pacific Subtropical Gyre. In: P. J. le B. Williams, D. R. Thomas and C. S. Reynolds, Eds., Phytoplankton Productivity and Carbon Assimilation in Marine and Freshwater Ecosystems, Blackwell Publishers, London, 222-64.

Keeling, C. D., Brix, H. and Gruber, N. 2004. Seasonal and long-term dynamics of the upper ocean carbon cycle at Station ALOHA near Hawaii. *Global Biogeochem. Cycles* **18**: 4006-32.

Laws, E. A. 2003. Partitioning of microbial biomass in pelagic aquatic communities: maximum resiliency as a food web organizing construct. *Aquatic Micr. Ecol.* **32**:1-10.

Laws, E. A., DiTullio, G. R. and Redalje, D. G. 1987. High phytoplankton growth and production rates in the North Pacific subtropical gyre. *Limnol. Oceanogr.* **32**: 905-18.

Letelier, R.M., Bidigare, R. R., Hebel, D.V., Ondrusek, M., Winn, C.D. and Karl, D.M. 1993. Temporal variability of phytoplankton community structure based on pigment analysis. *Limnol. Oceanogr.* **38:** 1420-37.

Letelier, R.M., Dore, J.E., Winn, C.D. and Karl, D.M. 1996. Seasonal and interannual variations in photosynthetic carbon assimilation at Station ALOHA. *Deep-Sea Res. II* **43**:467-87.

Letelier, R. M., Karl, D. M., Abbott, M. R., Flament, P., Freilich, M. , Lukas, R. and Strub, T. (2000). Role of late winter mesoscale events in the biogeochemical

variability of the upper water column of the North Pacific Subtropical Gyre. *J. Geophys. Res.* **105**: 28723-39.

Longhurst, A., Sathyendranath, S., Platt, T. and Caverhill, C. 1995. An estimate of global primary production in the ocean from satellite radiometer data. *J. Plankton Res.* **17**: 1245-71.

Lukas, R. 2001. Freshening of the upper thermocline in the North Pacific subtropical gyre associated with decadal changes of rainfall. *Geophys. Res. Lett.* **28**: 3485-3488.

Mackey, M.D., Mackey, D.J., Higgins, H.W. and Wright, S.W. 1996. CHEMTAX- a program for estimating class abundances from chemical markers: application to HPLC measurements of phytoplankton. *Mar. Ecol. Prog. Ser.* **144**: 265-283.

Magnuson, J.J. 1990. Long-Term research and the invisible present. *BioScience* **40**: 495-501.

Mantua, N., Hare, S., Zhang, Y., Wallace, J. and Francis, R. 1997. A Pacific interdecadal climate oscillation with impacts on salmon production. *Bull. Am. Meteorol. Soc.* **78**: 1069-79.

Maranon, E., Behrenfeld, M. J., Gonzalez, N., Mourino, B. and Zubkov, M. V. 2003. High variability of primary production in oligotrophic waters of the Atlantic Ocean: uncoupling from phytoplankton biomass and size structure. *Mar. Ecol. Prog. Ser.* **257**: 1-11.

Martin, J. H., Knauer, G. A., Karl, D. M. and Broenkow, W. W. 1987. VERTEX: carbon cycling in the northeast Pacific. *Deep-Sea Res. I* **34**: 267-285.

McPhaden, M.J. and Zhang, D. 2004. Pacific Ocean circulation rebounds. *Geophys. Res. Lett.* **31**: 18301-5.

Moore, L. R., Goericke, R. and Chisholm, S. W. 1995. Comparative physiology of *Synechococcus* and *Prochlorococcus*: influence of light and temperature on growth, pigments, fluorescence, and absorptive properties. *Mar. Ecol. Prog. Ser.* **116:** 259-275

Moore, L. R., Post, A. F., Rocap, G., and Chisholm, S. W. 2002. Utilization of different nitrogen sources by the marine cyanobacteria, *Prochlorococcus* and *Synechococcus*. *Limnol. Oceanogr.* **47**: 989-96.

Ropelewski, C.F., and M.S. Halpert, 1987: Global and regional scale precipitation patterns associated with the El Niño/Southern Oscillation. Mon. Wea. Rev., 115, 1606-1626.

Ropelewski, C.F., and M.S. Halpert, 1996: Quantifying Southern Oscillation-precipitation relationships. J. Climate, 9, 1043-1959.

Sakamoto, C., Karl, D. M., Jannasch, H.W., Bidigare, R. R., Letelier, R. M., Walz, P. M., Ryan, J. R., Polito, P. S. and Johnson, K. S. 2004. Influence of Rossby waves on nutrient dynamics ad the plankton community structure in the North Pacific subtropical gyre. *J. Geophys. Res.* **109**: 5032-44.

Venrick, E. L., McGowan, J. A., Cayan, D. R. and Hayward, T. L. 1987. Climate and chlorophyll *a* : Long-term trends in the Central North Pacific Ocean. *Science* **4823**: 70-72.

Wilson, C. 2003. Late summer chlorophyll blooms in the oligotrophic North Pacific Subtropical Gyre. *Geophys. Res. Lett.* **30**: 1942-46

Wolter, K., and Timlin, M. S. 1998: Measuring the strength of ENSO - how does 1997/98 rank? *Weather* **53**: 315-24.

Table 2.1. Ecosystem variations at Sta. ALOHA during periods characterized by different ENSO and PDO variations, as defined in the text. Values represent the mean and 1 SD for each period. Units are mol C $m^{-2}$ $d^{-1}$ for PP, mol C mol Chl $a^{-1}$ $d^{-1}$ for PP/Chl *a*, mol C mol quanta $^{-1}$ for PP/Light, $10^{11}$ cells $m^{-2}$ for flow cytometric measurements, μmol $m^{-2}$ for N+N and SRP, mol C $m^{-2}$ $day^{-1}$ for particulate flux, mol:mol for particulate ratio (e.g. PC:PN,…), m for MLD (*i* and *ii* refer to the 0.125 surface offset and 0.005 slope difference in $\sigma_\theta$, respectively, as defined in the text), º C for temperature and rad/s for $N^2$ (Brunt-Väisälä frequency). For each variable, common letters (i.e. a, b,…) next to values indicate no statistically significant difference between values (ANOVA and t-test, $p<0.005$).

| | 1989-1990 | 1991-1994 | 1995-1996 | 1997-1998 | 1999-2004 |
|---|---|---|---|---|---|
| PP | 0.033 ± 0.004 [a] | 0.041 ± 0.001 [b] | 0.041 ± 0.003 [b] | 0.042 ± 0.002 [b] | 0.052 ± 0.002 [c] |
| PP/Chl *a* | 0.0021 ± 0.001 [a] | 0.0023 ± 0.005 [a] | 0.0022 ± 0.006 [a] | 0.0022 ± 0.001 [a] | 0.0023 ± 0.003 [a] |
| PP/Light | 0.020 [a] | 0.022 [b] | 0.025 [c] | 0.023 [b] | 0.027 [c] |
| $PP_{0\text{-}45m}$ | 0.015 ± 0.001 [a] | 0.022 ± 0.001 [b, c] | 0.025 ± 0.001 [c] | 0.021 ± 0.001 [b] | 0.024 ± 0.001 [c] |
| $PP_{75\text{-}125m}$ | 0.0072 ± 0.0006 [a] | 0.0065 ± 0.0005 [a] | 0.0061 ± 0.0007 [a] | 0.0077 ± 0.0006 [b] | 0.0082 ± 0.0003 [b] |
| PP Winter | 0.026 ± 0.002 [a] | 0.036 ± 0.002 [b] | 0.036 ± 0.001 [b] | 0.044 ± 0.003 [c] | 0.049 ± 0.004 [c] |
| PP Spring | 0.036 ± 0.002 [a] | 0.054 ± 0.005 [b] | 0.050 ± 0.006 [b] | 0.045 ± 0.005 [b] | 0.0050 ± 0.002 [b] |
| PP Summer | 0.030 ± 0.005 [a] | 0.042 ± 0.002 [b] | 0.043 ± 0.002 [b] | 0.045 ± 0.004 [b] | 0.058 ± 0.004 [c] |
| PP Fall | 0.033 ± 0.001 [a] | 0.043 ± 0.001 [b] | 0.029 ± 0.004 [a] | 0.037 ± 0.004 [a] | 0.045 ± 0.002 [b] |
| *Prochlorococcus* spp. $_{0\text{-}45m}$ | n/a | 74 ± 3 [a] | 104 ± 4 [b] | 96 ± 5 [c] | 55 ± 4 [d] |
| *Synechococcus* $spp._{0\text{-}45m}$ | n/a | 0.66 ± 0.01 [a] | 0.84 ± 0.08 [b] | 0.94 ± 0.1 [b] | 0.81 ± 0.1 [b] |
| Picoeukaryotes $_{0\text{-}45m}$ | n/a | 0.24 ± 0.03 [a] | 0.31 ± 0.04 [b] | 0.44 ± 0.07 [c] | 0.48 ± 0.03 [c] |
| *Prochlorococcus* spp. $_{75\text{-}125m}$ | n/a | 57 ± 4 [a] | 77 ± 8 [b] | 72 ± 6 [b] | 60 ± 3 [a] |
| *Synechococcus* spp. $_{75\text{-}125m}$ | n/a | 0.47 ± 0.07 [a] | 0.68 ± 0.11 [b] | 0.59 ± 0.07 [a, b] | 0.56 ± 0.05 [a, b] |
| Picoeukaryotes $_{75\text{-}125m}$ | n/a | 0.46 ± 0.05 [a] | 0.42 ± 0.10 [a] | 0.61 ± 0.05 [b] | 0.54 ± 0.03 [b] |
| N+N $_{0\text{-}45\ m}$ | 475 ± 274 [a] | 127 ± 19 [b] | 110 ± 23 [b] | 40 ± 6 [c] | 70 ± 12 [d] |
| SRP $_{0\text{-}45\ m}$ | 4039 ± 430 [a] | 2820 ± 284 [b] | 3010 ± 440 [b] | 1650 ± 180 [c] | 2170 ± 150 [d] |
| N+N $_{75\text{-}125\ m}$ | 3547 ± 360 [a] | 3880 ± 890 [a] | 5416 ± 200 [b] | 5366 ± 190 [b] | 5972 ± 140 [c] |
| SRP $_{75\text{-}125\ m}$ | 4293 ± 470 [a] | 3707 ± 310 [a] | 3850 ± 510 [a] | 2970 ± 400 [b] | 2830 ± 180 [b] |
| Particulate C flux | 0.0040 ± 0.0002 [a] | 0.0030 ± 0.0002 [b] | 0.0025 ± 0.0001 [c] | 0.0030 ± 0.0001 [b] | 0.0028± 0.0001 [b, c] |
| PC: PN | 8.0 ± 0.1 [a] | 8.1 ± 0.2 [a] | 8.7 ± 0.2 [b] | 8.3 ± 0.3 [a] | 7.6 ± 0.2 [c] |
| PC: PP | 197 ± 9 [a] | 167 ± 5 [b] | 206 ± 11 [a] | 215 ± 6 [a] | 227 ± 5 [c] |
| PN: PP | 24 ± 1 [a] | 20 ± 1 [b] | 23 ± 2 [a] | 25 ± 1 [a] | 30 ± 1 [c] |
| MLD (*i*), (*ii*) | 55 ± 7 [a], 34 ± 5 [a] | 50 ± 3 [b], 28 ± 2 [b] | 50 ± 2 [b], 30 ± 2 [b] | 56 ± 4 [a], 35 ± 5 [a] | 66 ± 3 [c], 36 ± 2 [a] |
| Temperature | 24.8 ± 0.2 [a] | 24.8 ± 0.2 [a] | 25.2 ± 0.3 [b] | 24.5 ± 0.2 [c] | 24.8 ± 0.2 [a] |
| $N^2$ | 0.0351 [a] | 0.0426 [b] | 0.0525 [c] | 0.0282 [d] | 0.0294 [d] |

Table 2..2. Conceptualized ecosystem behavior in the NPSG relative to large-scale climate forcing. Each condition is defined according to (i) the status of the ENSO index (negative, positive (0-1), and very positive (1-3)) and (ii) statistical correlation between ENSO and PDO during the period considered). ‘Normal’ condition’ refers to negative ENSO, not significantly correlated to the PDO index. ‘ENSO condition’ occurs when the ENSO is positive or very positive, but not significantly correlated with the PDO (the first ENSO event during 1991-1994). Finally, the ‘ENSO and PDO condition’ indicates a very positive ENSO significantly correlated with the PDO (the second ENSO event during 1997-1998).

| | **'Normal' condition *** | **ENSO condition*** | **ENSO and PDO condition** |
|---|---|---|---|
| MLD | Variable MLD | Shallow MLD | Variable and Deep MLD |
| SST | Warm | Warm | Cooler |
| Main Nutrient | -Ammonium | -Ammonium | -Ammonium |
| | -Recycled Nutrients | -$N_2$-Fixation | -Deep new nutrients |
| Primary Production | -Moderate | -Periods of high production | -Low then high and sustained |
| | - $NH_4$ based production | -$N_2$ based new production | -$NO_3$ based new production |
| Export production | Moderate | Low or High (blooms) | High |
| Community shift | *Prochlorococcus* spp. | *Trichodesmium* spp., *Richelia intracellularis* | Picoeukaryotes, prymnesiophytes |

* Adapted from Karl *et al.* (1995)

## 2.8 Figure Legend

Figure 2.1 Temporal variations in physical properties in the NPSG during 1989-2004, as indicated by (a) the ENSO and PDO anomalies, (b) the SSH monthly average anomaly (i.e. z-score as defined in the text) between Hilo and Honolulu, (c) the monthly anomaly of the mixed layer depth (MLD) at Sta. ALOHA, the monthly anomaly of the mean potential density ($\sigma_\theta$) difference between (d) the MLD+ 20m layer and the mixed layer, and (e) the MLD+ 20m layer and the 140-160 m layer at Sta. ALOHA. The red line in panels b, c, d and e represents the 3-point running average. The temporal boundaries for the five periods used in the statistical analysis (based on different ENSO and PDO variations, as defined in the text) are also shown (vertical black lines in panel a).

Figure 2.2. Temporal variations in mixed layer density anomaly (seasonal cycle removed) with the mixed layer temperature and salinity anomalies scaled by their contributions to density at Sta. ALOHA during 1989-2004.

Figure 2.3. Temporal and vertical variations in the buoyancy frequency (low-pass filtered) at Sta. ALOHA during 1989-2004. Buoyancy frequency units are in cycle hour$^{-1}$ (cph). The black line represents the depth where potential temperature is 0.5° C less than the surface, while the white line represents the depth where $\sigma_\theta$ is 0.125 kg m$^{-3}$ heavier than the surface (i.e. the equivalent density difference if salinity is held constant).

Figure 2.4. Seasonal variations in MLD (based on 0.125 kg $m^{-3}$ surface offset in $\sigma_\theta$) anomaly at Sta. ALOHA during 1989-2004. (a) Winter variations include December through February, (b) spring refers to March through May, (c) summer is June through August and (d) fall is September through November.

Figure 2.5. Temporal variations for (a) salinity, (b) temperature and (c) surface PAR anomaly in near-surface waters at Sta. ALOHA. The salinity and temperature records are from 5 m depth at Sta. ALOHA, while the light is the sea surface PAR measured by a Licor meter on deck. The red line in each panel represents the 3-point running average.

Figure 2.6. Temporal and vertical variability in salinity in the upper water column (surface to 200m) at Sta. ALOHA during the 1989-2004 period. Salinity units are in practical salinity units (psu).

Figure 2.7. Temporal variations in nitrogen (N+N) and phosphorous (SRP) concentrations in the upper (0-45 m) (a and b, respectively) and lower (75-125 m) (c and d, respectively) euphotic zone at Sta. ALOHA. The red line in each panel represents the 3-point running average.

Figure 2.8. Temporal variations in integrated (a) $PP_{0\text{-}125m}$, (b) PP/Chl *a* and (c) PP/Light (c) anomaly at Sta. ALOHA during 1989-2004. The PP/Chl *a* was

calculated as depth integrated (0-125 m) PP and Chl *a*, respectively. The PP/Light was calculated based on PP at 5m depth and surface PAR flux with adjustments for seasonally dependent changes in light extinction coefficients.

Figure 2.9. Temporal variations in PP anomaly at Sta. ALOHA during 1989-2004 in (a) the surface to 125 m layer, (b) the upper and (c) lower euphotic zone. Similar colors indicate the same observation period characterized by different ENSO and PDO variations, as defined in the text.

Figure 2.10. Seasonal anomaly variations in PP at Sta. ALOHA during 1989-2004. Seasonal groupings are the same as for Fig. 4.

Figure 2.11. Temporal variations in major photoautotrophs concentrations anomaly at Sta. ALOHA during 1989-2004, based on flow cytometric measurements. Temporal variations for *Prochlorococccus* spp., *Synechococcus* spp. and picoeukaryotes are shown for the upper (a,c,e) and lower (b,d,f) euphotic zone, respectively. The red line in each panel represents the 3-point running average.

Figure 2.12. Temporal variations in selected pigment concentrations at Sta. ALOHA during 1989-2004, based on HPLC determination. Pigment concentrations for Chl *b*, 19′-Hex and zeaxanthin are shown for the upper (a,c,e) and lower (b,d,f) euphotic zone, respectively. The red line in each panel represents the 3-point running average.

Figure 2.1

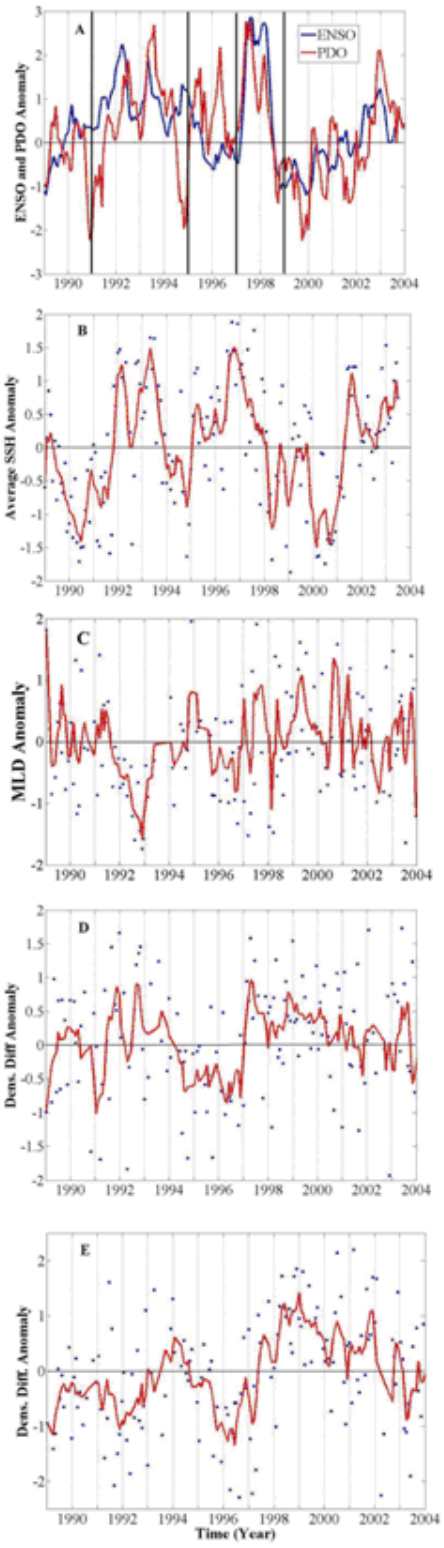
A
ENSO
PDO
ENSO and PDO Anomaly
B
Average SSH Anomaly
C
MLD Anomaly
D
Dens. Diff Anomaly
E
Dens. Diff. Anomaly
1990 1992 1994 1996 1998 2000 2002 2004
Time (Year)

Figure 2.2

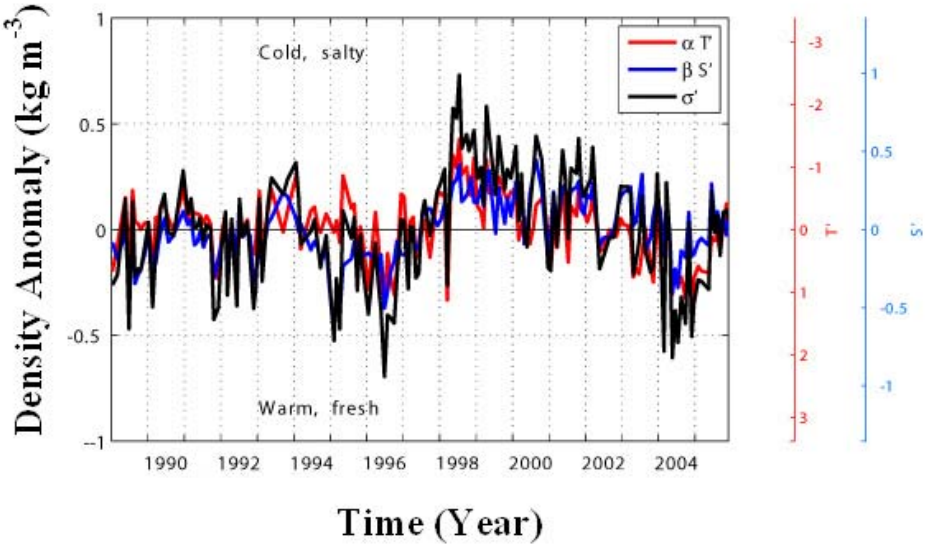
Density Anomaly (kg m-3)
Cold, salty
Warm, fresh
α T'
β S'
σ'
T'
S'
Time (Year)
1990
1992
1994
1996
1998
2000
2002
2004

Figure 2.3

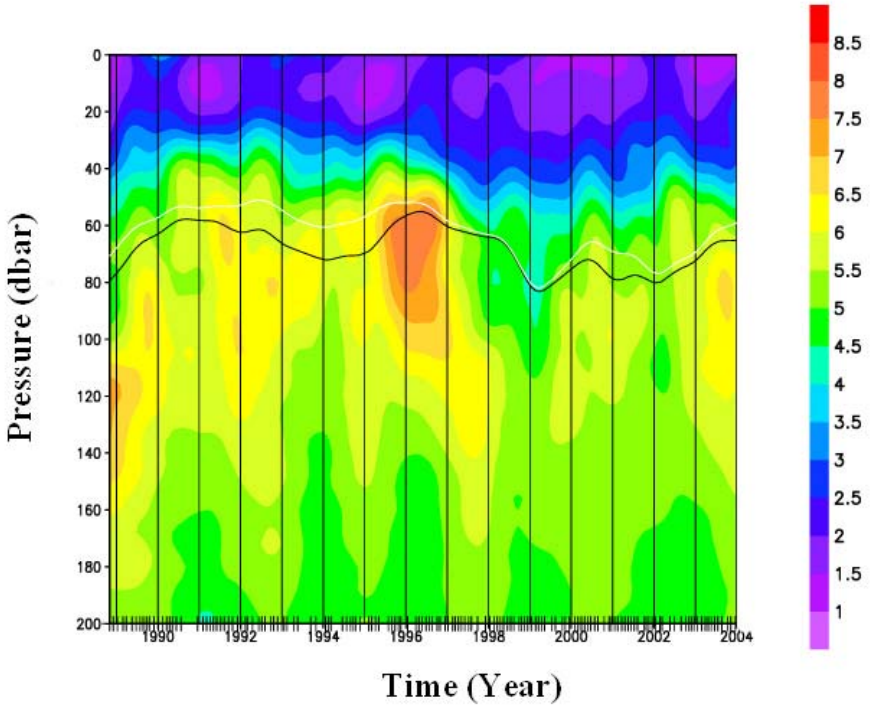
Pressure (dbar)
0
20
40
60
80
100
120
140
160
180
200
1990
1992
1994
1996
1998
2000
2002
2004
Time (Year)
8.5
8
7.5
7
6.5
6
5.5
5
4.5
4
3.5
3
2.5
2
1.5
1

Figure 2.4

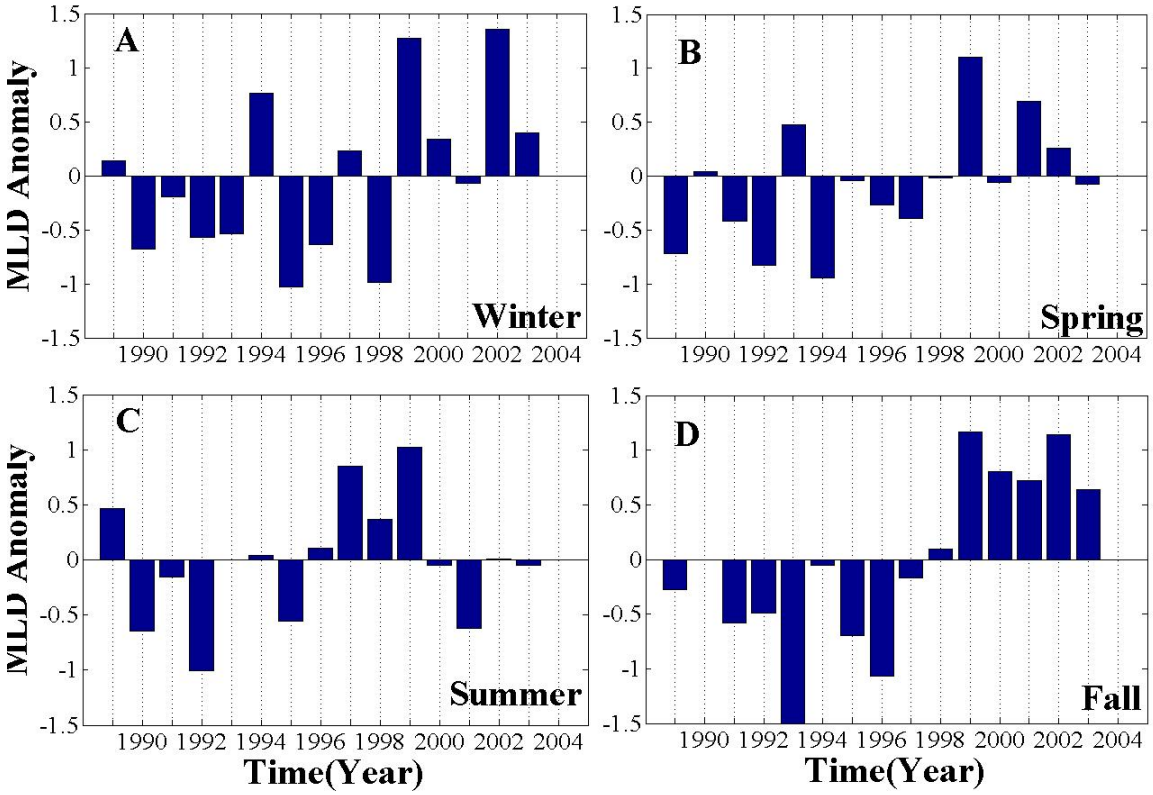
A
B
C
D
Winter
Spring
Summer
Fall
MLD Anomaly
MLD Anomaly
Time(Year)
Time(Year)
1.5
1
0.5
0
-0.5
-1
-1.5
1990 1992 1994 1996 1998 2000 2002 2004

Figure 2.5

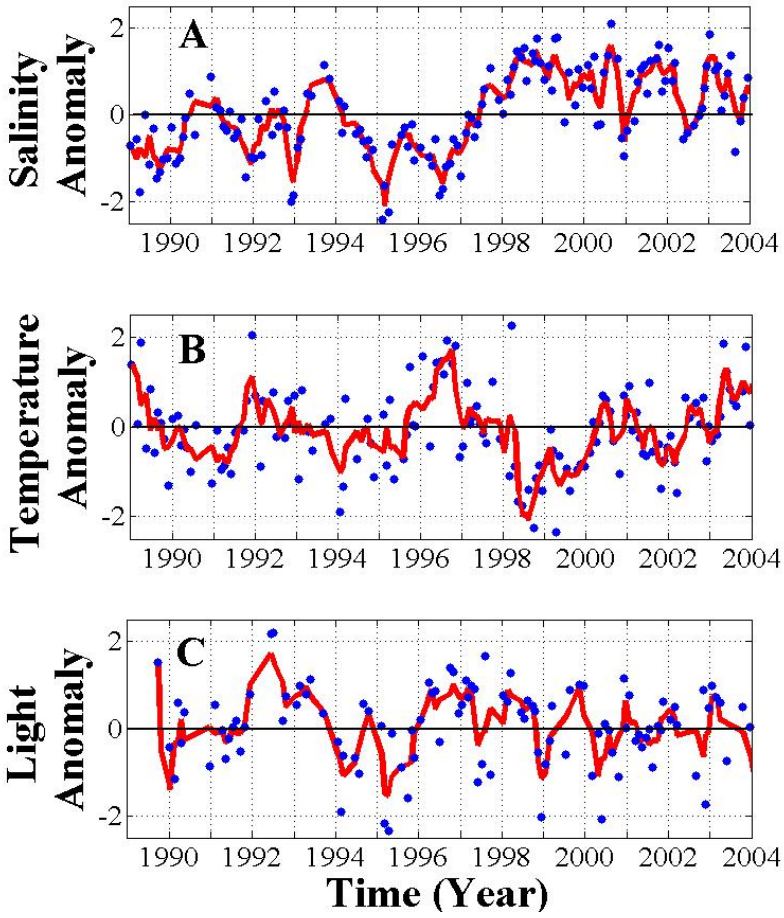
A
Salinity Anomaly
2
0
-2
1990 1992 1994 1996 1998 2000 2002 2004
B
Temperature Anomaly
2
0
-2
1990 1992 1994 1996 1998 2000 2002 2004
C
Light Anomaly
2
0
-2
1990 1992 1994 1996 1998 2000 2002 2004
Time (Year)

Figure 2.6

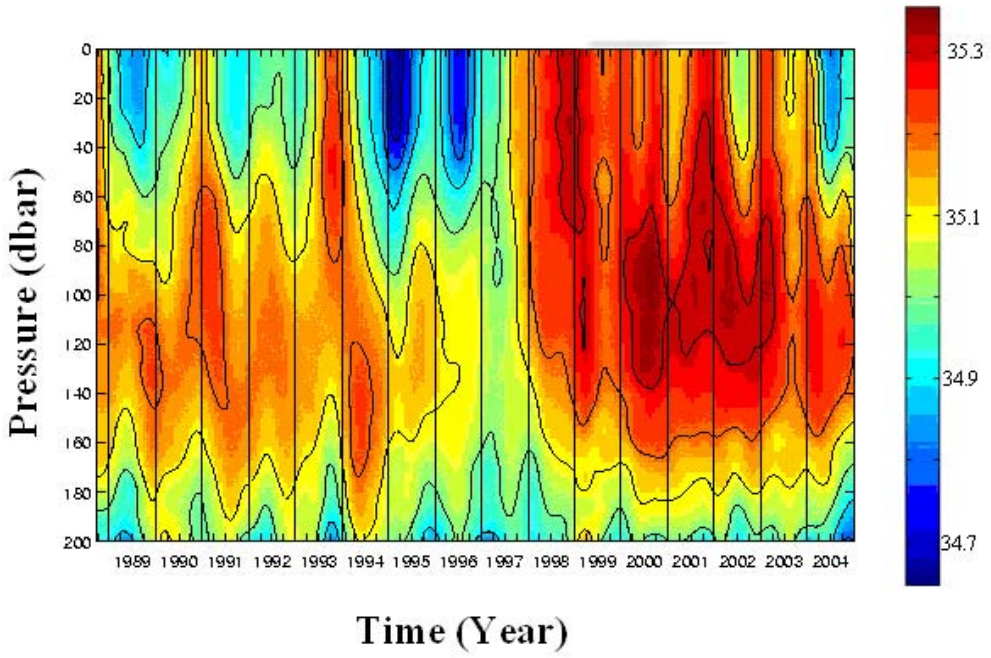
Pressure (dbar)
0
20
40
60
80
100
120
140
160
180
200
1989 1990 1991 1992 1993 1994 1995 1996 1997 1998 1999 2000 2001 2002 2003 2004
Time (Year)
35.3
35.1
34.9
34.7

Figure 2.7

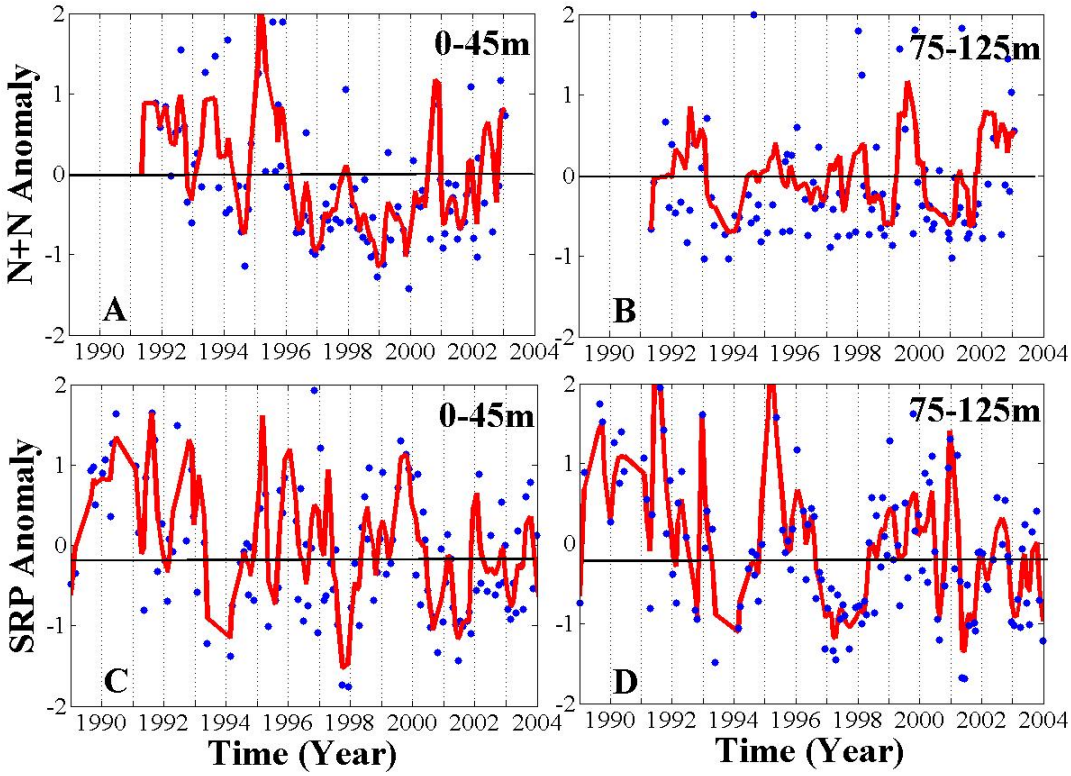

Figure 2.8

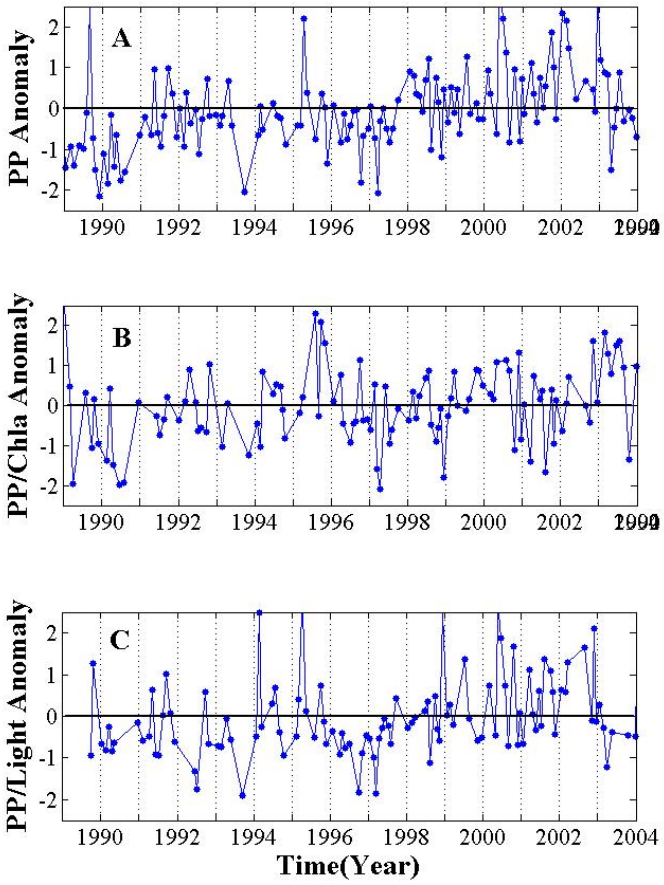
A
PP Anomaly
B
PP/Chla Anomaly
C
PP/Light Anomaly
2
1
0
-1
-2
1990
1992
1994
1996
1998
2000
2002
2004
Time(Year)

Figure 2.9

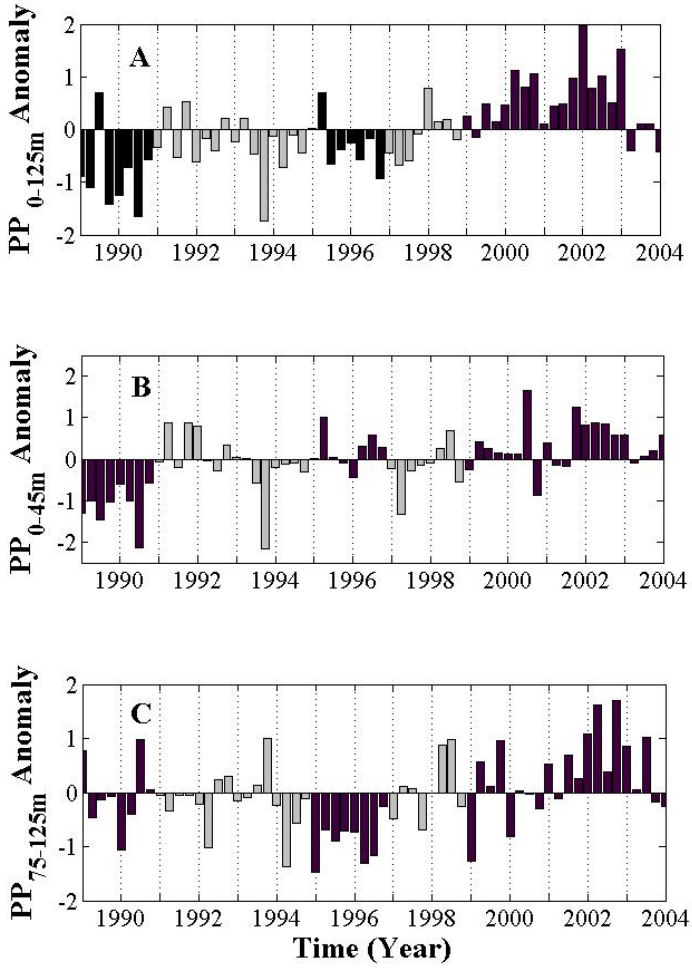
A
B
C
PP 0-125m Anomaly
PP 0-45m Anomaly
PP 75-125m Anomaly
2
1
0
-1
-2
1990
1992
1994
1996
1998
2000
2002
2004
Time (Year)

Figure 2.10

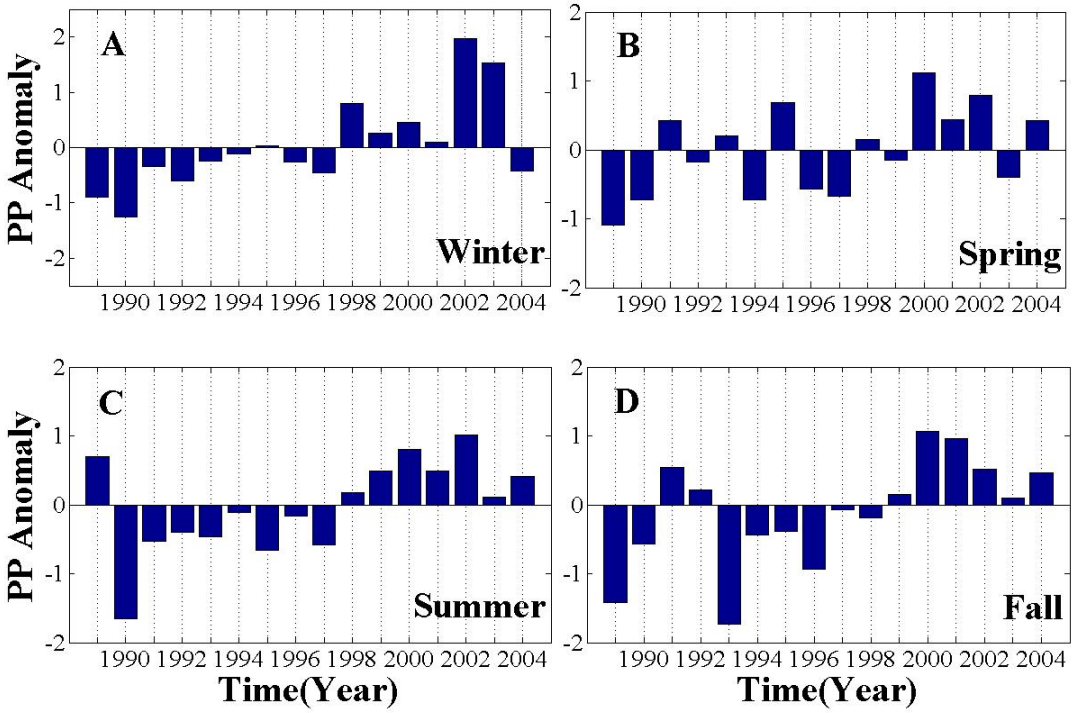
A
B
C
D
Winter
Spring
Summer
Fall
PP Anomaly
PP Anomaly
2
1
0
-1
-2
1990 1992 1994 1996 1998 2000 2002 2004
Time(Year)
Time(Year)

Figure 2.11

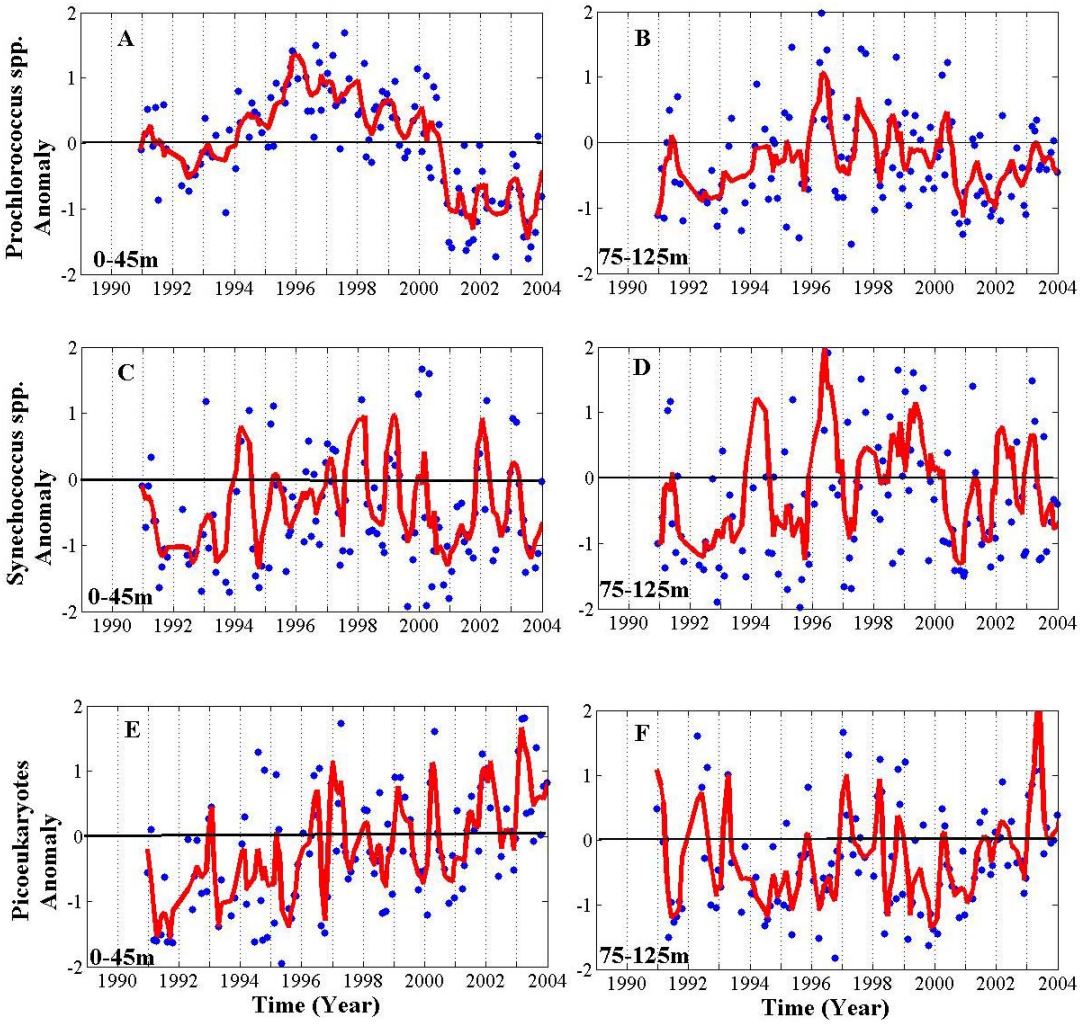
A
B
C
D
E
F
0-45m
75-125m
Prochlorococcus spp. Anomaly
Synechococcus spp. Anomaly
Picoeukaryotes Anomaly
Time (Year)
1990
1992
1994
1996
1998
2000
2002
2004
2
1
0
-1
-2

Figure 2.12

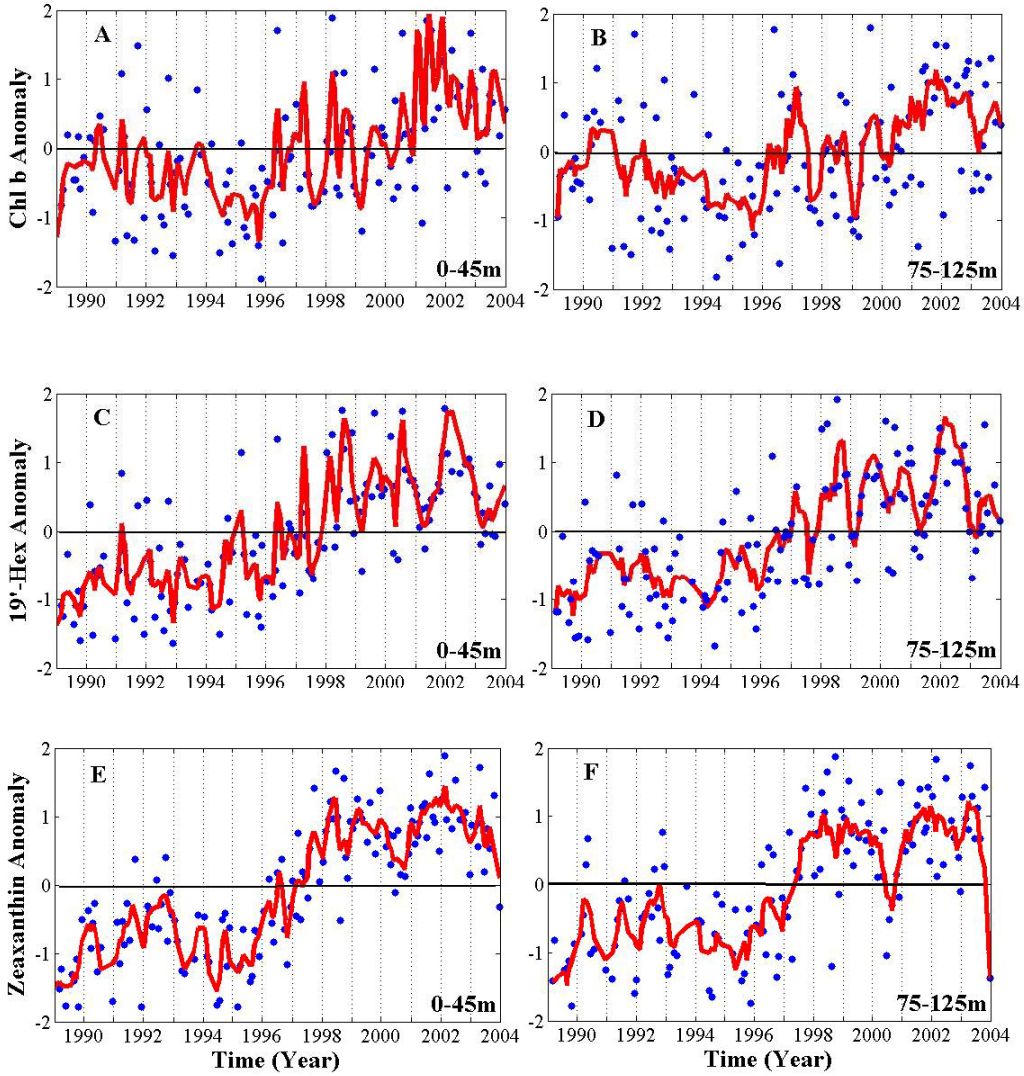
A
B
C
D
E
F
0-45m
75-125m
Chl b Anomaly
19'-Hex Anomaly
Zeaxanthin Anomaly
Time (Year)
Time (Year)
1990 1992 1994 1996 1998 2000 2002 2004
-2 -1 0 1 2

# 3. Assessing primary production variability in the North Pacific Subtropical Gyre: A comparison of Fast Repetition Rate Fluorometry and $^{14}C$ measurements

Guido Corno , Ricardo M. Letelier, Mark R. Abbott and David M. Karl

Issue manuscrispt appears in *Journal of Phycology* 42: 51-60

## 3.1 Abstract

*In situ* $^{14}C$ uptake (dawn to dusk) and Fast Repetition Rate Fluorometry (FRRF) measurements at nearly monthly intervals were compared at Station ALOHA (22º 45' N, 158º 00' W) between August 2002 and September 2003 in order to determine the feasibility of using FRRF profiling as a means for estimating primary productivity (PP). The FRRF and $^{14}C$ rates were significantly correlated ($r^2$= 0.906, *p*-value < 0.05, *n*= 70) with slopes of 2.00 and 1.90 for chl *a* and light normalized data, respectively. However, the relationship between $^{14}C$ and FRRF derived carbon fixation varied vertically and temporally. The FRRF: $^{14}C$ ratio was > 1.5 in near surface water (5-25 m depth) and approached 1.0 deeper in the euphotic zone. Vertical variations probably reflected the effect of different physiological processes (i.e. Mehler reaction, dark respiration and excretion) on overall photoautotrophic respiration. In particular, the decrease in Mehler reaction rates with increasing water depth, may have accounted for the decrease in difference between $^{14}C$ and FRRF measurements with depth. The influence of *in situ* light field variability in controlling the absorption cross section of PSII ($\sigma_{PSII}'$) may also have been responsible for some of this difference. When compared to total community respiration (R), derived light-driven photoautotrophic respiration (reported here as the difference between FRRF and $^{14}C$ measurements) represented approximately 50% of R integrated over the euphotic zone. Our results show that FRRF and $^{14}C$ measurements were well correlated in oligotrophic waters but the exact relationship between the two processes varies both temporally and vertically, such that a unique relationship between these two techniques could not be derived from first-order principles.

## 3.2 Introduction

Fine vertical scale (~ 1 m) measurements of oceanic primary productivity (PP) are important as they can provide insights on possible "hot spots" in the water column (Cowles et al. 1998, Azam and Long 2001), with physiological and ecological consequences for both lower and higher trophic levels (Baines and Pace 1991, Carlson et al. 1994, Caron et al. 1999, Landry 2000). In the last decade, *in situ* active fluorescence techniques have provided a method to determine PP across fine vertical (cm to m) and temporal (minutes to days) scales (Kolber et al. 1998). Fast Repetition Rate Fluorometry (FRRF) represents an appealing technique because it is non-invasive, reports results in real-time and allows for the measurement of *in situ* photoautotrophic activity and the derivation of PP across spatial and temporal scales not achievable with other *in situ* techniques which require sample incubation or integration over larger time scale (i.e. $^{14}C$ uptake, $O_2$ evolution and fluxes, pH changes). Even though the method relies on several assumptions (e.g. fixed number of reaction centers for different species, and theoretical maximum ratio of functional reaction centers), some of which can introduce potential errors (Suggett et al. 2004), FRRF has proven to be a promising technique for deriving PP, as it targets electron transport rates between PSII and PSI, providing an estimate of the total energy flow derive through photosynthesis.

Major questions still remain on how FRRF results can be translated into photoautotrophic carbon fixation rates. Comparisons between *in situ* incubations and FRRF measurements are therefore needed in order to resolve some of these

uncertainties, to assess the feasibility of FRRF for determining vertical scales of PP, and possibly to improve estimates of oceanic PP. The only published comparisons between these two techniques (Suggett et al. 2001, Moore et al. 2003, Raateoja et al. 2004, Smyth et al. 2004) have found significant correlations between FRRF and $^{14}C$ measurements of PP, even though the slopes of the linear relationship are significantly different than one, suggesting possible discrepancies in PP estimated by the two techniques. These comparisons have been restricted to single cruises in highly productive regions (i.e. English Channel tidal front, Celtic Sea, Finnish coastal zone and cyanobacterial blooms). Additional field comparisons between other fluorescence-based PP estimates (i.e. Pump and Probe) and $^{14}C$ have also found significant relationships, but with slopes closer to 1 (Kolber and Falkowski 1993, Boyd et al. 1997).

All these comparisons were normalized to chl *a* concentrations, as a proxy for photoautotrophic biomass, in order to exclude the effect of biomass in the relationship. However, they were not normalized to photon flux, which represents a significant factor in controlling photosynthetic rates in the euphotic zone. Both normalizations could help explain which physical and physiological processes account for potential discrepancies between methods. However, from a practical perspective, such normalizations are not needed when the goal is to assess the reliability of FRRF in estimating water column PP.

To date there has been no published comparison between FRRF and $^{14}C$ derived PP in the oligotrophic ocean, despite the global significance of these regions (Karl 1999). Here, we report the results of the first comparison between $^{14}C$ uptake

and FRRF techniques for the North Pacific Subtropical Gyre (NPSG) over the course of a full year. In this study region, PP derived from $^{14}C$ uptake measurements during the Hawaii Ocean Time-series (HOT) program (1988-present) has been shown to vary significantly across different temporal and vertical scales (Letelier et al. 1996, Karl et al. 2001, Karl 2002). However, sampling has been limited in time (one day per month) and in space (fixed depths). This discrete sampling approach may bias the characterization of the variability in space and time (Karl 1999). By comparing $^{14}C$ uptake and FRRF at HOT, we sought to complete a detailed analysis of the relationship between these two techniques. If FRRF methodology is used to estimate carbon fixation, we need to assess carefully the spatial and temporal relation between FRRF and $^{14}C$ or $O_2$ derived productivity rates.

### 3.3 Materials and Methods

In situ *FRRF and the $^{14}C$ uptake method measurements. In situ* FRRF measurements were obtained at Station ALOHA (22º 45' N, 158º 00' W) between August 2002 and August 2003 during 12 cruises, as part of the ongoing HOT Bio-optical component. A FAST-TRACKA (Chelsea Instruments S/N 182047) FRR fluorometer with dual 'Light' and 'Dark' chambers (defined by 'L' and 'D') was used to measure active fluorescence. From the L and D chambers, measurements of minimal and maximal fluorescence ($F_O$ and $F_M$, respectively), and a value termed the variable fluorescence ($F_V$), defined as the quantity [$F_M$-$F_O$], were obtained. The maximum change in the quantum yield of fluorescence (i.e. the efficiency of photosystem II (PSII), $F_V/F_M = (F_M - F_O)/ F_M$), the effective absorption cross-section for

PSII, $\sigma_{PSII}$, and the minimum turnover time of electron transfer between reaction centers, ($\tau$), were also derived. A list of bio-optical terminology is given in Table 3.1.

The FRRF was an integral component of an instrument package that also included a Seabird CTD and a WetLabs ac-9. The instrument was oriented horizontally (with light chamber facing upward). A grooved sun-block, designed to prevent ambient sunlight from degrading the quality of near-surface fluorescence response in the L chambers, was mounted facing the emission window of the FRRF light chamber. The package was lowered at a constant speed of 10 m•min$^{-1}$ to a final depth of approximately 250 m. This speed was empirically determined to: (i) best resolve the fluorescence response of small scale (~ 0.5 m) variations in photoautotrophic assemblages and (ii) allow enough time for the instrument to switch gains without losing significant vertical resolution. Depth (dbar) and in situ irradiance (PAR, μmol photons•m$^{-2}$ •s$^{-1}$) were logged with each profile.

For each cruise, three profiles were obtained, two around noon and one during the night. The rationale behind this sampling strategy was to obtain physiological measurements of light-adapted cells, an estimation of photochemical and non-photochemical quenching, a precise assessment of $F_V/F_M$ and $\sigma_{PSII}$ (night samples by excluding photochemical quenching effects on the fluorescence yield), as well as the variability in these parameters between night and day.

*In situ* $^{14}C$ uptake measurements were conducted during the diurnal FRRF casts. A full description of the $^{14}C$ uptake method applied is given elsewhere (Karl et al. 1998). Briefly, water samples were collected from six depths (5, 25, 45, 75, 100,

and 125 m) and were sub-sampled directly into clean 500-mL polycarbonate bottles. Typically, three separate 500-mL polycarbonate bottles were prepared from each depth, for incubation in the light. Each bottle was spiked with $H^{14}CO_{3-}$ to yield a final radioactivity of approximately 1.9-3.7 MBq•$L^{-1}$ and deployed from dawn to dusk while attached to a free-drifting array. Following *in situ* incubations, the entire contents of each bottle was filtered onto a 25-mm-diameter Whatman glass fiber (Whatman-GF/F, Boston, MA, USA) filter, and each filter was placed into a glass vial for subsequent measurement of $^{14}C$ incorporation into particulate matter. The sample vials were stored for 2-3 days at -20º C until processed at the land laboratories. After acidification and venting to remove excess $^{14}C\text{-}HCO_3^-$ , 10 mL of Aquasol-II (New England Nuclear, Boston, MA, USA) was added and the samples were counted immediately and again after approximately 30 days. The final (30 day) $^{14}C$ activity was used in all primary productivity calculations.

*Data processing.* Data were downloaded from the FRRF in binary format and analyzed using the FRS software provided by Chelsea instrumentation. A comparison, using a sub-sample of the full data set, between the FRS software and the V6 (Laney 2003) was done to determine the potential errors in estimating FRRF parameters using the FRS software. Differences in the derived $F_O$, $F_M$ and $\sigma_{PSII}$ using both software were not significant. The nocturnal raw data were quality controlled by subtracting the mean + 1 SD of the blank for $F_O$, $F_M$ and $\sigma_{PSII.}$ Filtered seawater (0.2 μm) from 250 m was chosen as a blank, based on signal comparisons with deep-water

samples (Corno unpublished data). The ratio $F_V/F_M$ was then recalculated using $F_O$ and $F_M$ values obtained after blank subtraction.

*FRRF- derived carbon fixation. In situ,* electron transport rates ($ETR^{Chl}$) and volumetric gross oxygen evolution (GOE) rates were derived from FRRF measurements. $ETR^{Chl}$ and GOE were calculated using the following equations (Kober et al. 2000, Kolber and Falkowski 1993), respectively:

$$ETR^{Chl}(z) = E(z)\ \sigma_{PSII}'(z)\ qP(z)\ n_{PSII}\ (F_V/F_M(z)/0.65) \quad \text{(Eq. 1)}$$

$$GOE(z) = 2.0256 \times 10^{-8}\ E(z)\ qP(z)\ F_V/F_M(z)\ \sigma_{PSII}'(z)\ [\text{chl } a](z)\ \Phi_e\ n_{PSII} \quad \text{(Eq.2)}$$

The constant $2.0256 \times 10^{-8}$ includes the following conversions: $10^{20}$ photons•$m^{-2}$, 3600 s•$h^{-1}$, $6.023 \cdot 10^{23}$ molecules•$mol^{-1}$, and 892 g chl *a*•$mol^{-1}$. It also assumes that four photons are delivered to reaction centers (RCII) per $O_2$ molecule evolved, that the maximum value of $F_V/F_M(z)$ equals 0.65, and that photosynthetic unit size is 300 chl *a*•$RCII^{-1}$ for this particular oceanic environment (characteristic of prokaryotes, Falkowski et al. 1981). The *in situ* light at depth z, E(z), was obtained from daily-integrated surface light value from the ship's LI-COR sensor and calculated using the appropriate extinction coefficient (0.039 and 0.044 for summer and winter, respectively; Letelier et al. 2004) . These light values were chosen (i) to approximate the light conditions experienced by *in situ* $^{14}C$ measurements and (ii) to minimize a source of variability between the $^{14}C$ and FRRF comparison estimates. The chl *a* concentrations were computed from $F_M$, after a significant (Least squares model II regression, $r^2 = 0.77$, $n = 95$, $p$-value$<0.05$) regression was obtained between

$F_M$ and discrete chl *a* samples collected as part of HOT core program. The photon yield of electron transfer by PSII is $\Phi_e$.

The carbon fixation estimates from FRRF (FRRF-PP) were then obtained considering a photosynthetic quotient (PQ) of 1.1 for growth on ammonium (Laws 1991), characteristics of more than 90% of our samples:

$$\text{FRRF-PP}(z) = \text{GOE}(z) / \text{PQ} \quad \text{(Eq.3)}$$

In order to compare discrete depth samples of $^{14}C$ measurements with continuous FRRF measurements, FRRF measurements from an interval of 1 m around the same discrete depth of $^{14}C$ were considered. Volumetric PP from FRRF and $^{14}C$ were then normalized to chl *a* concentrations, in order to remove biomass effect on the regression. Quantum yields for both FRRF and $^{14}C$ were also obtained to remove the light effect from the regression analysis. Finally, PP from both techniques was normalized to chl *a* concentrations and mole quanta to determine differences in the derived biomass normalized photosynthetic quantum yield.

*Data analysis.* Least squares model II linear regression (95% confidence interval) was applied to determine significant (with relative confidence intervals) slope coefficient and y-axis intercept between FRRF (both GOE and PP) and $^{14}C$ measurements. For model II regression, the geometric mean was used to determine significance relationship (McArdle 2003). Analysis of variance (ANOVA) was applied to determine significant differences between the FRRF: $^{14}C$ ratios for the three normalizations by adjusting alpha (Bonferroni corrections) (Miller 1981) for multiple comparisons at different depths.

### 3.4 Results

The FRRF-GOE and $^{14}C$ rate estimates were significantly correlated ($r^2$= 0.906; *p*-value< 0.05, *n*=70) when all data were pooled (Fig. 3.1). The slope was significantly greater than 1 (2.90 ± 0.23) and the intercept was not significantly different from zero (Table 3.2). Considering absolute values, higher scatter and variability were observed at higher PP estimates (Fig. 3.1). The chl *a* normalized data also yielded a significant relationship ($r^2$= 0.946, p-value < 0.05, n= 70), but the slope was lower than that derived from volumetric estimates (slope=2.00, Fig. 3.2 and Table 3.2). Axis intercepts were not significantly different from zero. A further decrease in slope occurred when data were normalized to photon flux (Fig. 3.3). Significant regressions ($r^2$= 0.873, *p*-value < 0.05, *n*= 70) yielded a slope of 1.90 ± 0.17 (Table 3.2). Residuals from chl *a* and light normalized regression were analyzed to determine their dependence on chl *a* and light, respectively, and were found to be randomly distributed.

*Vertical variations in the FRRF:$^{14}C$ ratio.* When FRRF-PP was considered (Eq. 3), the FRRF:$^{14}C$ ratio was higher in near surface waters (5-25 m) than deeper in the water column (Fig. 3.4, *p*-value< 0.05, *n*=36). Mean values from volumetric and chl *a* normalized data displayed similar values. For both these normalizations, ratios were greater than 1.50 at 5 m, significantly decreasing to 1.10 at 45 m (*p*-value< 0.05, *n*=24). From 45 to 125 m, the FRRF:$^{14}C$ relationship from volumetric normalization varied between 1.10 and 1.40 with no particular trend. On the other hand, ratios from

chl *a* normalization significantly increased from 1.10 (45 m) to 1.40 (125 m) (*p*-value< 0.05, *n*=24). For light normalized data, mean values were always greater than or equal to 1.50. The ratio was greater than 2 at 5m, decreasing exponentially to 1.50 at 75 m. Between 75 and 125 m, the FRRF:$^{14}$C relationship increased to a final value of 1.70. The variability in the ratio (indicated by the standard deviation) increased with depth for all normalizations.

*Temporal variations in the FRRF:$^{14}$C ratio.* Temporal (i.e. grouped by seasons, centered on equinoxes and solstices) data analysis showed a seasonal pattern for the FRRF:$^{14}$C ratio, when light normalized data were considered (Fig. 3.5). The ratio gradually increased from 1.50 in winter to 2.10 in fall (significant increase, *p*-value< 0.05, *n*=72). A clear seasonal pattern was not apparent for the other two data normalizations. However, maximum values of the ratio also occurred in fall for both the volumetric and light normalization (1.70 and 1.60, respectively). The ratio variability (indicated by the standard deviation) was not significantly related to any significant seasonal pattern.

**3.5 Discussion**

Our results indicate a statistically significant correlation between FRRF and $^{14}$C estimates of PP in the NPSG. The slope and ratio between FRRF and $^{14}$C was greater than 1.0 for the overall data set. The significant correlation between FRRF and $^{14}$C indicates that these independent methods both track similar PP changes across different levels of productivity and vertical scales. These findings are of

practical significance because they provide an experimental basis for deriving PP from FRRF measurements in oligotrophic oceans. The FRRF can obtain much higher frequency measurement than is possible with the *in vitro* based $^{14}C$ method, and can also be used for unattended remote surveillance.

There are several possible explanations for the divergence between the FRRF and $^{14}C$-based values. First, the quantitative difference between FRRF and $^{14}C$ estimates indicate that a portion of the available energy stored in the form of ATP or NADPH during the photosynthetic light reactions (and approximated by the gross electron flow measured by FRRF) is utilized for metabolic processes other than carbon fixation (i.e. as approximated by $^{14}C$). A great number of metabolic processes utilize of such energy (e.g. secondary metabolites production), nutrition (e.g. nutrient uptake) and reproduction (e.g. DNA replication). These processes will influence the intracellular energy availability, depending on the cell cycle stage and/or particular environmental conditions.

The divergence between FRRF and $^{14}C$ results also possibly reflects the different theoretical basis of these two techniques (i.e. gross electron transfer rate measured by FRRF vs. net carbon incorporation measured by $^{14}C$). For the purpose of this discussion, GPP is defined as the available intracellular energy resulting from photosynthetic light reactions as indicated by the gross electron transport rates between PSI and PSII during the photoperiod. The NPP is considered as the stored intracellular energy in term of net carbon fixation during the photoperiod (and therefore excluding (i) energy storage in terms of N and P, (ii) the energy costs associated with N and P metabolic processes and (iii) nocturnal dark respiration). In

the case of $^{14}C$, some production may be lost to respiration ($^{14}C$-$CO_2$) or excretion ($^{14}C$-DOC); NPP measured by $^{14}C$ will then be a lower estimate of the true NPP. Measurements of DO$^{14}C$ at Sta. ALOHA indicate that this fraction can reach up to 30% of the measured $^{14}C$ particulate incorporation in standard PP experiments (Karl et al. 1998). Incubation time is also critical to understand the relationship to NPP and GPP. Incubation time has been shown, by theoretical (Dring and Jewson 1982) and experimental (Grande et al. 1989) approaches, to approximate net carbon fixation in incubations < 12 h. However, a clear relationship between incubation time and the degree of net carbon fixation measured is yet to be achieved. Laboratory experiments have shown that the measurement of net carbon fixation may also be achieved in incubations < 2 h (Jespersen 1994). Incubation time during this study varied between 10-12 h from dawn to dusk. Thus, we suggest that our $^{14}C$ measurements approximate net carbon fixation. Carbon uptake must be less than the oxygen evolution fluxes, because there are sources of carbon within the cell from mitochondrial respiration (Marra et al. 1988) and also because ATP and NADPH can be utilized by other redox reactions. Such considerations agree with our results, as comparison between FRRF-PP and $^{14}C$ yielded relative large slopes (i.e. > 2). If this interpretation is correct, the $^{14}C$ method will provide an estimate that is closer to net carbon fixation relative to the $O_2$ evolution method (Marra 2002). Uptake of labeled DO$^{14}C$ by heterotrophic bacteria and aerobic anoxygenic photosynthetic (AAnP) microorganisms, respectively, can also add uncertainties to the estimates of photoautotrophic NPP (Kolber et al. 2001). The influence of these organisms on the measured $^{14}C$ activity is

yet to be determined. All these processes preclude a strict interpretation of C uptake estimates derived by $^{14}C$.

Finally, we must also consider the possibility that errors associated in estimating $\sigma_{PSII}'$ can contribute to the observed divergence between both methods. The measured $\sigma_{PSII}'$ was not corrected for variability in the spectral quality of the *in situ* light field (Suggett et al. 2001, Raateoja et al. 2004). In case 2 waters, such corrections can result in an overestimation of the true *in situ* $\sigma_{PSII}'$ up to a factor of 2 (Raateoja et al. 2004); however, this error has yet to be quantified in case I waters, such as those in the NPSG. Other errors associated with the parameterization of FRRF-PP in this specific ecosystem (i.e. fixed number of $n_{PSII}$, PQ and diel variability in photophysiology) have been evaluated to account between 3-15% of the FRRF: $^{14}C$ ratio, which is well below the 2:1 ratio observed. We postulate that FRRF and $^{14}C$ rate measurements at HOT can be used to estimate the variability between GPP and NPP in the NPSG, respectively. Other studies comparing these techniques (Suggett et al. 2001, Moore et al. 2003) have also found slopes greater than 1, suggesting consistent differences in PP estimated by FRRF and $^{14}C$ in different oceanic habitats.

*Differences in ratios for normalized data.* Differences in the FRRF:$^{14}C$ ratio for normalized data can be interpreted both analytically and ecologically. Volumetric and chl *a* comparisons (hereafter, VC and CC, respectively) displayed similar ratios. This similarity indicates that the influence on the FRRF:$^{14}C$ relationship by photoautotrophic biomass (chl *a*) in this region is not significant.

The light-normalized data comparisons (hereafter, LC) show significant differences in the ratio value from both VC and CC in the upper water column (5-45m). As discussed below, this divergence can be explained by photorespiration processes. The similarity between ratios among all normalizations, observed deeper in the water column, suggests that environmental and physiological variables do not significantly influence the FRRF and $^{14}C$ relationship.

*Divergence of energy capture from carbon fixation in the NPSG.* A unique relationship between $^{14}C$ and FRRF rate measurements was not found in this study. The relationship (indicated by the ratio) varied vertically and, to some extent, temporally. Based on information presented above, higher ratios in near surface waters (5-25m) represent an increase in electron transfer rates through PSII, relative to net carbon fixation. This may possibly indicate (i) an increase in GPP relative to NPP, (ii) an increase in photo-autotrophic respiration processes, or (iii) variations in other selected physiological processes responsible for the divergence of intracellular energy from carbon fixation. For example, $N_2$ fixation represents a possible physiological route acting as a sink of ATP and NADPH. This pathway is particularly relevant at Station ALOHA (Karl et al. 1997), where up to 50% of new production is supported by $N_2$ fixation. This estimate is also consistent with the observed differences between GPP and NPP for LC at the surface. The most important depth-related variable in the upper 100 m of the water column at Station ALOHA is light, so we consider this to be the root cause of the patterns observed for FRRF and $^{14}C$ incorporation. Increase in GPP relative to NPP can then be explained by greater light

intensity at the surface, which will drive higher electron transport rates across photosystems. A simultaneous and/or independent increase in GPP (i.e. increase in FFRF estimates) and respiration (i.e. decrease in $^{14}C$ estimates) rates can also account for ratio variations among the different data sets.

Three photoautotrophic respiration processes can account for larger differences between $^{14}C$ and FRRF estimates, and in turn between GPP and NPP in surface layers (Bender et al. 1999, Suggett et al. 2001). They include: (i) "dark" respiration, (ii) photorespiration, and (iii) the Mehler reaction. These physiological processes may all play a role in explaining higher ratios at the surface and their vertical variations.

The difference in the $^{14}C$-FRRF relationship between surface and deep layers may also be due to a vertical shift in (i) *Prochlorococcus* sp. populations and/or (ii) community structure in the NPSG. At Station ALOHA two clades of *Prochlorococcus* sp. have been recognized based on genetic analysis: a high- and a low-light adapted population, respectively (Campbell and Vaulot 1993). A vertical change in the photoautotrophs assemblage has also be found in the central North Pacific (Venrick 1993). These vertical shifts may influence the $^{14}C$ and FRRF measurements differently, as different populations most likely possess different physiological adaptations.

No clear seasonal cycle was observed for the difference between FRRF and $^{14}C$, and in turn for the GPP versus NPP relationship, when VC and CC were considered. These results would indicate that the overall GPP versus NPP relationship is not influenced by the annual light and temperature cycle. At Station ALOHA, a

clear seasonal cycle in PP and chl *a* has been found based on 15 years of time-series sampling (Karl et al. 2001). However, little is known regarding the seasonal variation (if any) of respiration processes in this region. Such variation may be represented by the FRRF and $^{14}C$ relationship shown here by VC and CC. The maximum of the ratio in fall indicates that the peak in photorespiration activity may occur during this period. A clear seasonal cycle was observed when LC is considered. Ratios increased gradually from winter to fall, suggesting that respiration processes (in particular photorespiration) increase their relative influence on PP dynamics in correspondence with seasonal light cycle of this particular environment.

*Empirical and theoretical derivation of light-driven photoautotrophic respiration.*

Based on the information presented here, the divergence from a 1:1 relationship between FRRF and $^{14}C$ represents the difference between GPP and NPP during the photoperiod. The linear comparison between PP from FRRF $_{(GPP)}$ and $^{14}C$ $_{(NPP)}$ yield a relationship such as:

$$FRRF\ (z)_{(GPP)} = m\ ^{14}C\ (z)_{(NPP)} + c \quad \text{(Eq. 4)},$$

where m is the slope and c is the y-axis intercept. Biologically, m is an indication of the GPP versus NPP relationship, and the x-axis (-c/m) intercept may represent the uptake of labeled $H^{14}CO_3^-$ by other photoautotrophs organisms not relying on chl a, as major light harvesting pigment (i.e. AAnP which will not be measured by FRRF). The light-driven photoautotrophic community respiration (R) (i.e. processes including Mehler reaction, photorespiration and community mitochondrial respiration) can then be estimated by:

$$R\ (z) = FRRF\ (z)_{(GPP)} - {}^{14}C\ (z)_{(NPP)} \text{ (Eq. 5).}$$

Community photorespiration was then calculated using the full data set for different depths and data were normalized (Eq.4). For VC and CC, R decreased exponentially with depth (Fig. 3.6). Best-fit lines were $R\ (z) = 0.00007e^{-0.0197z}$ ($r^2$= 0.962, $p$-value < 0.05, $n$= 70) and $R\ (z) = 0.0006e^{-0.0297z}$ ($r^2$= 0.996, $p$-value < 0.05, $n$= 70) for VC and CC, respectively.

The depth dependence of R can be related to the exponential decrease of light with increasing water depth. There have been only a few theoretical (Dring and Jewson 1982) or experimental (Weger et al. 1989, Xue et al. 1996, Williams 1998) studies on photoautotrophic respiration; its experimental determination is not trivial. Laboratory experiments have shown how a unique relationship between rates of respiratory carbon flow and photosynthesis does not exist in some green algae (Xue et al. 1996). These observations suggest interactions between photosynthesis and respiration at more than one level. Mitochondrial respiration has also been found to vary during photosynthesis in relation to substrate supply and light variations (Weger et al. 1989). *In situ* investigations indicate a depth dependence of photoautotrophic respiration, suggesting that cells become more efficient in incorporating carbon as light decreases due to changes in respiration rates (in particular light-driven respiration processes) (Williams 1998). When compared to *in situ* total community respiration (TCR) at Station ALOHA (Fig. 3.7 and Table 3.3, Williams et al. 2004), R appears to be of the same magnitude as TCR (20-100%). Near the surface (< 5 m), R is approximately equivalent to the TCR, while it represents approximately 50% of TCR between 25 and 100 m. The relative fraction decreases below 20% deeper in the

water column. These results suggest that light-driven photoautotrophic respiration is similar to the surface respiration budget. The decrease with depth of the R/TCR percentage is a direct function of the exponential light decrease in the water column, which will lower light-driven photoautotrophic respiration rates.

*Empirical and theoretical derivation of autotrophic status of photoautotrophs.* To a first approximation, net carbon fixation can be considered as the major energy-storage process in photoautotrophs. In this context, the ratio R/NPP can therefore be a proxy of the efficiency by photoautotrophs in transferring biological energy to next trophic level (in the form of carbon), or in other terms of the autotrophic status of photoautotrophs. If R is obtained by (4), the ratio R/NPP can be derived by

$$R/NPP= [\ FRRF\ (z)_{(GPP)} - {}^{14}C\ (z)_{(NPP)}\ ] / {}^{14}C\ (z)_{(NPP)},$$

$$R/NPP= [FRRF\ (z)_{(GPP)} / {}^{14}C\ (z)_{(NPP)}\ ]\text{-}1 \quad \text{(Eq. 6)}.$$

It follows that greater growth efficiency and available energy in the form of C to the ecosystem will be achieved as R/NPP tends to 0, or the FRRF: $^{14}C$ ratio tends to 1. If R/NPP becomes greater than 1, or the FRRF: $^{14}C$ ratio becomes greater than 2, photoautotrophic storage of carbon is less efficient (i.e. greater portion of available intracellular energy directed toward other metabolic processes rather than carbon fixation).

The FRRF: $^{14}C$ ratio was greater than two at the near surface (5 m) for LC, suggesting the greater redistribution of the intracellular energy budget toward other processes rather than carbon fixation. According to the arguments presented here, in deeper layers, photoautotrophic cells are more efficient in storing carbon (the FRRF:

$^{14}C$ ratio < 2) per unit light and biomass. Thus, surface populations would be less efficient in transferring biomass and energy (in the form of C) to the next trophic level (i.e. micro and macro-grazers). The FRRF: $^{14}C$ ratio increased from winter to fall (1.50 to 2.10) for LC data. Such a seasonal pattern suggests that this ecosystem increases its efficiency in storing carbon (and trophic energy transfer) inversely in relation to the seasonal light cycle. The seasonal change in the FRRF: $^{14}C$ ratio also provides preliminary evidence of a seasonal cycle in light-driven photoautotrophic respiration processes in this ecosystem.

*Ecological implications.* The observations reported here have potentially significant ecological and biogeochemical implications for this biome. First, if light-driven photoautotrophic respiration is equivalent to the overall total community respiration at the surface, variations in physiological status could contribute significantly to the regulation of $O_2$ and $CO_2$ fluxes from and to the atmosphere. The background metabolic state of this system may be poised by the activities of the photoautotrophs. Furthermore, the increase in efficiency of carbon storage by photoautotrophs with depth also highlights the greater efficiency of this ecosystem in recycling biomass (in terms of C) at depth. The relative effects of such increase, on appropriate time scales, for higher and lower trophic levels are yet to be fully assessed. These results suggest that deeper layers would be energetically more advantageous for micro-grazers and, if DOM production is considered a function of autotrophic efficiency, for bacterial populations.

*Conclusion*

Fast repetition rate fluorometry is a promising technique for estimating PP in oligotrophic oceans. This study suggests that FRRF measurements estimate instantaneous GPP at Station ALOHA. However, care should be taken when interpreting measurements based on FRRF, especially with respect to errors associated with the PP parameterization and *in situ* light effects. The good correlation with $^{14}C$ measurements across different water column depths also indicates that FRRF is able to estimate PP across the euphotic zone. Despite a robust linear relationship between $^{14}C$ and FRRF measurements, a unique quantitative correlation could not be derived. The relationship was found to vary vertically and, to some extent, temporally. Such variations indicate that (i) these two techniques are approximating different aspects of PP and (ii) the available intracellular energy, derived from photosynthetic light reactions, is not uniformly distributed across different populations within the water column.

As indicated by Marra and Barber (2004), a long-standing problem in biological oceanography is the measurement of the components of respiration (photoautrophic vs. heterotrophic) in plankton communities. The analysis (i.e. difference between FRRF and $^{14}C$ measurements) presented here represents a possible solution for evaluating light-driven photoautotrophic respiration in the ocean. However, further comparisons on appropriate time scales are needed for different oceanic regions to determine the generality of such relationships. As more data from Station ALOHA become available, additional analysis of the temporal variability of $^{14}C$ and FRRF different depths will be possible. A further understanding of the light

cycle influence, physical processing and relative community shift on the GPP/NPP changes is needed for a complete understanding of biological dynamics in this oceanic region.

### 3.6 References

Azam, F. & Long, R. A. 2001. Sea snow microcosms. *Nature* 414:495-98.

Baines, S. & Pace, M. L. 1991. The production of dissolved organic matter by phytoplankton and its importance to bacteria: patterns across marine and freshwater systems. *Limnol. Oceanogr.* 36:1078-90.

Bender, M. L., Grande, K., Johnson, K., Marra, J., Williams, P., Sieburth, J., Pilson, M., Langdon, C., Hitchcock, G., Orchado, J., Hunt, C., Donaghay, P. & Heinemann, K. 1987. A comparison of four methods for the determination of planktonic community metabolism. *Limnol. Oceanogr.* 32:1085-98.

Bender, M., Orchado, J., Dickson, M., Barber, R. & Lindley, S. 1999. In vitro $O_2$ fluxes compared with $^{14}C$ production and other rate terms during the JGOFS Equatorial Pacific experiment. *Deep-Sea Res. I* 46:637-54.

Boyd, P. W., Aiken, J. & Kolber, Z. 1997. Comparison of radiocarbon and fluorescence based (pump and probe) measurements of phytoplankton photosynthetic characteristics in the Northeast Atlantic Ocean. *Mar. Ecol. Prog. Ser.* 149:215-26.

Campbell, L. & Vaulot, D. 1993. Photosynthetic picoplankton community structure in the subtropical North Pacific Ocean near Hawaii (station ALOHA). *Deep-Sea Res. I* 40:2043-60.

Carlson, C. A., Ducklow, H. W. & Micheals, A. F. 1994. Annual flux of dissolved organic carbon from the euphotic zone in the northwestern Sargasso Sea. *Nature* 371:405-08.

Caron, D. A., Peele, E. R., Lim, E. L. & Dennett, M. R. 1999. Picoplankton and nanoplankton and their trophic relationships in surface waters of the Sargasso Sea south of Bermuda. *Limnol. Oceanogr.* 44:259-72.

Corno, G., Letelier, R. M., Abbott, M. R. & Karl, D. M. 2005. Photosynthetic activity and variability in the North Pacific Subtropical Gyre (NPSG) determined by Fast Repetition Rate Fluorometry (FRRF). Submitted to *Deep-Sea Res I.*

Cowles, T. J., Desiderio, R. A. & Carr, M-E. 1998. Small-scale planktonic structure: persistence and trophic consequences. *Oceanography* 11:4-9

Dring, M. J. & Jewson, D. H. 1982. What does $^{14}C$ uptake by phytoplankton really measure? A theoretical modeling approach. *Proc. R. Soc. Lond.* 214:351-68.

Falkowski, P. G., Owens, T. G., Ley, A. C. & Mauzerall, D. C. 1981. Effects of growth irradiance levels on the ratio of reaction centers in two species of marine phytoplankton. *Plant. Physiol.* 68:969-73.

Grande, K., Williams, P. J. le B., Marra, J., Purdie, D. A., Heinemann, K., Eppley, R. W. & Bender, M. L. 1989. Primary production on the North Pacific gyre: a comparison of rates determined by the $^{14}C$ , $O_2$ concentration and $^{18}O$ methods. *Deep-Sea Res.I* 36:1621-34.

Jespersen, A. M.. 1994. Comparison of $^{14}CO_2$ and $^{14}CO_2$ uptake and release rates in laboratory cultures of phytoplankton. *Oikos* 69:460-8.

Karl, D. M. 1999. A sea of change: biogeochemical variability in the North Pacific Subtropical Gyre. *Ecosystems* 2:181-214.

Karl, D. M. 2002. Nutrient dynamics in the deep blue sea. *Trends in Microbiology* 10:410-18.

Karl, D. M., Letelier, R. M., Tupas, L., Dore, J., Christian, J. & Hebel, D. 1997. The role of nitrogen fixation in biogeochemical cycling in the subtropical North Pacific Ocean. *Nature* 388:533-38.

Karl, D. M., Hebel, D. V., Björkmann, K. & Letelier, R. M. 1998. The role of dissolved organic matter release in the productivity of the oligotrophic North Pacific Ocean. *Limnol. Oceanogr.* 43:1270-86.

Karl, D. M., Bidigare, R. R. & Letelier, R. M. 2001. Long-term changes in plankton community structure and productivity in the North Pacific Subtropical Gyre: The domain shift hypothesis. *Deep-Sea Res. II* 43:539-68.

Kana, T. M. 1992. Relationship between photosynthetic oxygen cycling and carbon assimilation in *Synechococcus* WH7803 (Cyanophyta). *J. Phycol.* 28:304-08.

Kolber, Z. & Falkowski, P. G. 1993. Use of active fluorescence to estimate phytoplankton photosynthesis in situ. *Limnol. Oceanogr.* 38:1646-65.

Kolber, Z. S., Prasil, O. & Falkowski, P. G., 1998. Measurements of variable chlorophyll fluorescence using fast repetition rate techniques: defining methodology and experimental protocols. *Biochim. Biophys. Acta* 1367:88-106.

Kolber, Z. S., van Dover, C. L., Niederman, R. A. & Falkowski, P. G. 2001. Bacterial photosynthesis in surface waters of the open ocean. *Nature* 407:177-9.

Landry, M. R. 2000. Biological response to iron fertilization in the eastern equatorial Pacific (IronEx II). III. Dynamics of phytoplankton growth and microzooplankton grazing. *Mar. Ecol. Prog. Ser.* 201:57-72.

Laney, S. R. 2003. Assessing the errors in photosynthetic properties determined with Fast Repetition Rate fluorometry. *Limnol. Oceanogr.* 48:2234-42.

Laws, E. A. 1991. Photosynthetic quotients, new production and net community production in the open ocean. *Deep-Sea Res.I* 38:143-67.

Letelier, R. M., Dore, J. E., Winn, C. D. & Karl, D. M. 1996. Seasonal and interannual variations in photosynthetic carbon assimilation at Station ALOHA. *Deep-Sea Res.II* 43:467-90.

Letelier, R. M., Karl, D. M., Abbott, M. R. & Bidigare, R. R. 2004. Light-driven seasonal patterns of chlorophyll and nitrate in the lower euphotic zone of the North Pacific Subtropical Gyre. *Limnol. Oceanogr.* 49:508-19.

Marra, J. 2002. Approaches to the measurement of plankton production. Phytoplankton productivity: carbon assimilation in marine and freshwater ecosystems. P. J. le B. Williams, D. N. Thomas, C. S. Reynolds. Cambridge, Blackwells, 78-108.

Marra, J. & Barber, R. T. 2004. Phytoplankton and heterotrophic respiration in the surface layer of the ocean. Geophys. Res. Lett. 31:19-24.

Marra, J., Haas, L. W. & Heinemann, L. W. 1988. Time course of C assimilation and microbial food-web. *J. Mar. Biol. Exp. Ecol.* 115:263-80.

McArdle, B. H. 2003. Lines, models, and errors: regression in the field. *Limnol. Oceanogr.* 48:1363-6.

Mehler, A. H. 1951. Studies on the reactions of illuminated chloroplasts: I. Mechanism of the reduction of oxygen and other Hill reagents. *Arch. Biochem. Biophys.* 33**:**65-77.

Miller, R. G. 1981. Simultaneous Statistical Inference. 2nd Edition, Springer Verling, 50-75.

Moore, M. C., Suggett, D., Holligan, P. M., Sharples, J., Abraham, E. R., Lucas, M. I., Rippeth, T. P., Fisher, N. R., Simpson, J. H. & Hydes, D. J. 2003. Physical control on phytoplankton physiology and production at a shelf sea front: a fast repetition-rate fluorometer-based field study. *Mar. Ecol. Prog. Ser.* 259:29-45.

Raateoja, M., Seppala, J. & Kuosa, H. 2004. Bio-optical modeling of primary production in the SW Finnish coastal zone, Baltic Sea: fast repetition rate fluorometry in Case 2 waters. *Mar. Ecol. Prog. Ser.* 267:9-26.

Raven, J. A. & Beardall, J. 1981. Respiration and photorespiration. In: Platt, T. ed. Physiological bases of phytoplankton ecology. Ottawa: *J. Can. Fish. Res. Bd.* 55-82.

Smyth, T. J., Pemberton, J., Aiken, J. & Geider, R. J. 2004. A methodology to determine primary production and phytoplankton photosynthetic parameters from Fast Repetition Rate Fluorometry. *J. Plankton Res.* 26:1337-50.

Suggett, D. J., Kraay, G., Holligan, P., Davey, M., Aiken, J., Geider, R. 2001. Assessment of photosynthesis in a spring caynobacterial bloom by use of a fast repetition rate fluorometer. *Limnol. Oceanogr.* 46:802-10.

Suggett, D. J., MacIntyre, H. L. & Geider, R. J. 2004. Evaluation of biophysical and optical determinations of light absorption by photosystem II in phytoplankton. *Limnol. Oceanogr. Meth.* 2: 316-32.

Venrick, E. L. 1993. Phytoplankton seasonality in the central North Pacific: the endless summer reconsidered. *Limnol. Oceanogr.* 38:1135-49.

Weger, H. G. , Herzig, R., Falkowski, P. G. & Turpin, D. H. 1989. Respiratory losses in the light in a marine diatom: Measurements by short-term mass spectrometry. *Limnol. Oceanogr.* 34:1153-61.

Williams, P. J. le B. 1998. The balance of plankton respiration and photosynthesis in the open oceans. *Nature* 394:55-7.

Williams, P. J. le B., Morris, P. J. & Karl, D. M. 2004. Net community production and metabolic balance at the oligotrophic ocean site, Station ALOHA. *Deep-Sea Res. I* 51:1563-78.

Williams, P. J. le B. & Robertson, J. E. 1991. Overall oxygen and carbon dioxide metabolisms: the problem of reconciling observations and calculations of photosynthetic quotients. *J. Plankton. Res.* (suppl.) 13:153-69.

Xue, X., Gauthier, D. A., Turpin, D. H. & Weger, H. C. 1996. Interactions between Photosynthesis and Respiration in the Green Alga *Chlamydomonas reinhardtii*. *Plant. Physiol.* 112:1005-14.

Table 3.1. Definitions of bio-optical, environmental and productivity parameters used in the text.

| Parameter | Definition | Units |
|---|---|---|
| E | Irradiance | μmol photons•$m^{-2}$•$s^{-1}$ |
| $F_O$ , $F_M$ | Initial and maximal fluorescence yield in absence of non-photochemical quenching | relative |
| F ', $F_M$' | Initial and maximal fluorescence yield at ambient irradiance in presence of non-photochemical quenching | relative |
| $F_O$' | Fluorescence yield at ambient irradiance, measured after 1to 2 s of dark adaptation | relative |
| $F_V$, $F_V$' | Variable fluorescence yield in dark adapted and under ambient light, derived as ($F_M$ - $F_O$) and ($F_M$'- $F_O$'), respectively | relative |
| $F_V/F_M$ , $F_V'/F_M'$ | Potential photochemical efficiency of open RCIIs, in dark adapted and under ambient light, respectively | dimensionless |
| $F_q$' | Difference between fluorescence yields $F_M$' and F ' | relative |
| qP | Photochemical quenching, derived as $F_q'/F_V'$ | between 0 and 1 |
| $\sigma_{PSII}$ , $\sigma_{PSII}$ ' | Effective absorption cross section of PSII in dark adapted and under ambient light condition, respectively | $10^{-20}$•$m^2$•$quanta^{-1}$ |
| $n_{PSII}$ | Photosynthetic unit size of PSII | mol RCII•mol chl *a*$^{-1}$ |
| τ | Electron turnover rate per functional PSII | μs |
| $\Phi_e$ | Photon yield of electron transfer by PSII | mol $O_2$•mol $photon^{-1}$ |
| $ETR^{Chl}$ | Electron transport rate | e•mol chl *a*•mol RCII $^{-1}$•$s^{-1}$ |
| GOE | Gross oxygen evolution rates | mol $O_2$•$m^{-3}$•$h^{-1}$ |
| FRRF-PP | Primary productivity rates derived by FRRF measurements | mol C•$m^{-3}$•$h^{-1}$ |

Table 3.2. Statistical parameters from model II regression (geometric mean) between FRRF-GOE and $^{14}C$ rate estimates for different data normalizations .Values not significantly different than zero are indicated by ns. The x-intercepts and C.I. of the y-intercept are not presented because they were not significantly different than zero for all regression models.

| Statistical parameters | Volumetric-normalized | chl *a*-normalized | Light-normalized |
|---|---|---|---|
| *n* | 72 | 72 | 72 |
| Slope | 2.90 | 2.00 | 1.90 |
| y-intercept | ns | ns | ns |
| C.I. slope | 0.23 | 0.13 | 0.17 |
| $r^2$ | 0.90 | 0.94 | 0.87 |
| *p*-value | <0.05 | <0.05 | <0.05 |

Table 3.3. Measured rates of total community respiration (TCR) at Sta. ALOHA (Williams et al. 2004), derived light-driven photoautotrophic respiration (R) (after Eq. 4 in the text) and the percentage contribution of PR to TCR. Depth-integrated rates are given as mmol $O_2 \bullet m^{-2} \bullet d^{-1}$.

| Depth (m) | Total Community Respiration (TCR) (mmol $O_2 \bullet m^{-3} \bullet d^{-1}$) | Photo-autotrophic respiration (R) (mmol $O_2 \bullet m^{-3} \bullet d^{-1}$) | Percentage of Photoautotrophic Respiration (R/TCR•100%) |
|---|---|---|---|
| 5 | 0.80 ± 0.10 | 0.90 ± 0.18 | 100 ± 12 |
| 25 | 0.93 ± 0.05 | 0.60 ± 0.25 | 66 ± 26 |
| 45 | 0.83 ± 0.06 | 0.33 ± 0.09 | 40 ± 11 |
| 75 | 0.57 ± 0.04 | 0.27 ± 0.05 | 47± 10 |
| 100 | 0.37 ± 0.05 | 0.17 ± 0.05 | 46± 13 |
| 125 | 0.30± 0.06 | 0.06 ± 0.02 | 20± 6 |
| $\Sigma_{0\text{-}125m}$ | 80.0± 1.00 | 46.1± 1.40 | 58± 10 |

**3.7 Figure Legend**

Figure 3.1. Volumetric measurements of primary productivity as derived by *in situ* FRRF-GOE and $^{14}C$ uptake at Station ALOHA over the course of one year. The dashed and solid lines represent a 1:1 relationship and the regression fit, respectively. Horizontal and vertical bars are ± 1 SD for each measurement. Regression statistics are given in Table 3.2.

Figure 3.2. Chl *a* normalized measurements of primary productivity as derived by *in situ* FRRF-GOE and $^{14}C$ uptake at Station ALOHA over the course of one year. The dashed and solid lines represent a 1:1 relationship and the regression fit, respectively. Horizontal and vertical bars are ± 1 SD for each measurement. Regression statistics are given in Table 3.2.

Figure 3.3. Light normalized measurements of primary productivity as derived by *in situ* FRRF-GOE and $^{14}C$ uptake at Station ALOHA over the course of one year. The dashed and solid lines represent a 1:1 relationship and the regression fit, respectively. Horizontal and vertical bars are ± 1 SD for each measurement. Regression statistics are given in Table 3.2.

Figure 3.4. Vertical variations of the ratio FRRF-PP: $^{14}C$ for normalized data. Horizontal bars represent 1 SD for each depth ($n$ = 12).

Figure 3.5. Temporal variations of the ratio FRRF-PP: $^{14}$C for normalized data. For each season, the ratio is an average of all depths. Vertical bars represent 1 SD for each depth ($n$ = 36).

Figure 3.6. Photoautotrophic respiration, volumetric (A) and chl *a* normalized (B), derived from the difference between FRRF and $^{14}$C rate measurements at Station ALOHA. Horizontal bars represent ±1 SD. Dashed lines represent the best fist to the experimental data. For volumetric and chl *a* normalized data, equations are $y= 7 \cdot 10^{-2} e^{-0.0197x}$ and $y= 6 \cdot 10^{-1} e^{-0.0276x}$, respectively.

Figure 3.7. Comparison of *in situ* total community respiration (TCR) (Williams et al. 2004) and light-driven photoautrophic respiration (R) derived from Eq. 4. Horizontal bars represent ±1 SD.

Figure 3.1

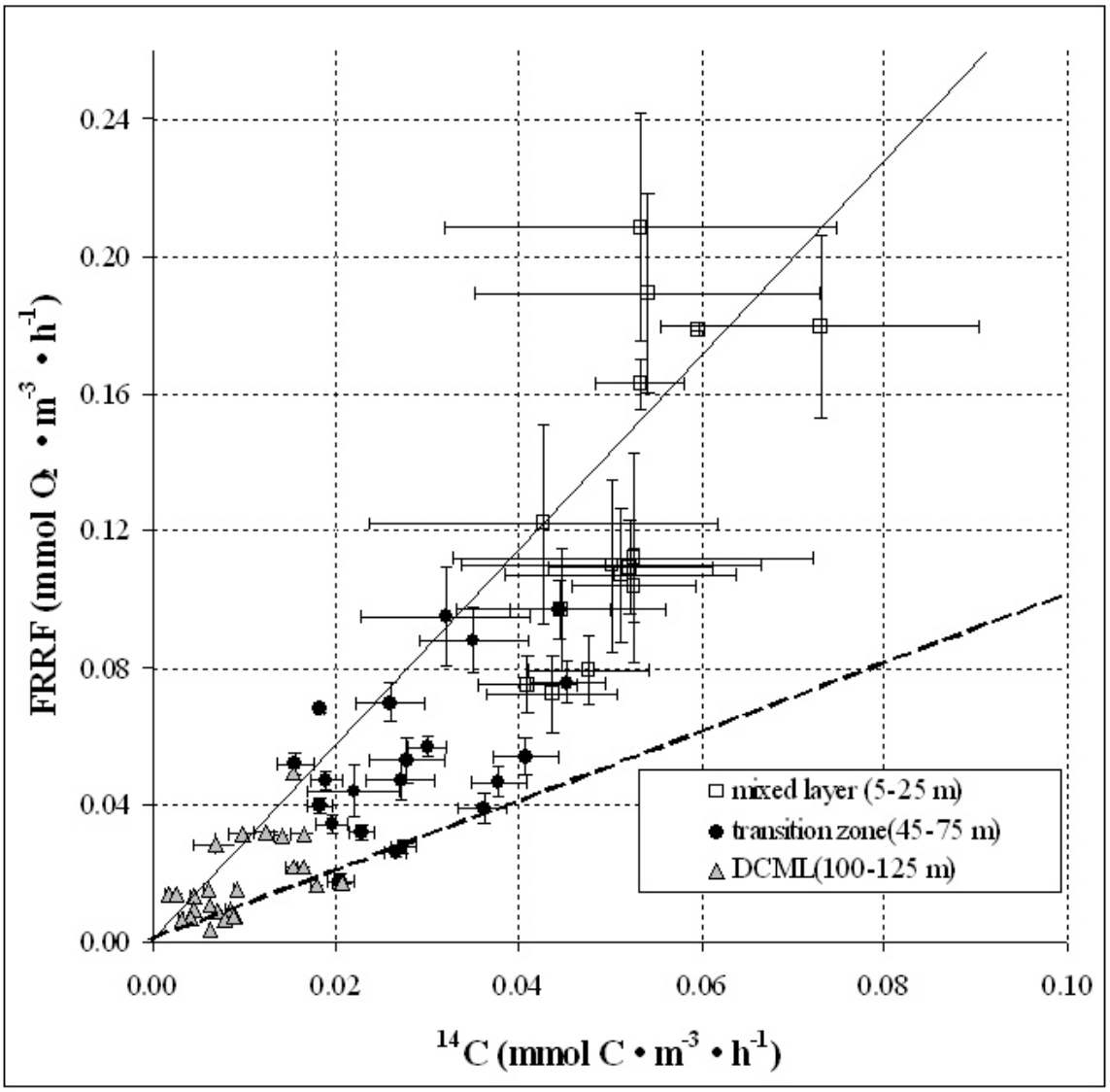
0.24
0.20
0.16
0.12
0.08
0.04
0.00
0.00
0.02
0.04
0.06
0.08
0.10
FRRF (mmol O2 • m-3 • h-1)
14C (mmol C • m-3 • h-1)
mixed layer (5-25 m)
transition zone(45-75 m)
DCML(100-125 m)

Figure 3.2

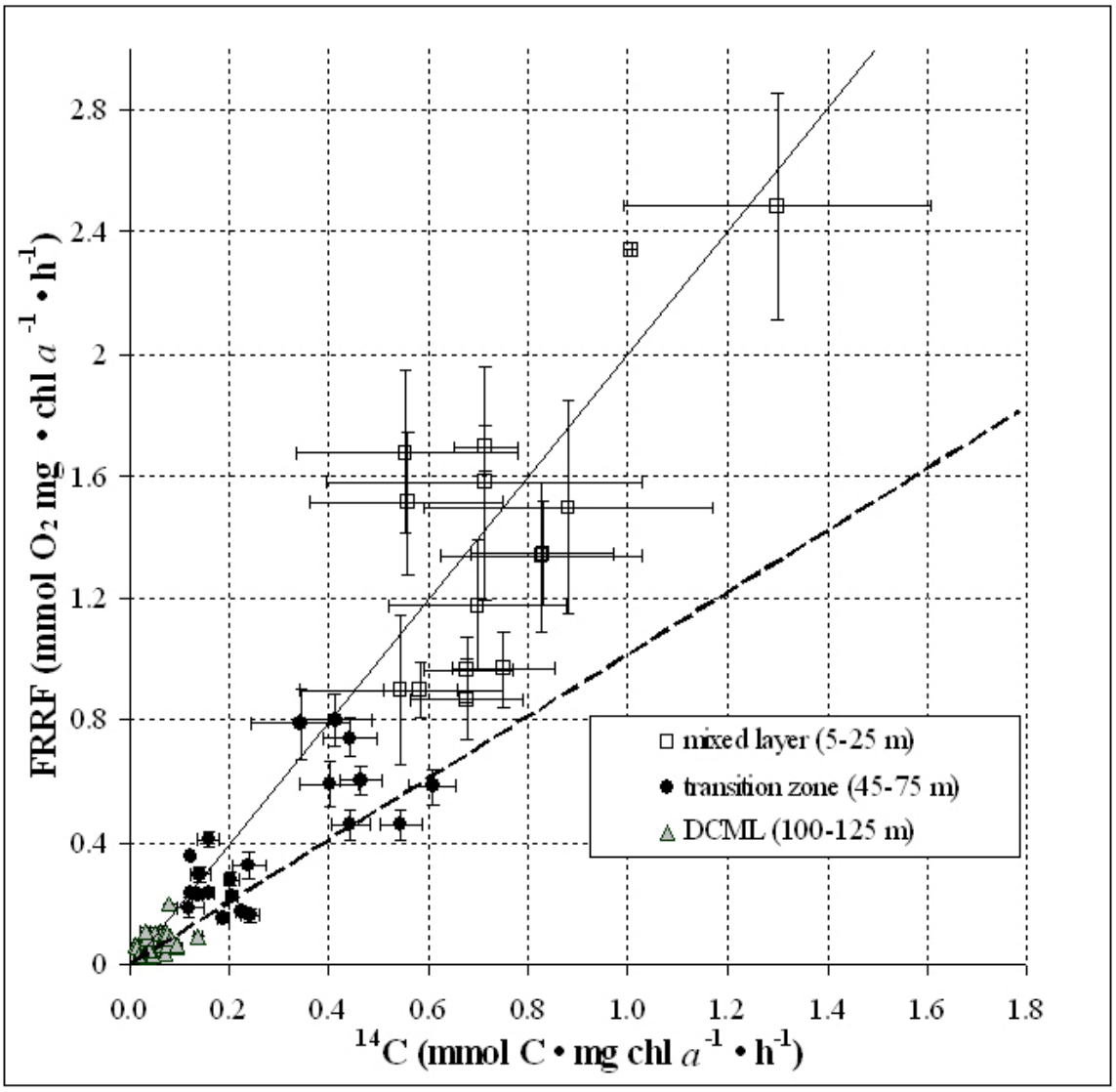
FRRF (mmol O2 mg • chl a -1 • h-1)
14C (mmol C • mg chl a -1 • h-1)
0
0.4
0.8
1.2
1.6
2
2.4
2.8
0.0
0.2
0.4
0.6
0.8
1.0
1.2
1.4
1.6
1.8
mixed layer (5-25 m)
transition zone (45-75 m)
DCML (100-125 m)

Figure 3.3

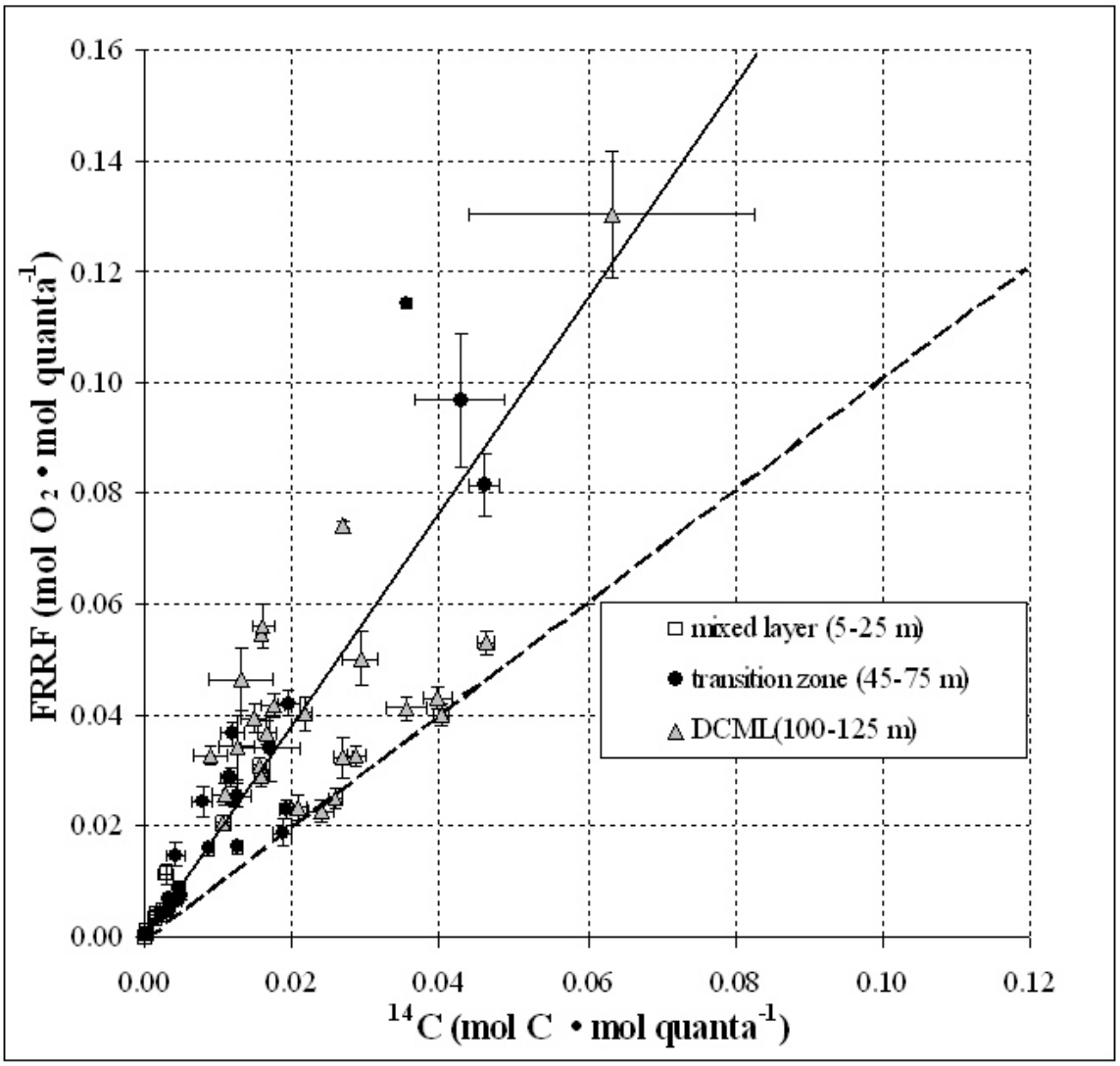
0.16
0.14
0.12
0.10
0.08
0.06
0.04
0.02
0.00
FRRF (mol O2 • mol quanta-1)
0.00
0.02
0.04
0.06
0.08
0.10
0.12
14C (mol C • mol quanta-1)
mixed layer (5-25 m)
transition zone (45-75 m)
DCML(100-125 m)

Figure 3.4

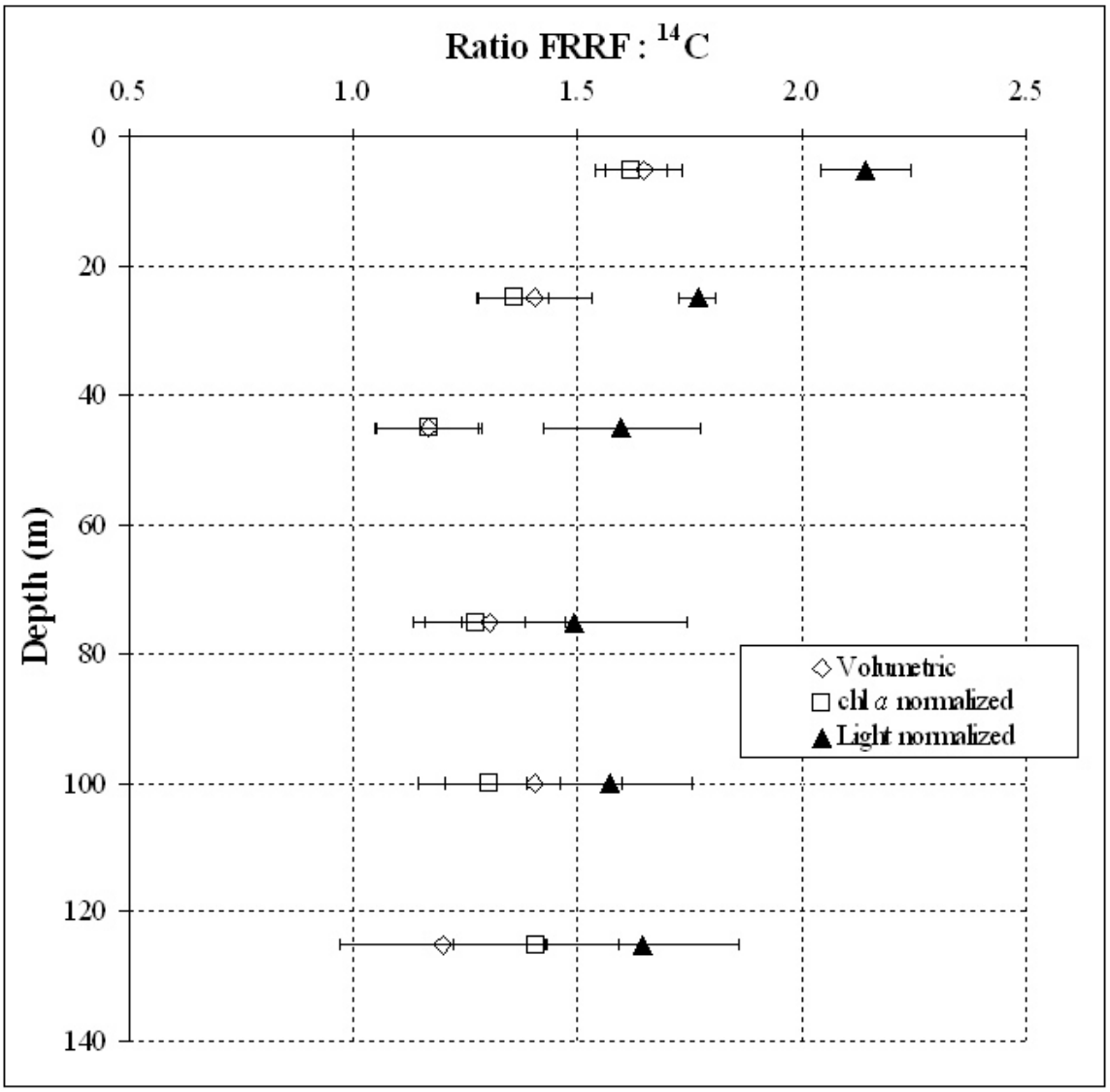
Ratio FRRF : $^{14}$C
0.5
1.0
1.5
2.0
2.5
0
20
40
60
80
100
120
140
Depth (m)
Volumetric
chl a normalized
Light normalized

Figure 3.5

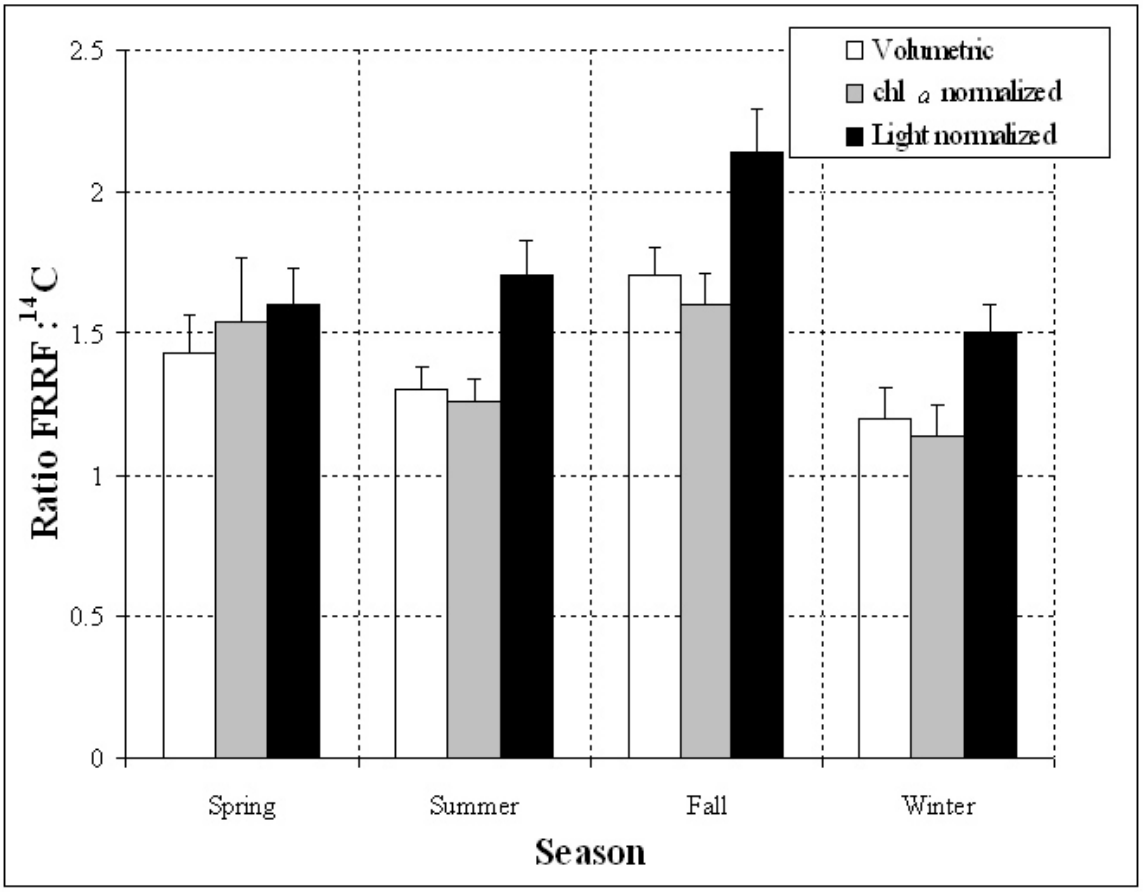
Volumetric
chl a normalized
Light normalized
2.5
2
1.5
1
0.5
0
Ratio FRRF:14C
Spring
Summer
Fall
Winter
Season

Figure 3.6

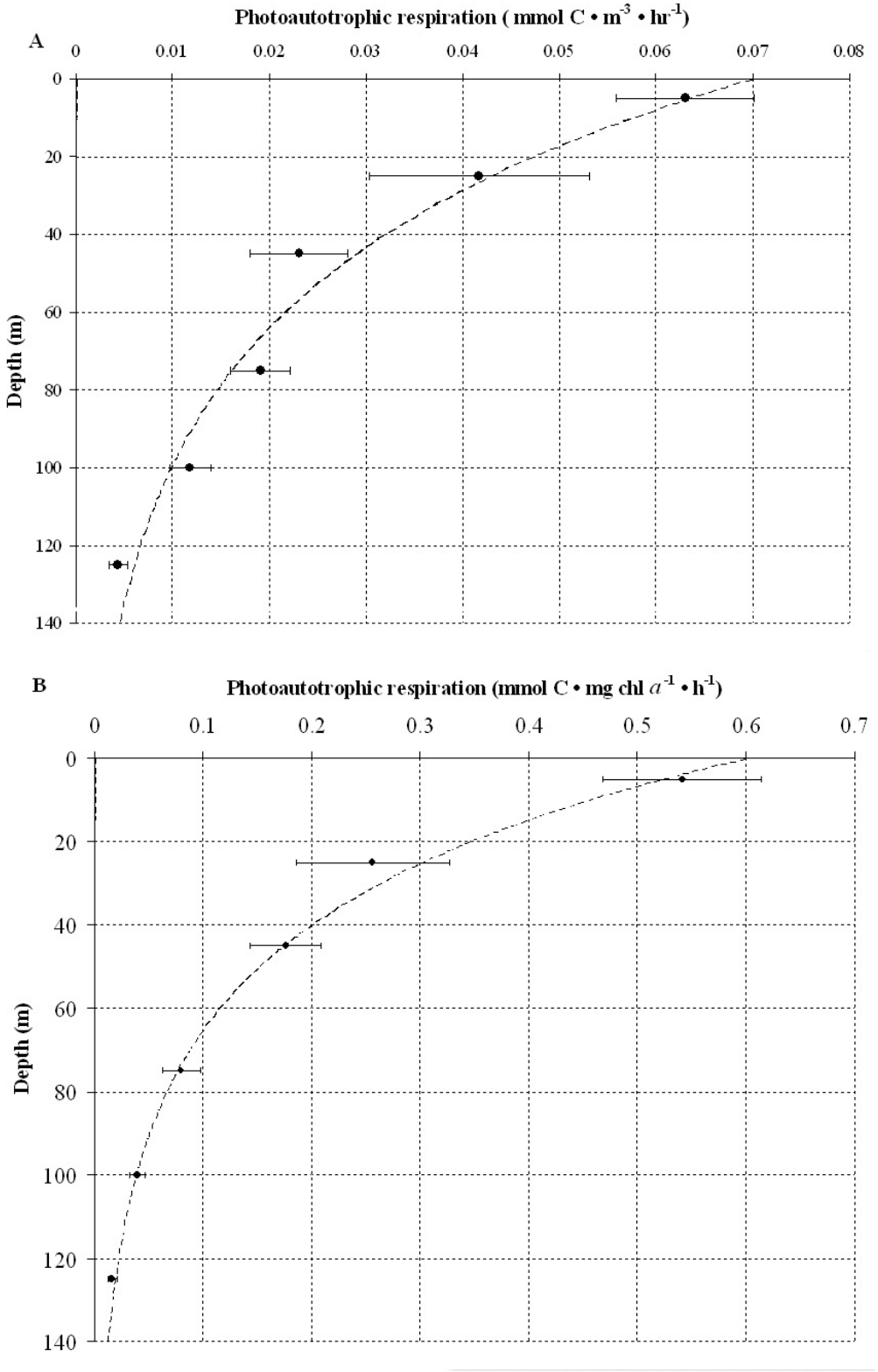
A
Photoautotrophic respiration ( mmol C • m-3 • hr-1)
0
0.01
0.02
0.03
0.04
0.05
0.06
0.07
0.08
Depth (m)
0
20
40
60
80
100
120
140
B
Photoautotrophic respiration (mmol C • mg chl a-1 • h-1)
0
0.1
0.2
0.3
0.4
0.5
0.6
0.7
Depth (m)
0
20
40
60
80
100
120
140

Figure 3.7

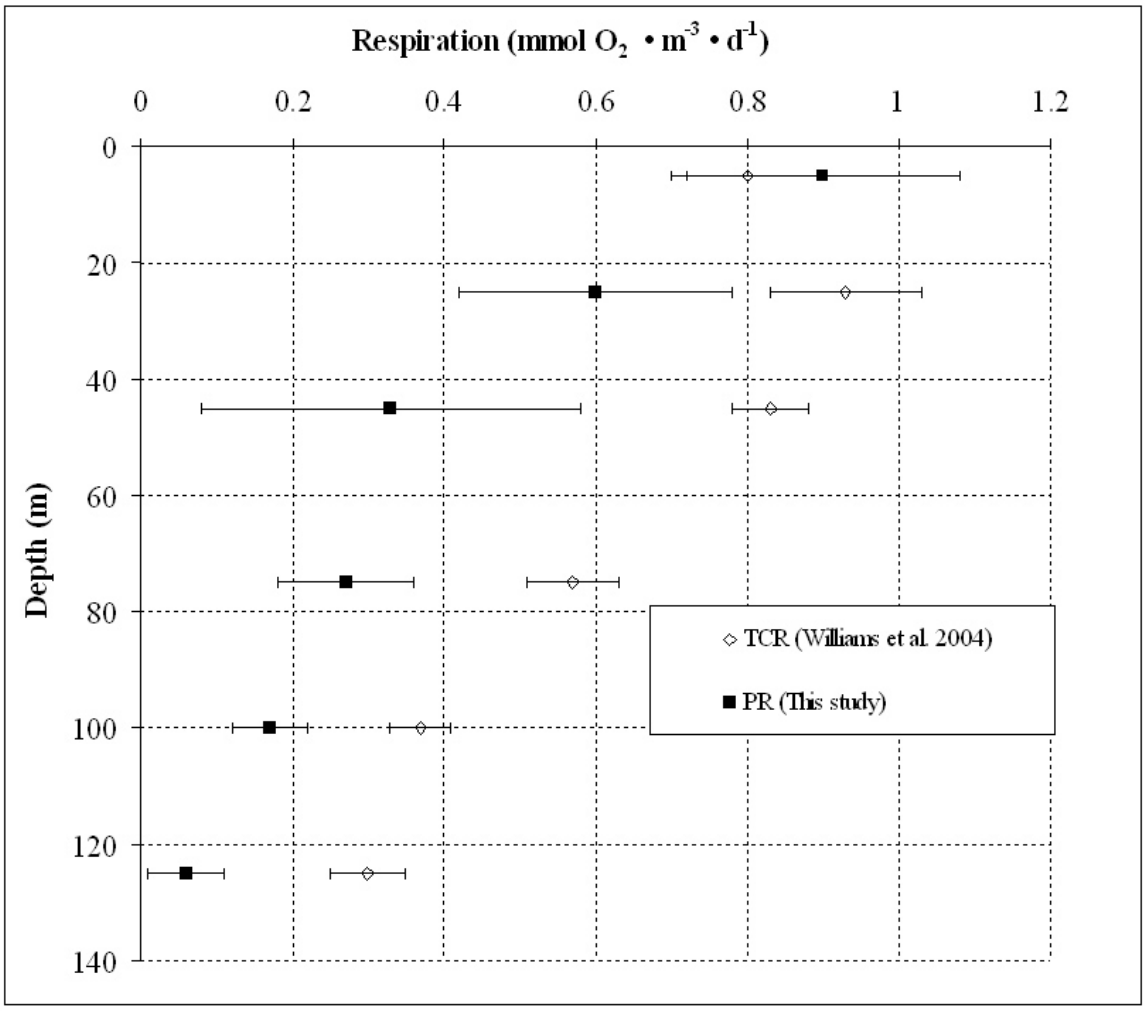
Respiration (mmol O2 • m-3 • d-1)
0
0.2
0.4
0.6
0.8
1
1.2
Depth (m)
0
20
40
60
80
100
120
140
TCR (Williams et al. 2004)
PR (This study)

# 4. Temporal and vertical variability in photosynthesis in the North Pacific Subtropical Gyre

Guido Corno , Ricardo M. Letelier, Mark R. Abbott and David M. Karl

Manuscript to be submitted to *Limnology and Oceanography*

## 4.1 Abstract

*In situ* Fast Repetition Rate Fluorometry (FRRF) was conducted in the North Pacific Subtropical Gyre (NPSG) at Station ALOHA (Sta. ALOHA, 22º 45' N 158º 00' W), from September 2002 to December 2004, to assess temporal and vertical photosynthetic variability in relation to environmental conditions. Night-time photosynthetic efficiency of the photoautotrophic microbial assemblage ($F_V/F_M$) was low in the mixed-layer and increased with depth. High $F_V/F_M$, with some values approaching the theoretical maximum for prokaryotes (0.60), were observed at and below the Deep Chlorophyll Maximum Layer (DCML). In contrast, the absorption cross section of PSII ($\sigma_{PSII}$) was high at the surface and decreased with depth, with minima (1000 $m^2$ $quanta^{-1}$) around the DCML. These vertical patterns suggest photosynthetic stress conditions in surface photoautotrophic population. No significant seasonal cycles were found for $F_V/F_M$, but surface $\sigma_{PSII}$ peaked in winter and decreased during summer, suggesting that seasonal variations in light availability may influence the observed $\sigma_{PSII}$ variability.

A significant correlation was found between surface $F_V/F_M$, $\sigma_{PSII}$ and the distance between the mixed layer depth (MLD) and the top of the nutricline. Neither nutrient nor light variations were significantly related to $F_V/F_M$ and $\sigma_{PSII}$ in the DCML. In this layer, $F_V/F_M$ variability was positively and negatively related to concentrations of chlorophyll *b* and zeaxanthin, respectively. Our results suggest that, at Sta. ALOHA, surface photosynthesis takes place under chronic nutrient limitation, while higher photosynthetic efficiency in the lower euphotic zone appears sensitive to community structure changes.

Keywords: Primary productivity, phytoplankton, photosynthesis, oligotrophic ocean, FRRF

Regional terms: USA, Hawaii, Station ALOHA

## 4.2 Introduction

In the ocean, variations in photosynthetic rates across different spatial and temporal scales can significantly influence ecosystem dynamics, including fishery yields and carbon sequestration (DiTullio and Laws 1991, Falkowski *et al.* 1998, Letelier *et al.* 2000). However, in oligotrophic regions of the ocean, these variations have been considered small due to chronic nutrient limitation (Berger 1989). This condition controls organic matter (dissolved and particulate) production and export (Karl 1999), and influences physiological and ecological adaptations of photoautotrophic organisms (Karl *et al.* 2001).

In the North Pacific Subtropical Gyre (NPSG) low assimilation numbers (i.e. light-saturated rates of gross carbon fixation normalized to total Chl *a*) have been interpreted as evidence of nutrient limitation of photosynthetic processes (Karl *et al.* 1996, Letelier *et al.* 1996). However, large (< 200 and > 900 mg C $m^{-2}$ $d^{-1}$) aperiodic variations from long-term mean (450 mg C $m^{-2}$ $d^{-1}$) production rates have also been observed in the NPSG (DiTullio and Laws 1991, Karl *et al.* 2001). These variations span different temporal scales (days to months) and are related to a variety of independent physical forcing events (e.g., variations in isolume depths, internal waves, mesoscale eddies, planetary Rossby waves; Letelier *et al.* 2000, Karl *et al.* 2001, Vaillancourt *et al.* 2003, Sakamoto *et al.* 2004). Temporal fluctuations can alter the quantum yield of photosynthesis (herein identified as the *in situ* quantum efficiency of carbon fixation, ΦC, with units of mol C mol $quanta^{-1}$) of the photoautotrophic assemblage.

A comprehensive understanding of the environmental factors (abiotic and biotic) that control ΦC variability in the NPSG over high frequency temporal (hours to days) and small spatial (meters) scales has not yet been achieved due to methodological

limitations. The $^{14}C$ radiotracer method (Steeman Nielsen 1951) that is widely used to derive photosynthetic activity in the NPSG (Platt 1984, Jones *et al.* 1996, Karl *et al.* 1998) has limited temporal resolution due to the requirement for *in situ* incubation and even more limited spatially because only a few discrete depths are typically analyzed in a given oceanic profile (Peterson 1980). These same restrictions apply to the light-dark oxygen method (Williams *et al*. 2004) and the $H_2{}^{18}O$ technique (triple oxygen isotope) for estimation of gross primary production (Grande *et al.* 1989). The $H_2{}^{18}O$ method is an instantaneous measurement that does not require an incubation step (Juranek and Quay 2005); however, it has a 2-3 week integration time-scale so it cannot be used to resolve high frequency events. Such limitations can affect precision and accuracy in assessing water column integrated photosynthetic activity, when interpolating between discrete temporal and vertical measurements (or determinations), and ultimately limits our ability to provide meaningful ecological interpretations. Furthermore, this temporal limitation could significantly affect our understanding of the metabolic balance variability of the system and, in turn, may generate aliasing against sampling the community response to mesoscale perturbations, such as the passage of eddies or summer bloom events in the NPSG (Karl *et al.* 2003).

Fast Repetition Rate Fluorometry (FRRF) represents an alternative high resolution method to characterize both vertical and temporal scale variability of photosynthetic processes (Kolber and Falkowski 1993, Kolber *et al.* 1998). By assessing the photosynthetic efficiency of photosystem II (PSII), through rapid, *in situ*, repetitive measurements of the fluorescence yield after deactiving the majority of the PSII reaction centers, FRRF can resolve small vertical (meters) and temporal (seconds) scale, compared to tens of meters and hours/weeks for the $^{14}C$ and the $H_2{}^{18}O$ methods, respectively. In addition, other photosynthetic parameters, such as the functional cross

section of PSII ($\sigma_{PSII}$), the minimum turnover time of the photosynthetic unit ($\tau$), primary production versus irradiance (P vs. E) curves, electron transport rates (ETR) and gross oxygen evolution rates (GOE), can also be derived using FRRF measurements. Possible bias associated with the inclusion, isolation, trace metal toxicity and light shock during $^{14}C$ and the $H_2{}^{18}O$ incubations is also reduced in discrete FRRF sampling or eliminated altogether during *in situ* FRRF measurements. However, the FRRF method has also some technical limitations that should be taken into account when interpreting its measurements. The major limitations include the poor sensitivity at low Chl *a* concentrations (increase of the noise to signal ratio), lack of spectral resolution (flash energy centered at 470 nm) and the measurement restrictions to PSII and not PSI activity. Nevertheless, a comparison between primary productivity (PP) estimates from FRRF and $^{14}C$ at Sta. ALOHA has highlighted the FRRF potential to determine PP variations in this environment (Corno *et al.* 2006). Furthermore, this analysis revealed that $\sigma_{PSII}$ variability can play a significant role for the observed variability in PP at Sta. ALOHA.

Previous attempts to model primary productivity (PP) at Sta. ALOHA have highlighted the need to describe the variability of ΦC across different temporal and vertical scales, in order to obtain more accurate estimates from such models (Ondrusek *et al.* 2001). In the present study, time-series FRRF measurements (August 2002-December 2004) are presented to describe photosynthetic efficiency and variability across vertical scales not achievable by the $^{14}C$ and the $H_2{}^{18}O$ technique. These data are used to determine the environmental factors controlling photosynthetic efficiency variations at Sta. ALOHA. In particular, the potential role of chronic nutrient limitation and community structure in determining photosynthetic efficiency is explored.

## 4.3 Methods

*Field sampling*

Quasi-monthly, *in situ* nighttime (between 12.00 and 3.00 AM local time) FRRF measurements were obtained at Sta. ALOHA between September 2002 and December 2004, as part of the ongoing HOT Bio-optical component. A full description of the sampling procedure can be found in Corno *et al.* (2006). Briefly, a FAST-TrackA (Chelsea Instruments S/N 182047) FRR fluorometer with dual 'Light' and 'Dark' chambers was used to measure active fluorescence. The package was lowered at a constant speed of 10 $m \bullet min^{-1}$ to a final depth of approximately 250 m. This speed was empirically determined to: (i) best resolve the fluorescence response of small scale (~ 0.5 m) variations in photoautotrophic assemblages, (ii) allow enough time for the instrument to switch gains without losing significant vertical resolution, and (iii) obtain statistically significant fluorescence saturation curves.

The FRRF protocol consisted of a saturation phase, where 100 excitation flashlets were delivered within 100 μs, and a relaxation phase, where 20 excitation flashlets were delivered within 50 μs. Measurements of minimal and maximal fluorescence in dark-adapted state ($F_O$ and $F_M$, respectively), and a value termed the variable fluorescence ($F_V$), defined as the quantity [$F_M$-$F_O$], were obtained. The maximum change in the quantum yield of fluorescence (i.e. the efficiency of photosystem II (PSII), indicated by $F_V/F_M = (F_M - F_O)/ F_M$, the effective absorption cross-section for PSII, $\sigma_{PSII}$, and the minimum turnover time of electron transfer between reaction centers, ($\tau$), were also derived. A list of bio-optical terminology is given in Table 4.1. In order to obtain statistically significant fluorescence parameters in these low Chl *a* waters, the quality of the fitted saturation curves to the physiological model of Kolber *et al.* (1998) was analyzed for different instrument gains. Overall, the fluorescence saturation curves were statistically significant ($p$-value < 0.05, $n$= 4000) from the surface to ~200 m. Below 200

m, the fluorescence transients became noisy and lost statistical significance. The best fit to the model occurred at gain 16 and 64 (characteristics of the depth interval 60-160 m), while fluorescence transients at gain 256 (typical at surface to 60 m, and below 160 m) displayed a statistically significant fit but with higher variance (10-15% variance from physiological model of Kolber *et al.* (1998); Fig.4.1A). In order to asses the data quality for gain 256, fluorescence transients were analyzed in relation to the instrument response function (IRF) at gain 256 (Fig. 4.1B), using dilute concentrations of rhodamine B, an inert fluorophore (R-6626, Sigma Chemical; Laney 2003). Only samples where raw FRRF data-IRF were statistically greater than the IRF were considered as valid fluorescence transients; samples where no significant difference was found, were disregarded.

As part of the ongoing HOT program, nitrogen and phosphorus concentrations were determined during each cruise by chemiluminescence (Garside *et al.* 1982) and magnesium-induced coprepitation (MAGIC; Karl *et al.* 2001), respectively. Pigment concentrations were also determined by reverse-phase high performance liquid chromatography (HPLC) as described by Letelier *et al.* (1993) and modified by Bidigare *et al.* (1989). These dataset can be obtained from the Hawaii Ocean Time-series Data Organization & Graphical System (HOT-DOGS) at http://hahana.soest.hawaii.edu/hot/hot-dogs/interface.html. Potential density, salinity and temperature data for each cruise was also obtained from HOT-DOGS. Time-series of the mixed layer depth (MLD) were calculated from the HOT CTD data archive as the depth where an offset of 0.125 in potential density ($\sigma_\theta$) from the surface occurred. The top of the nutricline was calculated following the derivation by Letelier *et al.* (2004). Briefly, the top of the nutricline was determined by a cubic spline interpolation for near inertial oscillation depth

corrected [$NO_3^-$ + $NO_2^-$] and defined as the shallowest depth at which the [$NO_3^-$ + $NO_2^-$] depth gradient exceeded 2 nmol $kg^{-1}$ $m^{-1}$. The *in situ* light at depth *z* was obtained from the daily-integrated surface light value from the ship's LI-COR sensor and calculated using the appropriate extinction coefficient (0.039 and 0.044 for summer and winter, respectively; Letelier *et al.* 2004).

*FRRF blank determination*

After analyzing fluorescence traces (from a Sea-Bird 911 fluorometer) to 1000 m depth from past CTD profiles in the region, a fluorescence minimum was determined to be present between 200 to 300 m. Seawater from this depth interval was then collected and analyzed in the dark for both 'Light' and 'Dark' FRRF chambers for the different instrument gains. Similar measurements were made for water collected at 1000 m and for filtered (0.2 μm) seawater collected at 250 m. Seawater between 200 to 300 m had the lowest fluorescence signal (t-test, $p$-value$< 0.05$, $n= 12$). For each cruise, fluorescence transients below 200 m were then used as a correction blank. The difference between the 200-300 m fluorescence and the other two blanks may be due to different concentrations of dissolved chlorophyll, other compounds that contribute to soluble fluorescence or possible scattering. Although the blank correction used here does not take into account potential changes with pressure and temperature (however, accounts for possible temporal variations), it represents a practical solution to this critical correction when dealing with *in situ* fluorescence measurements, as highlighted by Cullen and Davis (2003).

*Data processing and Statistical analyses*

Data were downloaded from the FRR fluorometer and analyzed using the V6 software (provided by Sam Laney), which represents an updated version of the V5 (Laney 2003). The raw data were quality controlled (QC) by (i) disregarding fluorescence measurements that did not significantly fit the saturation curves to the physiological model of Kolber *et al.* 1989, and (ii) subtracting the mean of the blank for $F_O$ and $F_M$. The ratio $F_V/F_M$ was then recalculated using $F_O$ and $F_M$ values obtained after blank correction.

Least squares Model II regression analysis and multiple linear regression (MLR, complete and stepwise model) were applied to determine significant correlation coefficients between FRRF parameters (i.e. $F_V/F_M$ and $\sigma_{PSII}$) and biological (i.e. HPLC pigments concentrations), chemical (i.e. N+N and SRP concentrations) and physical factors (e.g. density, light, salinity, temperature). For each variable, conditions of linearity and normality were evaluated and, where needed (N+N and SRP), variables were log-transformed to adhere to these statistical conditions. For Model II regression, the geometric mean was used to estimate slope and intercept confidence interval (McArdle 2003). Significant seasonal and vertical differences for each FRRF parameters were tested by t-tests and the analysis of variance (ANOVA, type I).

## 4.4 Results

*General environmental characteristics*

Major nutrient concentrations (corrected for near-inertial oscillations, Letelier *et al.* 1996) were low in the upper 100 m during all the sampling period (Fig. 4.2 and 4.3). N+N concentrations were less than 10 nmol $kg^{-1}$, while SRP less than 50 nmol $kg^{-1}$. Below 100 m, N+N and SRP increased sharply to values greater than 800 and 100 nmol $kg^{-1}$, respectively (Fig. 4.2 and 4.3). The top of nutricline depth (defined here as in

Letelier *et al.* 2004) was on average around 100 ± 8 m (winter average 90 ± 8 m, $n$ = 6, summer average 115 ± 5 m, $n$ = 5).

Sea surface temperature (SST) varied between 26.6 and 23.3 ° C (September 2003 and January 2003, respectively), was higher in summer (25.9 ± 0.1 ° C, $n$ = 5) and decreased in winter (24.0 ± 0.1 ° C, $n$ = 6). The MLD varied between 20 and 105 m (July 2003 and January 2004, respectively). Shallower MLD occurred during summer months (41 ± 4 m, $n$ = 5), while deeper MLD were recorded during winter (78 ± 7 m, $n$ = 6).

The minimal ($F_O$) and maximal ($F_M$) fluorescence displayed similar temporal and vertical patterns. However, greater variability was associated with $F_O$ than $F_M$. $F_M$ increased with depth reaching maxima between 90 and 120 m (Fig. 4.4A). This layer of high chlorophyll *a* fluorescence, previously defined as the Deep Chlorophyll Maximum Layer (DCML, Letelier *et al.* 1996), was deeper in summer (120 ± 2 m, $n$ = 5) than in winter (100 ± 4 m, $n$ = 6).

*Temporal and vertical variability in photosynthetic efficiency, $F_V/F_M$*

$F_V/F_M$ was significantly lower at the surface (i.e. 0-10m) than at the base of the MLD and in the DCML layer (Table 4.2). In general, $F_V/F_M$ increased with depth, reaching maxima (0.55-0.60) at and below the DCML (Fig. 4.2 and 4.4B). Below these maxima, $F_V/F_M$ decreased with increasing depth to values indistinguishable from zero, where no active fluorescence was detected. This threshold depth ranged from 160 to 190 m (Fig. 4.4B).

This clear vertical pattern changed during January 2004, when upper water column $F_V/F_M$ increased to values not significantly different than those at the DCML (t-test, $p<0.05$, $n$ = 12), as a result of the mixed layer eroding the top of the nutricline (Fig. 4.3 and 4.4B). During this period, $F_V/F_M$ was fairly constant with depth. In contrast, when

the MLD was shallower than the nutricline (21 out of 22 times), a significant increase (p-value < 0.05, n= 21) in $F_V/F_M$ was observed from the MLD to layers (i.e. 10m) below the MLD (Fig. 4.3 and 4.4B).

In contrast to the well-defined $F_V/F_M$ vertical patterns, distinct temporal variations were not present. Significant seasonal patterns in $F_V/F_M$ were not found for time-series surface and DCML values (Fig. 4.5A). However, peaks in $F_V/F_M$ occurred during winter both at the surface and the DCML, while for the remaining of the year $F_V/F_M$ remained relatively constant.

*Temporal and vertical variability in absorption cross section ($\sigma_{PSII}$)*

Vertical patterns in $\sigma_{PSII}$ were, to a first approximation, the opposite of those observed for $F_V/F_M$. $\sigma_{PSII}$ decreased with depth reaching minima (1000 $m^2$ quanta $^{-1}$) around the DCML (Fig. 4.2 and 4.4C). Overall, $\sigma_{PSII}$ was significantly higher at the surface than at the base of the MLD and in the DCML layer (Table 4.2).

As observed for $F_V/F_M$, upper water column $\sigma_{PSII}$ were not significantly different (t-test, p<0.05, $n$ = 12) than those at the DCML during January 2004 (Fig. 4.3 and 4.4C). During this period, upper water column $\sigma_{PSII}$ decreased resulting in a constant trace without trend with depth. Time-series analysis also revealed that during summer 2003, surface and DCML $\sigma_{PSII}$ were significantly different (t-test, p<0.05, $n$ = 12), even though the MLD was shallower than the top of the nutricline. As for $F_V/F_M$, a significant change ($p$-value < 0.05, $n$= 21) in $\sigma_{PSII}$ (lower values) was observed below the MLD, when the MLD was shallower than the nutricline (Fig. 4.2 and 4.4C).

Unlike the lack of clear temporal $F_V/F_M$ variations, a significant (sinusoidal fit, $p$-value<0.05, $n$= 22) seasonal pattern in $\sigma_{PSII}$ was present at the surface but not at the DCML which showed seasonality (Fig 4.5B). At the surface, $\sigma_{PSII}$ maxima occurred

during winter, while minima during summer. In the DCML, $\sigma_{PSII}$ varied little with a minimum value observed during October 2004.

*Relationship between photosynthetic efficiency and chemical-physical factors*

Photosynthetic efficiency showed correlation with chemical but not physical factors. In particular, no significant relationships were found between FRRF parameters and temperature. On the other hand considering all the available datasets, $F_V/F_M$ was positively related to N+N but not to SRP; $\sigma_{PSII}$ was negatively related to both nutrients concentrations (Table 4.4 and Fig. 4.6). However, photosynthetic parameters were not significantly related to nutrients concentrations for surface and DCML samples, respectively.

In order to understand the potential influence of nutrient diffusion variability on the photosynthetic efficiency in the upper water column, the distance MLD-top of the nutricline was derived. Surface and mixed layer $F_V/F_M$ were negatively related to this distance, while a positive relationship was found for $\sigma_{PSII}$ at the base of MLD (Table 4.4 and Fig. 4.7). When the MLD was shallower than the top of the nutricline, both $F_V/F_M$ and $F_M$ in the mixed layer were significantly ($p$-value < 0.05, $n$= 1500, Fig. 4.8A) lower than at depth. However when the MLD > the top of the nutricline, no significant difference between $F_V/F_M$ in the mixed layer and below it was found (Fig. 4.8B).

To further determine the potential role of nutrient vs. light in controlling photosynthetic efficiency, variations in DCML depth (corrected for near inertial oscillations), nutrient and light were also compared to photosynthetic parameters changes in the DCML. No significant relationships were found (Fig. 4.9), between photosynthetic parameters and the physical and chemical factors in this layer.

*Photosynthetic efficiency and pigment concentrations*

Selected pigments, including chlorophyll *b* (Chl *b*, a biomarker for prochlorophytes), zeaxanthin (Zea, a biomarker for cyanobacteria), 19′ -hexanoyloxyfucoxanthin (19′ -Hex, a biormaker for prymnesiophyes) and fucoxanthin (Fuco, a biomarker for diatoms) (Mackey *et al.* 1996), were used to assess the role of assemblage composition in the variability of photosynthetic parameters at Sta. ALOHA. Multiple linear regression (MLR) model between pigments concentrations and $F_V/F_M$ was significant for DCML but not for surface samples (Table 4.5). The MLR model between pigments and $\sigma_{PSII}$ was not significant for both surface and DCML samples. In addition, no significant relationships were found between pigments concentrations and the MLD-nutricline distance and DCML position, respectively. Stepwise MLR indicated that together [Chl *b*] and [Zea] accounted for > 95 % of $F_V/F_M$ variability in the DCML. In this region, $F_V/F_M$ was positively and negatively related to [Chl *b*] and [Zea], respectively, while no significant relationship was found at the surface (Fig. 4.10 and Table 4.5). However, the pigment concentrations at the DCML are calculated through extrapolation and are subject to some uncertainty.

## 4.5 Discussion

A complete understanding of the role of microorganisms in global elemental cycles will require a characterization of the variability in key environmental processes that drive the fluxes of energy and elements through the ecosystem. Consequently, we need to understand the physical processes that create habitat variability and the range of biological response to it. Foremost in importance in ecosystem analysis is the response of

the photoautotrophic assemblage, the base of the food web. Quantitative relationships between environmental conditions and photosynthesis are required when trying to predict PP variations in relation to chemical-physical forcing. This present study provides information on these key aspects of ocean ecology at an oligotrophic site in the NPSG.

At Sta. ALOHA, the photosynthetic efficiency was low in the upper water column, but increased in the lower euphotic zone. This vertical difference appeared to be the result of two distinct environmental conditions. While a chronic substrate limitation seemed to control photosynthetic processes in surface layers, community structure changes appeared to contribute to the observed variability in photosynthetic efficiency in the lower euphotic zone. The vertical difference in photosynthetic efficiency and relative controlling factors has added a new prospective to the previously proposed two-layer model for this oligotrophic ocean (Coale and Bruland 1987, Small *et al.* 1987, Knauer *et al.* 1990, Harrison *et al.* 1992).

*Vertical gradient in photosynthetic efficiency and associated environmental forcing*

The photosynthetic efficiency, as indicated by $F_V/ F_M$, is a function of light, nutrients, temperature, species composition and the recent history of environmental conditions in a particular environment. At Sta. ALOHA, the overall photosynthetic efficiency appeared to be correlated mainly with the availability of nutrients (in particular, N+N; Fig. 4.6, Table 4.3). The maxima in $F_V/ F_M$ were observed at and below the top of the nutricline, consistent with previous laboratory and field studies for nutrient-replete photoautotrophs (Kolber and Falkowski 1993, Kolber *et al.* 1998, Suggett *et al.* 2003). These maxima occurred within a region in the euphotic zone (i.e. DCML) where the vertical diffusive flux of inorganic nutrients is greatest (Dore and Karl 1996). This

constant supply of inorganic substrate can induce a greater efficiency in photosynthetic processes.

The role of nutrients in controlling photosynthetic efficiency was also indicated by the significant relationships between surface photosynthetic parameters and the distance MLD- the top of the nutricline. Even though there is not a clear physical explanation to this relationship, this distance may serve as a proxy for the undetectable flux of nutrients into the euphotic zone. The significant relationship between this distance and surface photosynthetic efficiency can then be interpreted as indication of nutrient control on surface photosynthetic processes. This proxy, however, still requires a theoretical bio-physical derivation linking this distance to the vertical nutrient diffusive flux, as it assumes a negligible horizontal diffusion and constant entrainment in the MLD. Alternatively, the observed relationship between surface photosynthetic processes and the MLD- top of the nutricline distance could be linked to the activity of vertical migrants (i.e. diatoms containing $N_2$-fixing endosymbionts and *Trichodesmium* spp.) in relation to stratification dynamics by uncoupling the physical dependence of nutrient delivery in the upper water column (Karl *et al.* 1992). The role of nutrient availability in controlling surface photosynthetic efficiency is also supported by regression with other environmental parameters. The lack of significant relationships between (i) surface photosynthetic parameters vs. surface pigments concentrations and (ii) surface pigments concentrations vs. the distance MLD-nutricline suggests that variations in community structure were not significantly influencing the observed variability in surface photosynthetic efficiency. The effect of nutrient limitation was clear when, in January 2004, the MLD became deeper than the top of the nutricline (Fig. 4.3 and 4.4). Even though an increase in major nutrients was not detected in surface waters (Fig. 4.3), increased $F_V/ F_M$ and decreased $\sigma_{PSII}$ were characteristics of nutrient stress reduction

(Kolber and Falkowski 1993, Suggett *et al.* 2003). These results are in agreement with previous investigations in the NPSG (Vaillancourt *et al.* 2003), which showed surface $F_V/F_M$ changes in relation to the intrusion of deep nutrient-rich waters. During January 2004, nutrient concentrations remain unchanged; rapid nutrient uptake by nutrient-starved photoautotrophs may have quickly consumed the hypothesized increase in nutrient input (Letelier *et al.* 2000, Vaillancourt *et al.* 2003). These results suggest variations in upper water column FRRF parameters can be used as a potential proxy, not only for photoautotrophs activity, but also for perturbations by aperiodic physical forcing.

In addition to the role that nutrient status plays in surface photosynthetic efficiency, other environmental factors may also contribute to the observed variations in photosynthetic efficiency in the lower euphotic zone. At Sta. ALOHA, it appears that changes in community structure can influence photosynthetic efficiency in the DCML, where photosynthetic efficiency suggests nutrient replete conditions. The increase in prochlorophytes (i.e. [Chl *b*]) relative to cyanobacteria (i.e. [Zea]) was associated to a rise in photosynthetic efficiency, suggesting that floristic shifts may significantly affect the photosynthetic efficiency of the DCML. The relationship between photosynthetic efficiency and pigments could also be explained by the different fluorescence yield of each group. Different pigments composition can control the energy transfer and emission within PSII, and therefore the FRRF measurements (Suggett *et al.* 2001). Furthermore, under nutrient replete condition different species can have different $F_V/F_M$ (Letelier unpublished data). This taxon related variability must be taken into account when interpreting the observed $F_V/F_M$ variability in the DCML.

The decrease in photosynthetic efficiency below 160m can be related to concomitant decrease in light availability. In this region, even though the inorganic substrate is high (N+N and SRP > 800 and 150 kg $L^{-1}$, respectively), light driven

photosynthesis is low due to limited photon flux. The interaction between nutrient and light in controlling photosynthetic efficiency is shown by the relationship between $F_M$ (proxy for Chl a concentrations) and $F_V/F_M$ (Fig. 4.8). For similar low $F_M$, photosynthetic efficiency varied greatly ($F_V/F_M$ range 0.25-0.60), indicating the role of high light-low nutrient (low $F_V/F_M$ at the surface) vs. low light-high nutrient (low $F_V/F_M$ in the DCML) condition in influencing photosynthetic processes.

Similarly to $F_V/F_M$, $\sigma_{PSII}$ is also a function of light, nutrients, temperature, species and their relative environmental history. $\sigma_{PSII}$ is the rate of PSII RC closure per absorbed light, and it is a measure of the "functional size" of the pigment antenna in terms of its ability to close the functional reaction centers. A large $\sigma_{PSII}$ means large antenna relative to a small number of PSII RC (such as under nutrient depletion), and a small $\sigma_{PSII}$ means the antenna is small relative to large number of PSII RC (typical of high nutrient availability) (Kolber and Falkowski 1993). At the surface, high $\sigma_{PSII}$ confirmed a nutrient stress condition, as previously indicated by $F_V/F_M$ values (Fig. 4.2 and Table 4.2). High $\sigma_{PSII}$ values are consistent with previous patterns in nutrient-poor waters (Behrenfeld and Kolber 1999).

The lack of significant relationship between photosynthetic efficiency and inorganic P availability found here is in apparent contradiction with previous findings at Sta. ALOHA (Björkman *et al.* 2000, Björkman and Karl 2003), which suggests that in this ecosystem photoautotrophic activity is under P-control. In contrast, results of the present investigation suggest that inorganic N may be controlling photosynthetic processes (Fig. 4.6, Table 4.3). In order to reconcile this apparent discrepancy, three explanations may be invoked. Firstly, even though a significant relationship between inorganic P and surface photosynthetic parameters was not found for the available data sets, on average lower $F_V/F_M$ and higher $\sigma_{PSII}$ (characteristics of physiological stress

conditions) were associated with low P concentrations. (Fig.4.6). Furthermore, the availability of P within different pool from the one considered here (i.e. inorganic vs. organic) and the high recycling rate of particular P-rich compounds (i.e. nucleotides) may have confounded any possible relationships between photosynthetic efficiency and P availability. At Sta. ALOHA, a fraction DOP has been found to be bio-available to the microbial community (Björkman and Karl 2003), with potential implications in influencing photosynthetic efficiency. In this case, our sampling strategy and methodology were not adequate on appropriate temporal scales to determine the possible P-control on photosynthetic processes. Finally, the lack of a bio-physical theoretical basis linking P and Chl *a* fluorescence may be responsible for the observed independence between P availability and photosynthetic parameters. While a good bio-physical understanding between N, Fe availability and Chl *a* fluorescence exists (i.e. the role of N and Fe in Chl *a* synthesis, elemental constituents of RCII centers and electron transport chain; Kiefer and Reynolds 1992, Kolber and Falkowski 1993), intracellular P is more related to energy sources (ATP and NADPH) rather than to the bio-physical processes occurring in PSII, where mostly of Chl *a* fluorescence generates. Considering the above arguments, results presented here do not preclude a possible P-control of photosynthetic processes.

Light availability can also influence $\sigma_{PSII}$ (Kolber and Falkowski 1993) and this relationship could help explaining the temporal $\sigma_{PSII}$ variations. The seasonal cycle in surface $\sigma_{PSII}$ was approximately the inverse of the seasonal light cycle at Sta. ALOHA. The increase in surface $\sigma_{PSII}$ during winter can be interpreted as a light stress condition due to seasonal decrease in surface light and increased mixing (deeper MLD). Surface photoautotrophic population would increase $\sigma_{PSII}$ to maximize the probability of absorbed photons to reach a functional RC (and in turn, keeping photosynthetic processes

balanced). On the other hand, the light increase during summer would have induced a decrease in the functional size of the antenna, as photons densities became higher. The summer decrease in surface $\sigma_{PSII}$ could also be related to the increased activity in microbial $N_2$-fixation, typical of this region (Letelier and Karl 1996, Karl *et al.* 1997). The availability of new N to surface populations might have increased the fraction of functional RC (decrease $\sigma_{PSII}$). Alternatively, an increase in the relative contribution of cyanobacteria to the photosynthetic efficiency during these periods could affect our interpretation of $\sigma_{PSII}$ variability.

*An updated view of the oligotrophic two-layer model*

The vertical difference in photosynthetic efficiency at Sta. ALOHA can be interpreted in the context of a two-layer model for this oligotrophic area (Coale and Bruland 1987, Small *et al.* 1987, Knauer *et al.* 1990, Harrison *et al.* 1992). The distinction between (i) high recycling-low new production in the upper water column and (ii) low recycling-high new production in the lower euphotic zone, can be extended to photosynthetic efficiency. As the present results indicated, photosynthetic processes at Sta. ALOHA are more efficient in the lower than upper water column. The transition in photosynthetic parameters around MLD (Fig. 4.2 and 4.5) was a further indication of the physiological distinction between upper and lower layer. This transition may be triggered by (i) particle accumulation at this density surface (false benthos model) with enhanced re-cycling and substrate availability, (ii) increased diffusive flux below the MLD and (iii) a change in species composition.

The two-layer model for this oligotrophic region should also be considered in terms of photosynthetic temporal variability. At Sta. ALOHA, the higher temporal variability observed in photosynthetic processes in surface relative to deep layers

indicates a vertical difference in physiological and ecological stability (i.e. balance in photosynthetic processes, light absorption, transfer and utilization). In the DCML, low variability in photosynthetic efficiency implies that the energy transfer (i.e. electron flow) between photosystems is well coupled with relatively little loss of energy in the forms of heat and fluorescence. It also indicates that the light energy absorbed is efficiently utilized, suggesting a concomitant high yield in intracellular energy in the forms of ATP and NADPH derived from the light reactions of photosynthesis. Conversely, the high variability in the upper water column means an unbalance between the capture and utilization of light within PSII RC.

The vertical gradient in photosynthetic efficiency could also be related to vertical difference in photoautrophs community structure in the NPSG (Venrick 1988, 1990). The vertical distribution of key photoautotrophs species indicates that a significant distinction between shallow and deep flora occurs in this environment (Venrick 1982, 1990). As different species have different fluorescence yields (therefore $F_V/ F_M$ and $\sigma_{PSII}$), the observed vertical gradient in photosynthetic efficiency may be partly controlled by this floristic shift. In this context, at Sta. ALOHA, the FRRF signal is mainly dominated by *Prochlorococcus* spp. fluorescence (Campbell *et al.* 1994), even though its relative Chl a fluorescence will be lower than for other eukaryotic cells, because of phycobilisomes and a Chl a/b antennae present in *Prochlorococcus* spp. (Moore *et al*. 1995, Ting *et al.* 2001). The vertical transition between physiologically distinct surface and deep *Prochlorococcus* spp. populations (Moore *et al*. 1995) could then account for some of the observed FRRF parameters variability. Furthermore, the relative increase of picoeukaryotes in the lower euphotic at Sta. ALOHA (Campbell *et al.* 2004) might be also related to vertical gradient in photosynthetic efficiency, as eukaryotes tend to have higher $F_V/ F_M$ under nutrient replete conditions than prokaryotes (Suggett *et al.* 2003).

*Theoretical considerations*

It is important to quantify, if possible, the effect of photosynthetic variability in terms of C or $O_2$ fluxes. FRRF derived parameters have been used to estimate ETR and GOE at Sta. ALOHA (Corno *et al.* 2006). To a first approximation, the equations used are (Kolber *et al.* 2000, Kolber and Falkowski 1993),

$$ETR\ (z) = E(z)\ \sigma_{PSII}\ (z)\ qP\ (z)\ n_{PSII}\ (F_V/F_M\ (z)\ /0.65) \qquad \text{(Eq. 1)}$$

$$GOE\ (z) = 2.0256 \times 10^{-8}\ E\ (z)\ qP\ (z)\ F_V/F_M\ (z)\ \sigma_{PSII}\ (z)\ [\text{chl } a]\ (z)\ \Phi_e\ n_{PSII}$$

(Eq.2) E(z) is the *in situ* light at depth z, qP the photochemical quenching (assumed to be 1 for the present calculation), $n_{PSII}$ the photosynthetic unit size of PSII (assumed to be 300 chl *a*•$RCII^{-1}$ for this particular oceanic environment, characteristic of prokaryotes, Falkowski *et al.* 1981), [chl *a*] (z) the chlorophyll *a* concentration at depth z, and $\Phi_e$ the photon yield of electron transfer by PSII (unity for the present calculation). The constant $2.0256 \times 10^{-8}$ includes the following conversions: $10^{20}$ photons•$m^{-2}$, 3600 s•$h^{-1}$, $6.023 \bullet 10^{23}$ molecules•$mol^{-1}$, and 892 g chl *a*•$mol^{-1}$. It also assumes that four photons are delivered to reaction centers (RCII) per $O_2$ molecule evolved and that the maximum value of $F_V/F_M(z)$ equals 0.65 (Kolber and Falkowski 1993).

Given the significant relationship between surface $F_V/F_M$ and the MLD- the top of the nutricline distance (Fig. 4.7 and Table 4.4), theoretical ETR and GOE change can be predicted (assuming constant light and a not significant variation in [chl *a*]) in relation to surface $F_V/F_M$ variations, when MLD is equal to the top of the nutricline depth. Such calculation represents the physical threshold for a possible nutrient input into the MLD. When the MLD is equal to the top of the nutricline depth (i.e. y-intercept equals to 0.44 $F_V/F_M$), a significant change of 0.07 $F_V/F_M$ from average surface values (Table 2) occurs.

As $\sigma_{PSII}$ was not found to change significantly in relation to MLD and the top of the nutricline dynamics (Table 4.3), the $F_V/F_M$ change reflects a theoretical 18-20% increase in ETR and GOE. Such theoretical derivation agrees remarkably well with independent observations of FRRF changes (0.06 $F_V/F_M$) in relation to nutrient input in surface waters (Vaillancourt *et al.* 2003). Furthermore, this theoretical increase in ETR and GOE is consistent with independent calculations of primary productivity changes (20-25%) in relation to nutrient input in the MLD at Sta. ALOHA due to Rossby waves (Sakamoto *et al.* 2004); this theoretical variation is also well related with an approximate 20% increase in ATP concentrations observed in the upper water column during December-January 2004 at Sta. ALOHA (data not shown). ETR and GOE can be interpreted as the total available intracellular energy; portion of this energy will be in form of ATP and, therefore, related to ETR and GOE variations. Even though this calculation does not take into account possible changes in qP, integrated light, [chl *a*] and photorespiration, it represents a theoretical prediction for surface ETR and GOE changes at Sta. ALOHA in relation to the physical mediated upward flux of nutrients. The fluorescence yield change observed here is lower than the change (3 fold increase) in passive chlorophyll fluorescence efficiency recorded at Sta. ALOHA during the passage of a mesoscale cyclonic eddy (Letelier *et al.* 2000). This difference can be explained mainly by the different methodological approaches (i.e. active vs. passive fluorescence).

Similar theoretical considerations can be made for ETR and GOE variations in the DCML. In theory, when the DCML community becomes dominated by prochlorophytes in relation to cyanobacteria (i.e. increase in Chl b compared to Zea), a change in 0.10 $F_V/F_M$ could take place (Fig. 4.10 and Table 4.5). Based on the same assumptions of the previous calculation, this variation indicates a theoretical increase of 20% in ETR and

GOE in the DCML. These values are within the range of the measured seasonal change in $^{14}$C-based PP at Sta. ALOHA in the DCML (Karl *et al.* 2002).

Variations in fluorescence yields can also be related to the changes in ΦC. Even though a theoretical derivation of ΦC from the fluorescence yield is still pending, the fluorescence yield ($F_V/F_M$) can be used as a proxy for ΦC (Kiefer and Reynolds 1992, Kolber and Falkowski 1993). At Sta. ALOHA, ΦC temporal and vertical variability has been suggested as a possible cause for the observed aperiodic PP changes (Karl *et al.* 2001) and for poor performance of a PP model (Ondrusek *et al.* 2001). Based on the present results, models that assume a constant vertical ΦC may generate error source (between 50-70%), as $F_V/F_M$ display some clear vertical gradients that should be taken into account in order to produce more reliable predictions. Furthermore, even though a predictable seasonal pattern in $F_V/F_M$ was not found, the observed $F_V/F_M$ temporal variability (Fig. 4.5) should also be considered when trying predicting temporal ΦC variations. Finally, it is also important noting that the vertical $F_V/F_M$ gradient (i.e. $\partial F_V/F_M / \partial z$) was not temporally variable, with the exception during the deep mixing event.

*Ecological implications*

The vertical gradient in photosynthetic efficiency has important implications for trophic dynamics and biogeochemical cycling for this particular ecosystem. The low photosynthetic efficiency suggests that chronic nutrient limitation restricts significantly the photosynthetic apparatus activity of the surface photoautotrophic assemblage through time. This effect would be most likely found in the molecular composition of RC (N requirements for PSII RC) and of electron transport carries (Fe requirements), as at Sta. ALOHA the majority of Fe in the MLD is considered to be in colloidal form and,

therefore, not ready available to photoautotrops (Wu *et al.* 2001). This inefficiency can influence the flux of energy to higher and lower trophic levels in surface waters. Conversely, the high photosynthetic efficiency observed in the DCML suggests high growth rates. These results are in agreement with independent growth rate estimates of *Prochlorococcus* spp. and other phototrophic eukaryotes for this environment (Laws *et al.* 1987, Jones *et al.* 1996, Liu *et al.* 1997). Since photoautotrophs standing stock in this layer remains relatively constant, the high photosynthetic efficiency implies rapid turnover of carbon (and associated bioelements) and the importance of a removal process (both grazing and sinking).

Photosynthetic processes variations in relation to environmental forcing have highlighted the important role of physical perturbations and community structure in influencing photosynthetic processes at Sta. ALOHA. The relative rapid photosynthetic response following a perturbation (MLD becoming deeper than the top of the nutricline) in the upper water column confirms that surface layers are dynamic systems with fast physiological responses. Such rapid changes in photoautotrophs activity could have important consequences for biological processes, such as bloom formation (by uncoupling respiration and photosynthesis), bacteria-photoautorophs interactions and larval survival. As suggested by Karl *et al.* (2003), sudden variations in photoautotrophs activity can control the metabolic balance of this ecosystem, with implications for $CO_2$ atmosphere-ocean fluxes. In addition, the relationship between community structure and photosynthetic efficiency in the DCML highlights the importance of succession in ecosystems dynamics. Environmental pressure controlling the abundance of prochlorophytes vs. cyanobacteria may result in a significant change in photoautotrophs community activity, with implications for this system efficiency.

To further understand the role of environmental pressure on photosynthetic and ecological processes in this oligotrophic region, future FRRF studies should be focused in understanding the possible relationship between the availability of different P forms (inogarnic vs. organic) and fluorescence transients. Such endeavor will help determining the role of P in influencing photosynthetic efficiency and photoautotrophic activity. The role of different photoautotrophic groups in controlling FRRF variations should also be investigated in order to understand the role of community shifts in photoautotrophic productivity of this ecosystem.

**4.6 Reference**

Baines, S. and Pace, M.L. 1991. The production of dissolved organic matter by phytoplankton and its importance to bacteria: patterns across marine and freshwater systems. *Limnol. Oceanogr*. **36**: 1078-1090.

Behrenfeld, M.J. and Kolber, Z.S. 1999. Widespread Iron Limitation of Phytoplankton in the South Pacific Ocean. *Science* **283**: 840- 843.

Berger, W.H. 1989. Global maps of ocean productivity. In : *Productivity of the ocean: Present and past*, Berger, W.H., Smetacek, V.S. and Wefer, G., editors, John Wiley and Sons, New York, 429-455.

Bidigare, R.R., Schofield, O. and Prezelin, B.B. 1989. Influence of zeaxanthin on quantum yield of photosynthesis of *Synechoccocus* clone WH7803 (DC2). *Mar. Ecol. Prog. Ser.* **56**: 177-188.

Björkman, K.M., Thomson-Bulldis, A.L. and Karl, D.M. 2000. Phosphorous dynamics in the North Pacific subtropical gyre. *Aquatic Microb. Ecol.* **22**: 185-198.

Björkman, K.M. and Karl, D.M. 2003. Bioavailability of dissolved organic phosphorous in the euphotic zone at Station ALOHA, North Pacific Subtropical Gyre. *Limnol. Oceanogr.* **48**: 1049-1057.

Campbell, L., Nolla, H.A. and Vaulot, D. 1994. The importance of *Prochlorococcus* to community structure in the central North Pacific Ocean. Limnol. Oceanogr. **39**: 954-961.

Corno, G., Letelier, R.M., Abbott, M.R. and Karl, D.M. 2006. Assessing the temporal variability of primary production in the North Pacific Subtropical Gyre: A comparison of Fast Repetition Rate Fluorometry and $^{14}C$ measurements. *J. of Phyc.* **42**: 51-60.

Coale, K.H. and Bruland, K.W. 1987. Oceanic stratified euphotic zone as elucidated by $^{234}Th$:$^{238}U$ disequilibria. *Limnol. Oceanogr.* **32**: 189-200

Cullen, J.J. and Davis, R.E. 2003. The blank can make a big difference in oceanographic measurements. *Limnol. Oceanogr. Bull.* **12**: 29-35.

DiTullio, G.R. and Laws, E. A. 1991. Impact of an atmospheric-oceanic disturbance on phytoplankton community dynamics in the North Pacific Central Gyre. *Deep-Sea Res. I* **38**: 1305-1329.

Dore, J. E. and Karl, D.M. 1996. Nitrite distributions and dynamics at Station ALOHA. *Deep-Sea Res. II* **43**: 385-402.

Falkowski, P.G. 1981. Light-shade adaptation and assimilation numbers. *J. Plankton Res.* **3**: 203-216.

Falkowski, P.G., Barber R.T. and Smetacek V**.** 1998. Biogeochemical controls and feedbacks on ocean primary production. *Science* **281**: 200–206.

Garside, C. 1982. A chemiluminescent technique for the determination of nanomolar concentrations of nitrate and nitrite in seawater. *Mar. Chem.* **11**:

159-167.

Grande, K., Williams, P. J. LeB., Marra, J., Eppley, R. and Bender, M. 1989. Primary production in the North Pacific Gyre: A comparison of rates determined by the $^{14}C$, $CO_2$, and $^{18}O$ methods. *Deep-Sea Res. I* **36**: 1621-1634.

Harrison, W.G., Harris, L.R., Karl, D.M., Knauer, G.A. and Redalje, D.G. 1992. Nitrogen dynamics at the VERTEX time-series site. *Deep-Sea Res. I* **39**: 1535-1552.

Hebel, D.V. and Karl, D.M. 2001. Seasonal, interannual and decadal variations in particulate matter concentrations and composition in the subtropical North Pacific Ocean. *Deep-Sea Res. II* **48**: 1669-1697.

Jones, D.R., Karl, D.M. and Laws, E.A. 1996. Growth rates and production of heterotrophic bacteria and phytoplankton in the North Pacific subtropical gyre. *Deep-Sea Res. I* **43**: 1567-1580.

Juranek, L.W. and Quay, P.D. 2005. In vitro and in situ gross primary and net community production in the North Pacific Subtropical Gyre using labeled and natural abundance isotopes of dissolved O2. *Glob. Biogeochem. Cycl.* **19**: 2384-2399.

Karl, D. M., Letelier, R.M., Hebel D.V., Bird, D.F. and Winn, C.D. 1992. *Trichodesmium* blooms and new nitrogen in the north Pacific gyre. In E. J. Carpenter, D. G. Capone and J. G. Rueter (eds.), Marine pelagic cyanobacteria: Trichodesmium and other diazotrophs, pp.219-237. Kluwer Academic Publishers, The Netherlands.

Karl, D.M., 1999. A sea of change: biogeochemical variability in the North Pacific Subtropical Gyre. *Ecosystems* **2**: 181-214.

Karl, D.M. 2002. Nutrient dynamics in the deep blue sea. *Trends in Microbiology* **10**: 410-418.

Karl, D. M., Christian, J.R. Dore, J.R., Hebel, D.V., Letelier, R.M., Tupas, L.M. and Winn, C.D. 1996. Seasonal and interannual variability in primary production and particle flux at Station ALOHA. *Deep-Sea Res. II* **43**: 539-568.

Karl, D.M., Letelier, R.M., Tupas, L., Dore, J., Christian, J. and Hebel, D. 1997. The role of nitrogen fixation in biogeochemical cycling in the subtropical North Pacific Ocean. *Nature* **388**: 533-538.

Karl, D.M., Hebel, D.V., Bjorkman, K. and Letelier, R.M. 1998. The role of dissolved organic matter release in the productivity of the oligotrophic North Pacific Ocean. *Limnol. Oceanogr.* **43**: 1270-1286.

Karl, D.M., Bidigare, R.R. and Letelier, R.M. 2001. Long-term changes in plankton community structure and productivity in the North Pacific Subtropical Gyre: The domain shift hypothesis. *Deep-Sea Res. II* **43**: 539-568.

Karl, D.M., Bidigare, R.R. and Letelier, R.M. 2002. Sustained and Aperiodic Variability in Organic Matter Production and Phototrophic Microbial Community Structure in the North Pacific Subtropical Gyre. In: P. J. le B. Williams, D. R. Thomas and C. S. Reynolds, Eds., Phytoplankton Productivity and Carbon Assimilation in Marine and Freshwater Ecosystems, Blackwell Publishers, London, 222-264.

Karl, D.M., Laws, E.A., Morris, P., Williams, P.J. le B. and Emerson, S. 2003. Metabolic balance of the open sea. *Nature* **426**: 32.

Kiefer, D.A. and Reynolds, R.A. 1992. Advances in understanding phytoplankton fluorescence and photosynthesis. *In* Falkowski, P.G. & Woodhead, A.D. [Eds] *Primary Productivity and Biogeochemical Cycles in the Sea.* Plenum Press, New York, pp 155-174.

Knauer, G.A., Redalje, D.G., Harrison, W.G. and Karl, D.M. 1990. New production at the VERTEX time-series site. *Deep-Sea Res. I* **37**: 1121-1134.

Kolber, Z.S. and Falkowski, P.G. 1993. Use of active fluorescence to estimate phytoplankton photosynthesis *in situ*. *Limnol. Oceanogr.* **38**: 1646-1665.

Kolber, Z.S., Prasil, O., Falkowski, P.G. 1998. Measurements of variable chlorophyll fluorescence using fast repetition rate techniques: defining methodology and experimental protocols. *Biochim. et Biophys. Acta* **1367**: 88-106

Kolber, Z.S., van Dover, C.L., Niederman, R.A. and Falkowski, P.G. 2000. Bacterial photosynthesis in surface waters of the open ocean. *Nature* **407**: 177-179.

Laney, S.R. 2003. Assessing the error in photosynthesis properties determined by fast repetition rate fluorometry. *Limnol. Oceanogr.* **48**: 2234-42.

Laws, E.A. 1987. High phytoplankton growth and production rates in the North Pacific Subtropical Gyre. *Limnol. Oceanogr.* **32**: 905-918.

Letelier, R.M., Bidigare, R.R., Hebel, D.V., Ondrusek, M., Winn, C.D. and Karl, D.M. 1993. Temporal variability of phytoplankton community structure based on pigment analysis. *Limnol. Oceanogr.* **38**: 1420-37.

Letelier, R.M., and Karl, D.M. 1996. The role of *Trichodesmium* spp. in the productivity of the subtropical North Pacific Ocean. *Mar. Ecol. Prog. Ser.* **133**: 263-273.

Letelier, R.M., Dore, J.E., Winn, C.D. and Karl, D.M. 1996. Seasonal and interannual variations in autotrophic carbon assimilation at Station ALOHA. *Deep-Sea Res. II* **43**: 467-490.

Letelier, R.M, Karl, D.M., Abbott, M.R., Flament, P., Freilich, M., Lukas, R. and Strub, T. 2000. Role of late winter mesoscale events in the biogeochemical variability of the upper water column of the North Pacific Subtropical Gyre. *J. of Geophys. Res.* **105**: 28,723-28,740.

Letelier, R.M, Karl, D.M., Abbott, M.R. and Bidigare, R.R. 2004. Light driven seasonal patterns of chlorophyll and nitrate in the lower euphotic zone of the North Pacific Subtropical Gyre. *Limnol. Oceanogr.* **49**: 508-519.

Liu, H., Nolla, H.A. and Campbell, L. 1997. *Prochlorococcus* growth rate and contribution to primary production in the equatorial and subtropical North Pacific Ocean. *Aquat. Micr. Ecol.* **12**: 39-47.

Mackey, M.D., Mackey, D.J., Higgins, H.W. and Wright, S.W. 1996. CHEMTAX- a program for estimating class abundances from chemical markers: application to HPLC measurements of phytoplankton. *Mar. Ecol. Prog. Ser.* **144**: 265-283.

McArdle, B.H. 2003. Lines, models, and errors: regression in the field. *Limnol. Oceanogr.* **48**: 1363-1366.

Moore, L.R., Goericke, R. and Chisholm, S.W. 1995. Comparative physiology of *Synechococcus* and *Prochlorococcus*: influence of light and temperature on growth, pigments, fluorescence and absorptive properties. *Mar. Ecol. Progr. Ser.* **116**: 259-275.

Ondrusek, M. E., Bidigare, R., Waters, K. and Karl, D.M. 2001. A predictive model for estimating rates of primary production in the subtropical North Pacific Ocean. *Deep-sea Res. II* **48**: 1837-1863.

Peterson, B.J. 1980. Aquatic primary productivity and $^{14}C$-$CO_2$ method: A history of the productivity problem. *Annual Rev. Ecol. Syst.* **11**: 359-385.

Platt, T. 1984. Primary productivity in the central North Pacific: comparison of oxygen and carbon fluxes. *Deep-Sea Res. I* **31**: 1311-1319.

Sakamoto, C. M., Karl, D. M., Jannasch, H. W., Bidigare, R. R., Letelier, R. M., Walz, P. M., Ryan, J. P., Polito, P. S. and Johnson, K. S. 2004. Influence of Rossby waves

on nutrient dynamics and the plankton community structure in the North Pacific subtropical gyre. *J. Geophys. Res.* **109**: 1976-1988.

Small, L.F., Knauer, G.A. and Tuel, M.D. 1987. The role of sinking fecal pellets in stratified euphotic zone. *Deep-Sea Res. I* **34**: 1705-1712.

Steeman-Nielsen, E. 1951. Measurement of the production of organic matter in the sea by means of carbon-14. *Nature* **167**: 684-685.

Suggett, D.J., Kraay, P., Holligan, P., Davey, M., Aiken, J. and Geider, R. 2001. Assessment of photosynthesis in a spring cyanobacterial bloom by use of a fast repetition rate fluorometer. *Limnol. Oceanogr.* **46**: 802-810.

Suggett, D.J., Oxborough, K., Baker, N.R., Macintyre, H.L., Kana, T.M. and Geider, R. J. 2003. Fast repetition rate and pulse amplitude modulation chlorophyll *a* fluorescence measurements for assessment of photosynthetic electron transport in marine phytoplankton. *Europ. J. of Phycol.* **38**: 371-384.

Ting, C.S., Rocap, G., King, J. and Chisholm, S.W. 2001. Phycobiliprotein genes of the marine photosynthetic prokaryote *Prochlorococcus*: evidence for rapid evolution of genetic heterogeneity. *Microbiology* **147**: 3171-3182.

Turpin, D.H. 1991. Effects of inorganic N availability on algal photosynthesis and carbon metabolism. *J. of Phyc.* **27**: 14-20.

Vaillancourt, R.D., Marra, J., Seki, M.P., Parsons, M.L. and Bidigare, R.R. 2003. Impact of a cyclonic eddy on phytoplankton community structure and photosynthetic competency in the subtropical North Pacific Ocean. *Deep Sea-Res. I* **50**: 829-847.

Venrick, E.L. 1988. The vertical distributions of chlorophyll and phytoplankton species in the North Pacific central environment. *J. of Plankton Res.* **10**: 987-998

Venrick, E.L. 1990. Phytoplankton in an oligotrophic ocean: species structure and interannual variability. *Ecology* **71**: 547-563.

Williams, P.J. le B., Morris, P.J. and Karl, D.M. 2004. Net community production and metabolic balance at the oligotrophic ocean site, station ALOHA. *Deep Sea-Res I* **51**: 1563-1578.

Wu, J., Boyle, E., Sunda, W. and Wen, L. 2001. Soluble and colloidal iron in the Oligotrophic North Atlantic and North Pacific. *Science* **293:** 847-849.

Tables

Table 4.1. Definitions of bio-optical, environmental and productivity parameters used in the text.

| Parameter | Definition | Units |
|---|---|---|
| E | Irradiance | μmol photons•$m^{-2}$•$s^{-1}$ |
| $F_O$ , $F_M$ | Initial and maximal fluorescence yield in absence of non-photochemical quenching | relative |
| $F_V$ | Variable fluorescence yield in dark adapted condition, derived as ($F_M$ - $F_O$) | relative |
| $F_V/F_M$ | Potential photochemical efficiency of open RCIIs normalized to FM in dark adapted condition | dimensionless |
| qP | Photochemical quenching | between 0 and 1 |
| $\sigma_{PSII}$ | Effective absorption cross section of PSII in dark adapted condition | $10^{-20}$•$m^2$•$quanta^{-1}$ |
| $n_{PSII}$ | Photosynthetic unit size of PSII | mol RCII•mol chl $a^{-1}$ |
| τ | Electron turnover rate per functional PSII | μs |
| $\Phi_e$ | Photon yield of electron transfer by PSII | mol $O_2$•mol $photon^{-1}$ |
| ΦC | Quantum yield of photosynthesis | mol C mol $quanta^{-1}$ |
| ETR | Electron transport rate | e•mol chl *a*•mol $RCII^{-1}$•$s^{-1}$ |
| GOE | Gross oxygen evolution rates | mol $O_2$•$m^{-3}$•$h^{-1}$ |

Table 4.2. Vertical variations (refer to text for definition of vertical interval) in average $F_V/F_M$ and $\sigma_{PSII}$ at Sta. ALOHA from August 2002 to December 2004. Values represent the mean and 1 SE for each vertical interval. For each variable, common letters indicate no statistically significant difference between values (ANOVA and t-test, $p<0.005$).

| | Surface | Base ML (± 5m) | DCML |
|---|---|---|---|
| $F_V/F_M$ | $0.37 \pm 0.01$ [a] | $0.46 \pm 0.01$ [b] | $0.55 \pm 0.01$ [c] |
| $\sigma_{PSII}$ | $1780 \pm 60$ [a] | $1630 \pm 62$ [b] | $1430 \pm 50$ [c] |

Table 4.3. Statistical parameters for model II linear regression between FRRF parameters and nutrient concentrations at Sta. ALOHA from August 2002 to December 2004. For each significant regression, the slope and confidence interval (CI), the y-intercept, the $r^2$ and *p*-value are given.

| | $F_V/F_M$ | | $\sigma_{PSII}$ | |
|---|---|---|---|---|
| | Log N+N | SRP | Log N+N | SRP |
| Slope | 0.034 | 0.10 | -134 | -4.60 |
| y-intercept | 0.41 | 0.09 | 1852 | 1800 |
| CI Slope | 0.004 | 0.02 | 20 | 0.10 |
| $r^2$ | 0.57 | 0.10 | 0.20 | 0.26 |
| *p*-value | <0.05 | NS | <0.05 | <0.05 |

Table 4.4. Statistical parameters for model II linear regression between FRRF parameters and the distance MLD- top of the nutricline (refer to text for definition) for different depth interval at Sta. ALOHA from August 2002 to December 2004. For each significant regression, the slope and confidence interval (CI), the y-intercept, the $r^2$ and *p*-value are given.

| | $F_V/F_M$ | | $\sigma_{PSII}$ | |
|---|---|---|---|---|
| | Surface | Base ML (± 5m) | Surface | Base ML (± 5m) |
| Slope | -0.0024 | -0.0029 | NS | 983 |
| y-intercept | 0.44 | 0.60 | NS | 22 |
| CI Slope | 0.007 | 0.008 | NS | 250 |
| $r^2$ | 0.60 | 0.74 | NS | 0.63 |
| *p*-value | <0.05 | <0.05 | NS | <0.05 |

Table 4.5. (a)Statistical parameters for multiple linear regressions between FRRF parameters and selected pigment concentrations at Sta. ALOHA from August 2002 to December 2004. (b) Statistical parameters for model II linear regression between photosynthetic efficiency ($F_V/F_M$) and [Chl *b*] and [Zea] in the DCML at Sta. ALOHA from August 2002 to December 2004. For each significant regression, the slope and confidence interval (CI), the y-intercept, the $r^2$ and *p*-value are given.

(a)

| | Surface | DCML |
|---|---|---|
| | $F_V/F_M$ | $F_V/F_M$ |
| $\beta_0$ | 0.60 | 0.50 |
| $\beta_1$ (Log Chl *a*) | -0.07 | -0.03 |
| $\beta_1$ (Log Chl *b*) | -0.01 | 0.02 |
| $\beta_2$ (Log 19-Hex) | 0.04 | -0.05 |
| $\beta_3$ (Zea) | -0.01 | -0.01 |
| $\beta_4$ (Fuco) | -0.01 | 0.01 |
| $r^2$ | 0.20 | 0.60 |
| *p*-value | NS | <0.05 |

(b)

| | $F_V/F_M$ | |
|---|---|---|
| | [Chl *b*] | [Zea] |
| Slope | 0.005 | -0.002 |
| y-intercept | 0.43 | 0.61 |
| CI Slope | 0.001 | 0.0001 |
| $r^2$ | 0.57 | 0.67 |
| *p*-value | <0.05 | <0.05 |

**4.7 Figure Legend**

Figure 4.1. Variations in the fluorescence yield, F (i.e. obtained by the ratio emission to excitation flashlets, EM/EX), induced by the saturation FRRF protocol used at Sta. ALOHA for different gain instrument (a). Black lines for each saturation curve represent the physiological model used to derive fluorescence parameters (Kolber *et al.* 1998). (b) Representative FRRF transients for gain 256 at Sta. ALOHA for raw and corrected data (i.e. raw data – IRF at gain 256).

Figure 4.2. Vertical profiles of temperature, N+N, SRP (a), $F_O$ and $F_M$ (b), $F_V/F_M$ (c) and $\sigma_{PSII}$ (d) at Sta. ALOHA during HOT-146 (March 2003). In panel (a) each tick corresponds to 2 °C for temperature (range 15-25 °C), 240 nmol kg $^{-1}$ for N+N (range 0-1200 nmol kg $^{-1}$) and 40 nmol kg $^{-1}$for SRP (range 0-200 nmol kg$^{-1}$). In the fluorescence plots (b, c, d), errors bars represent the ± 1 standard error, the solid line represents the 4-point running average and the horizontal dash line is the MLD.

Figure 4.3. Vertical profiles of temperature, N+N, SRP (a), $F_O$ and $F_M$ (b), $F_V/F_M$ (c) and $\sigma_{PSII}$ (d) at Sta. ALOHA during HOT-155 (January 2004). In panel (a) each tick corresponds to 2 °C for temperature (range 15-25 °C), 240 nmol kg $^{-1}$ for N+N (range 0-1200 nmol Kg $^{-1}$) and 40 nmol kg $^{-1}$for SRP (range 0-200 nmol kg$^{-1}$). In the fluorescence plots (b, c, d), error bars represent the ± 1 standard error, the solid line represents the 4-point running average and the horizontal dash line is the MLD.

Figure 4.4. Vertical and temporal variability in $F_M$ (a), $F_V/F_M$ (b) and $\sigma_{PSII}$ (c) at Sta. ALOHA from August 2002 to December 2004. Contours are 0.1 relative units for $F_M$, 0.05 dimensionless units for $F_V/F_M$ and 250 m$^2$ PSII $^{-1}$ for. White lines are isopycnal every 0.25 kg/m$^3$.

Figure 4.5. Temporal variation in $F_V/F_M$ and $\sigma_{PSII}$ at the surface (a) and at the DCML (b) at Sta. ALOHA from August 2002 to December 2004. Dashed vertical lines for each plot indicate the end of year. Error bars represent the ± 1 standard error.

Figure 4.6. Relationship between N+N, SRP and $F_V/F_M$ (a and b, respectively) and $\sigma_{PSII}$ (c and d, respectively) at Sta. ALOHA for the complete dataset. For each plot, mean and standard deviation for surface and DCML samples, respectively, are plotted by the red line. The statistical parameters for the regression are given in Table 2.

Figure 4.7. Relationship between $F_V/F_M$, $\sigma_{PSII}$ and the distance from the MLD to the nutricline (as defined in the text) for the surface (a and c, respectively) and the MLD (b and d, respectively) samples, respectively. Error bars represent the ± 1 standard error. The statistical parameters for the regression are given in Table 3.

Figure 4.8. Relationship between $F_V/F_M$ and $F_M$ at Sta. ALOHA when the MLD was shallower (a, HOT-146) and deeper (b, HOT-155) than the nutricline, respectively.

Figure 4.9. DCML $F_V/F_M$ and $\sigma_{PSII}$ at plotted against the mean DCML depth (corrected for near-inertial oscillation) (a and d, respectively), N+N (b and e, respectively) and light (c and f, respectively). Error bars represent the ± 1 standard error. All regressions were not significant.

Figure 4.10. Relationship between concentrations of Chl *b*, Zeaxanthin and $F_V/F_M$ for surface (a and c, respectively) and DCML (b and d, respectively) samples, respectively, at Sta. ALOHA for the complete dataset. Error bars represent the ± 1 standard error. For surface samples, all regressions were not significant. For the DCML samples, the statistical parameters for the regression are given in Table 4.

Figure 4.1

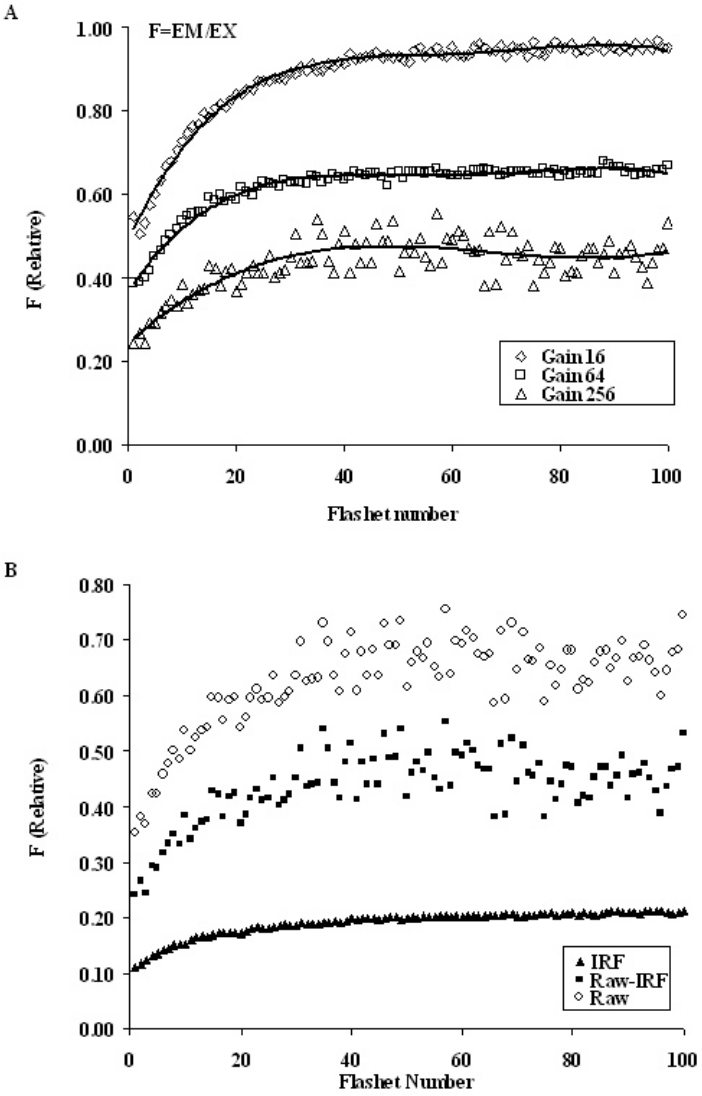
A
F=EM/EX
1.00
0.80
0.60
0.40
0.20
0.00
F (Relative)
0
20
40
60
80
100
Flashet number
Gain 16
Gain 64
Gain 256
B
0.80
0.70
0.60
0.50
0.40
0.30
0.20
0.10
0.00
F (Relative)
0
20
40
60
80
100
Flashet Number
IRF
Raw-IRF
Raw

Figure 4.2

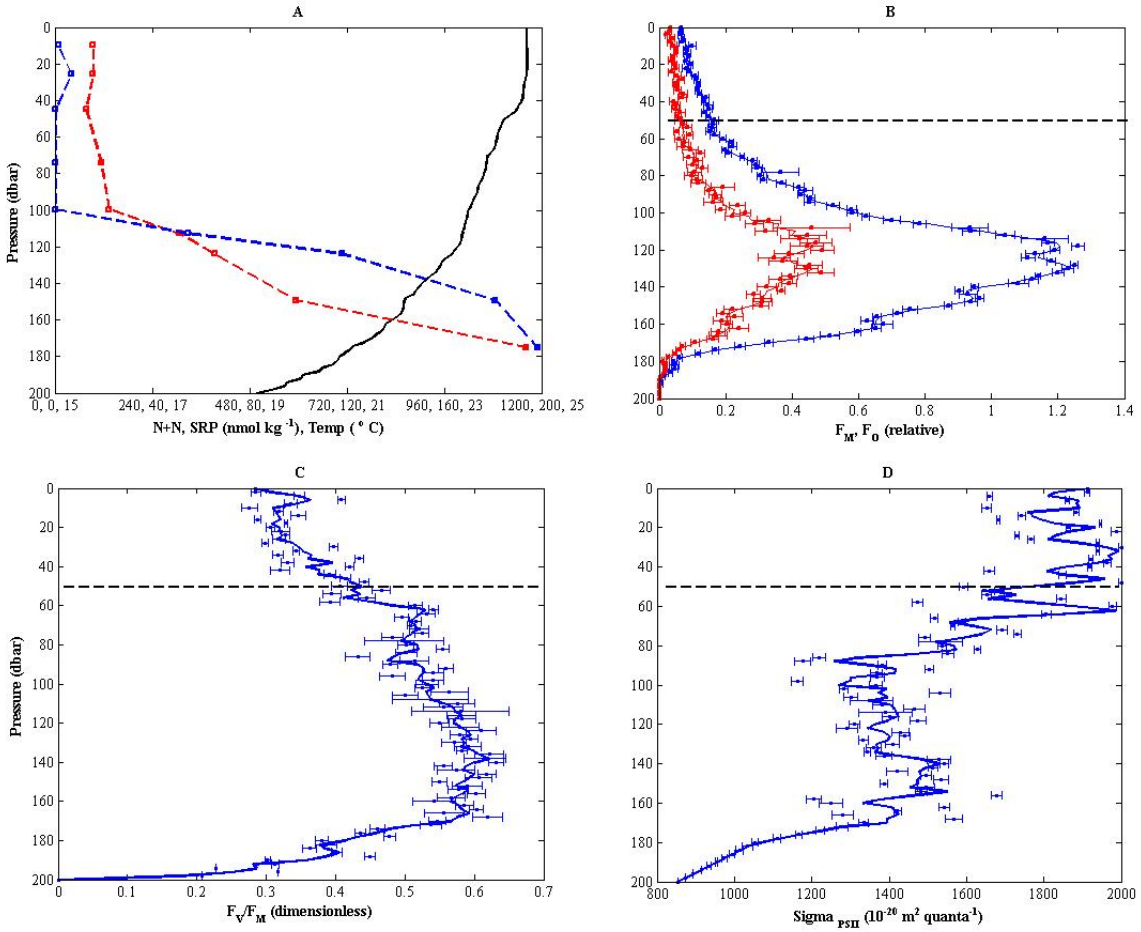
A
Pressure (dbar)
N+N, SRP (nmol kg -1), Temp ( ° C)
0, 0, 15
240, 40, 17
480, 80, 19
720, 120, 21
960, 160, 23
1200, 200, 25
B
F M, F 0 (relative)
C
F V/F M (dimensionless)
D
Sigma PSII (10-20 m2 quanta-1)

Figure 4.3

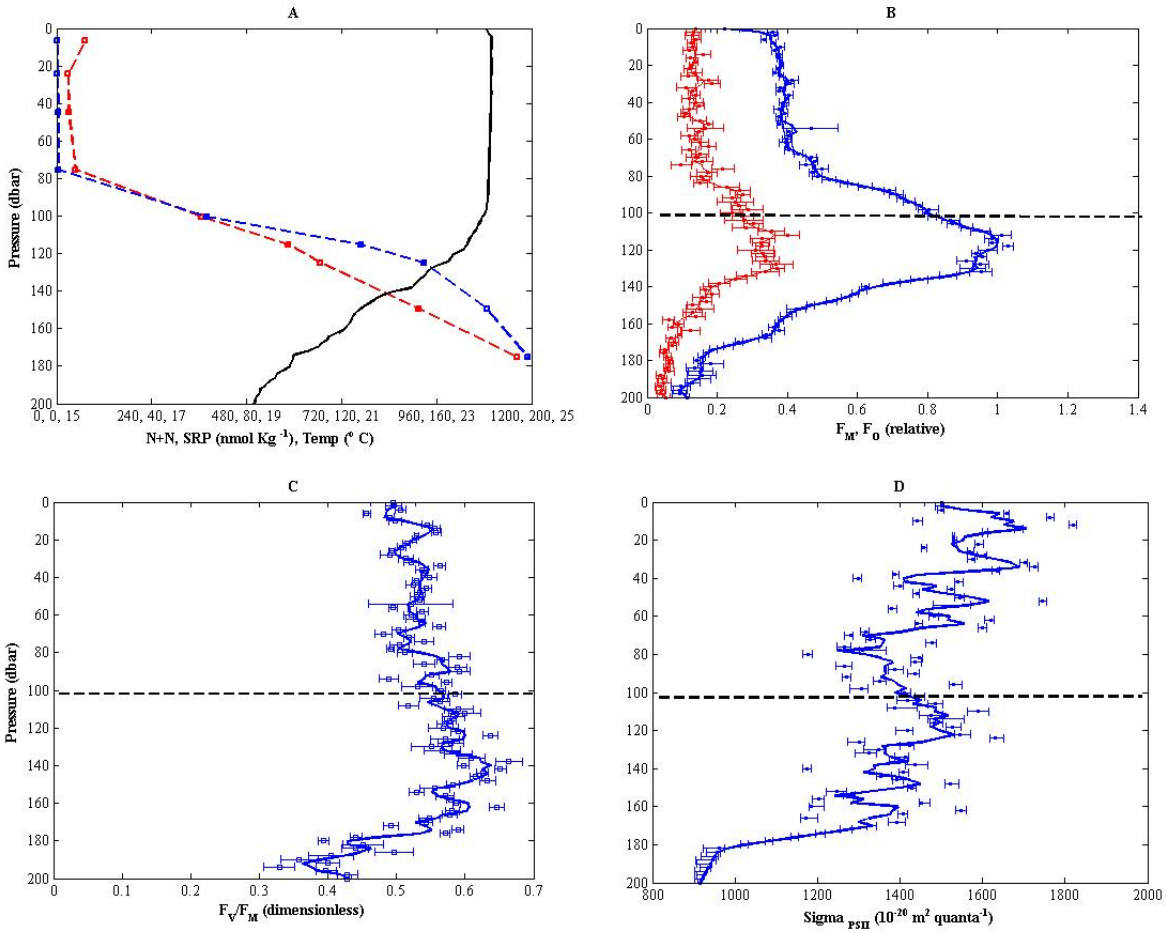
A
Pressure (dbar)
0, 0, 15
240, 40, 17
480, 80, 19
720, 120, 21
960, 160, 23
1200, 200, 25
N+N, SRP (nmol Kg-1), Temp (° C)
B
FM, FO (relative)
C
FV/FM (dimensionless)
D
Sigma PSII (10-20 m2 quanta-1)

Figure 4.4

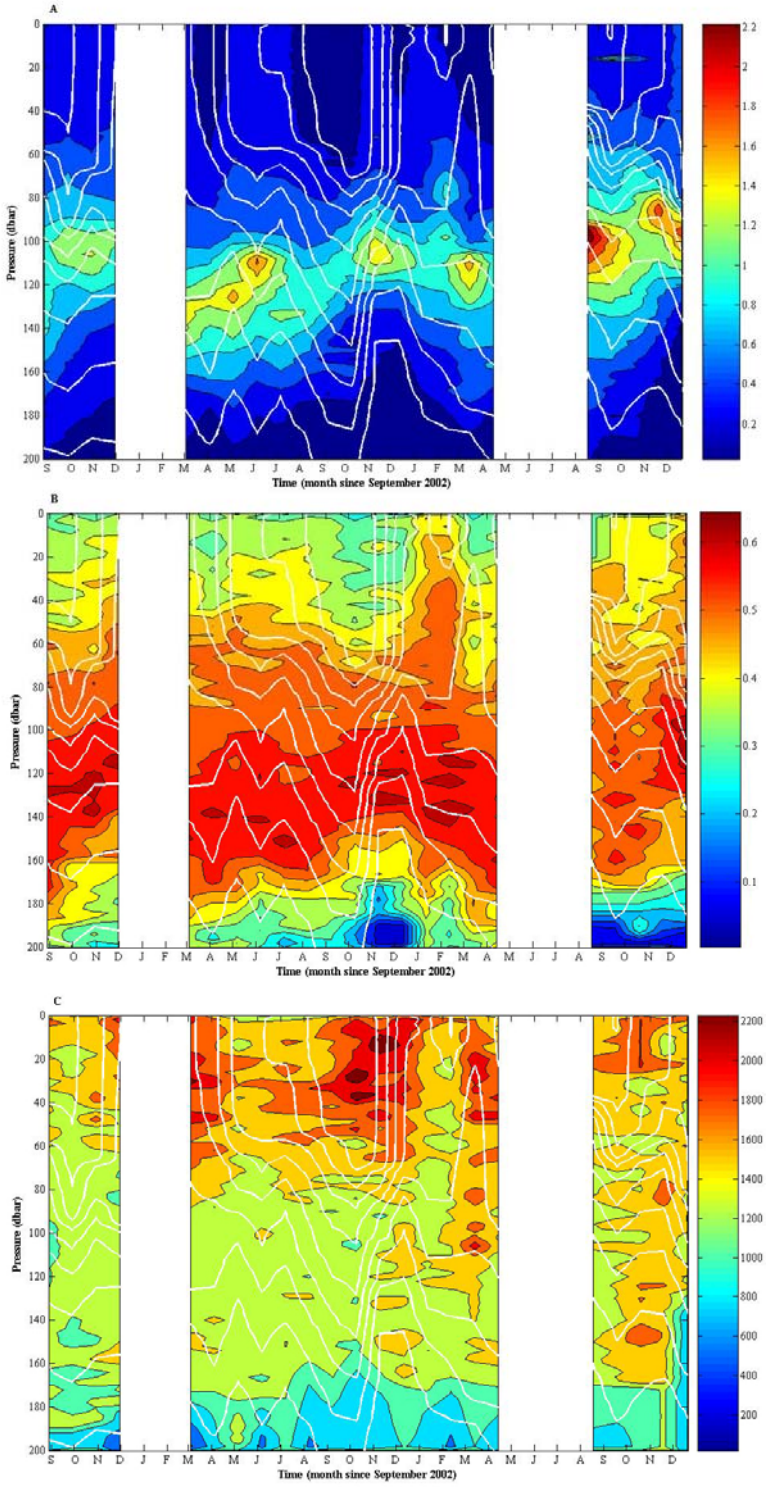
A
Pressure (dbar)
Time (month since September 2002)
B
Pressure (dbar)
Time (month since September 2002)
C
Pressure (dbar)
Time (month since September 2002)

Figure 4.5

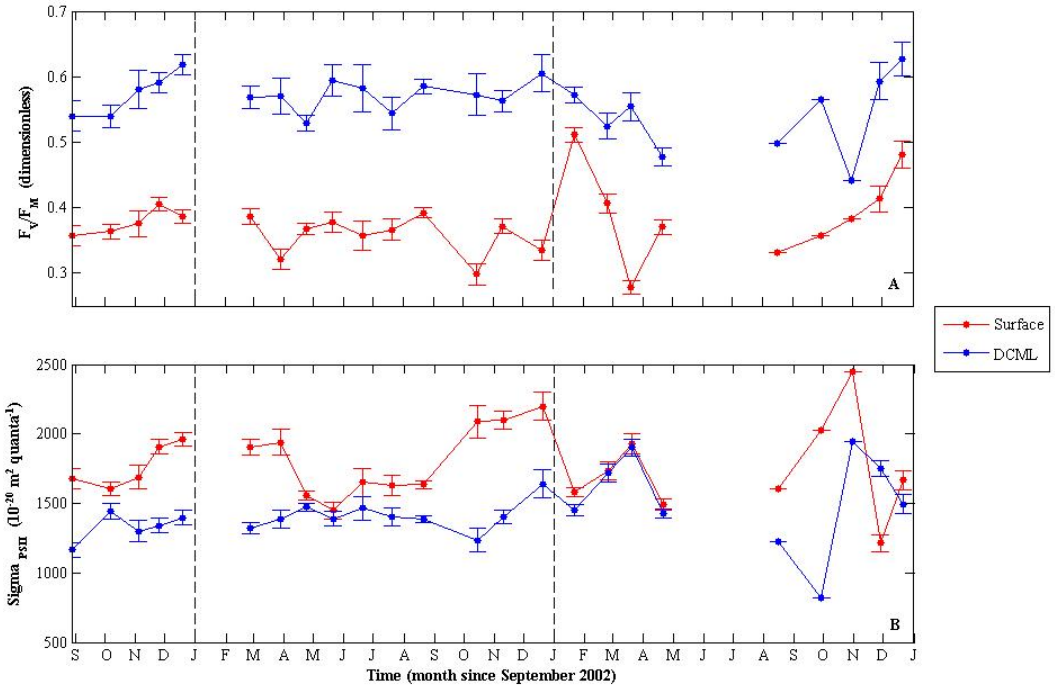
0.7
0.6
0.5
0.4
0.3
$F_V/F_M$ (dimensionless)
A
Surface
DCML
2500
2000
1500
1000
500
Sigma PSII ($10^{-20}$ m$^2$ quanta$^{-1}$)
B
S O N D J F M A M J J A S O N D J F M A M J J A S O N D J
Time (month since September 2002)

Figure 4.6

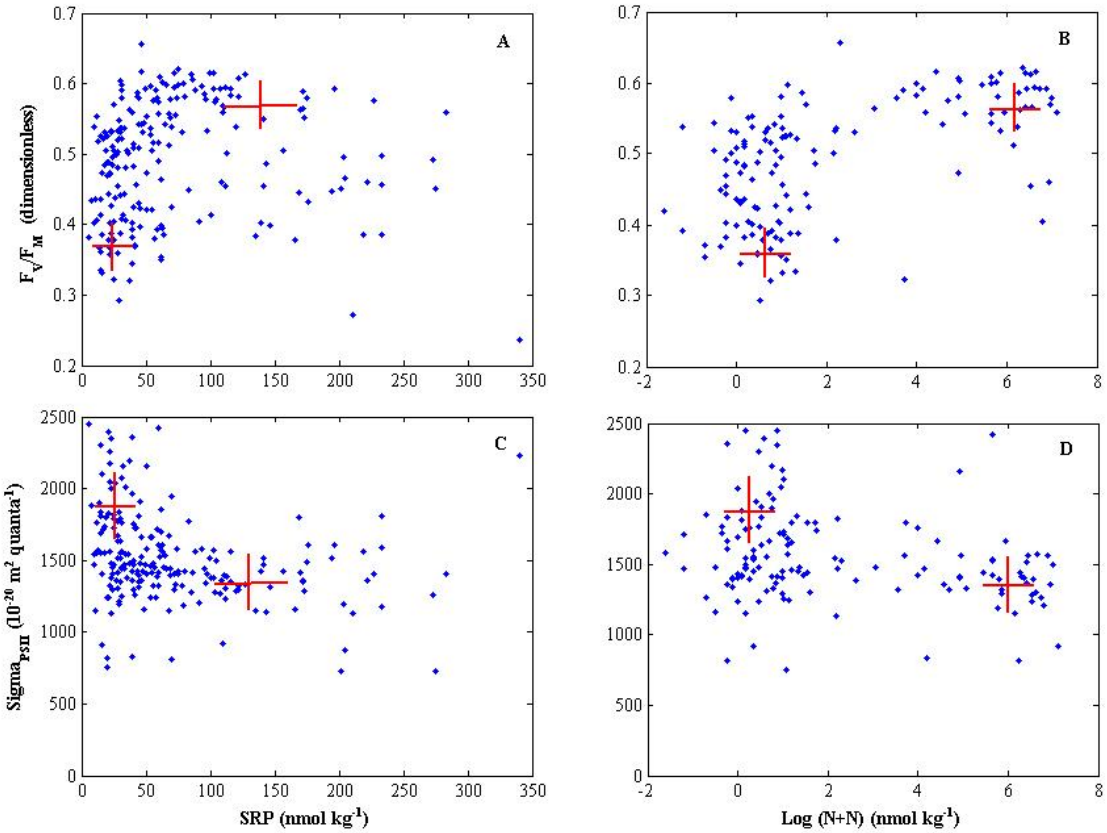
A
B
C
D
$F_V/F_M$ (dimensionless)
$Sigma_{PSII}$ ($10^{-20}$ m$^2$ quanta$^{-1}$)
SRP (nmol kg$^{-1}$)
Log (N+N) (nmol kg$^{-1}$)

Figure 4.7

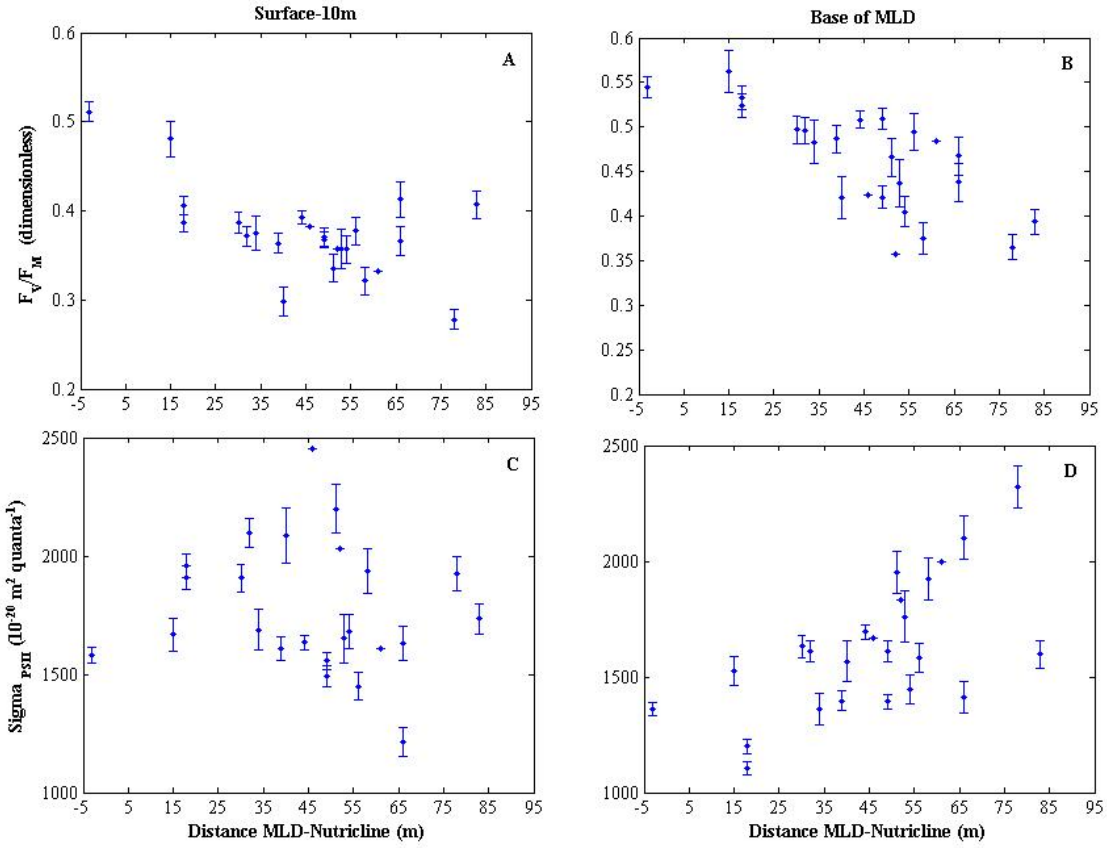
Surface-10m
Base of MLD
A
B
C
D
$F_V/F_M$ (dimensionless)
Sigma $_{PSII}$ ($10^{-20}$ m$^2$ quanta$^{-1}$)
Distance MLD-Nutricline (m)
Distance MLD-Nutricline (m)

Figure 4.8

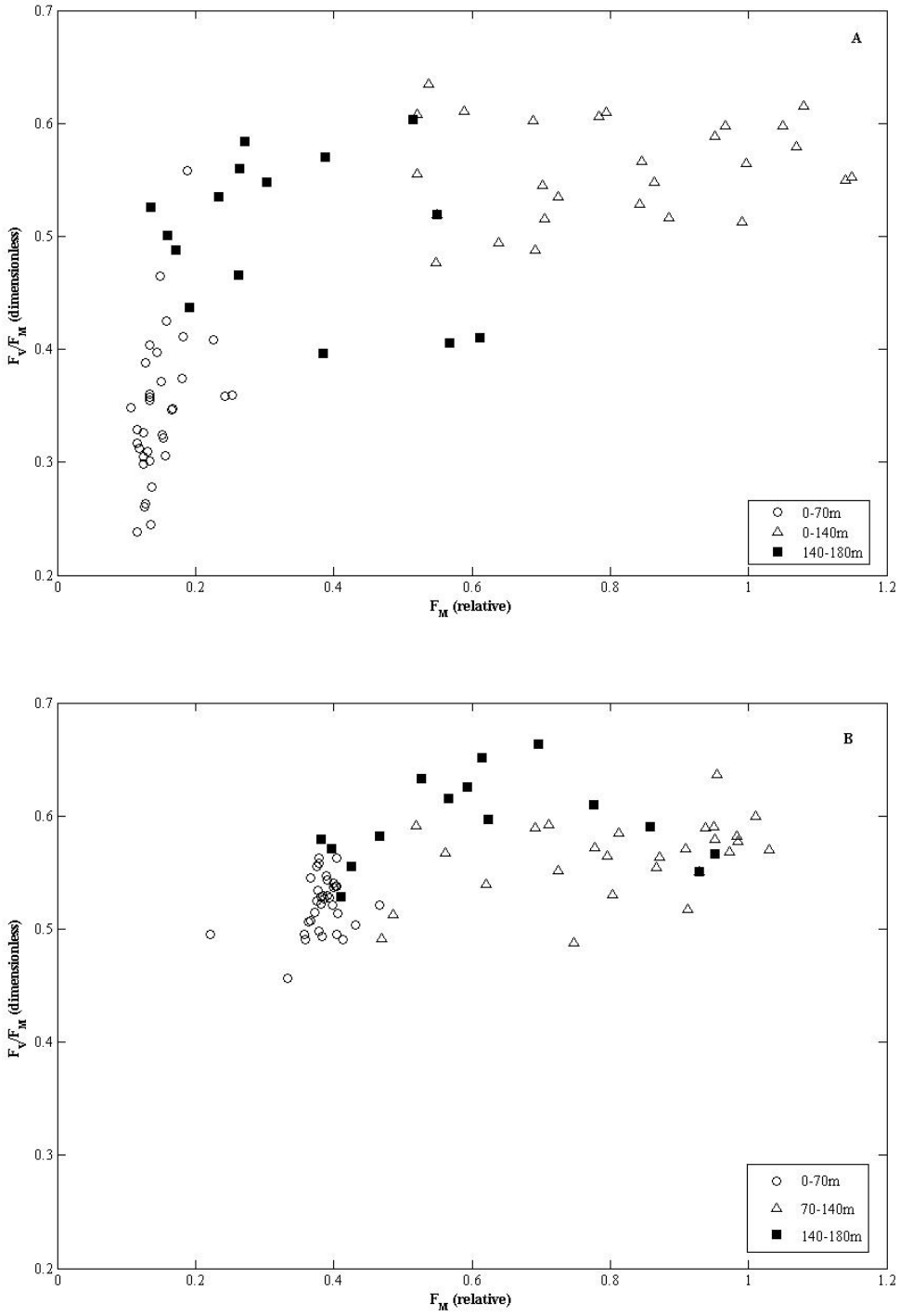
A
B
$F_V/F_M$ (dimensionless)
$F_M$ (relative)
0-70m
0-140m
70-140m
140-180m
0.2
0.3
0.4
0.5
0.6
0.7
0
0.2
0.4
0.6
0.8
1
1.2

Figure 4.9

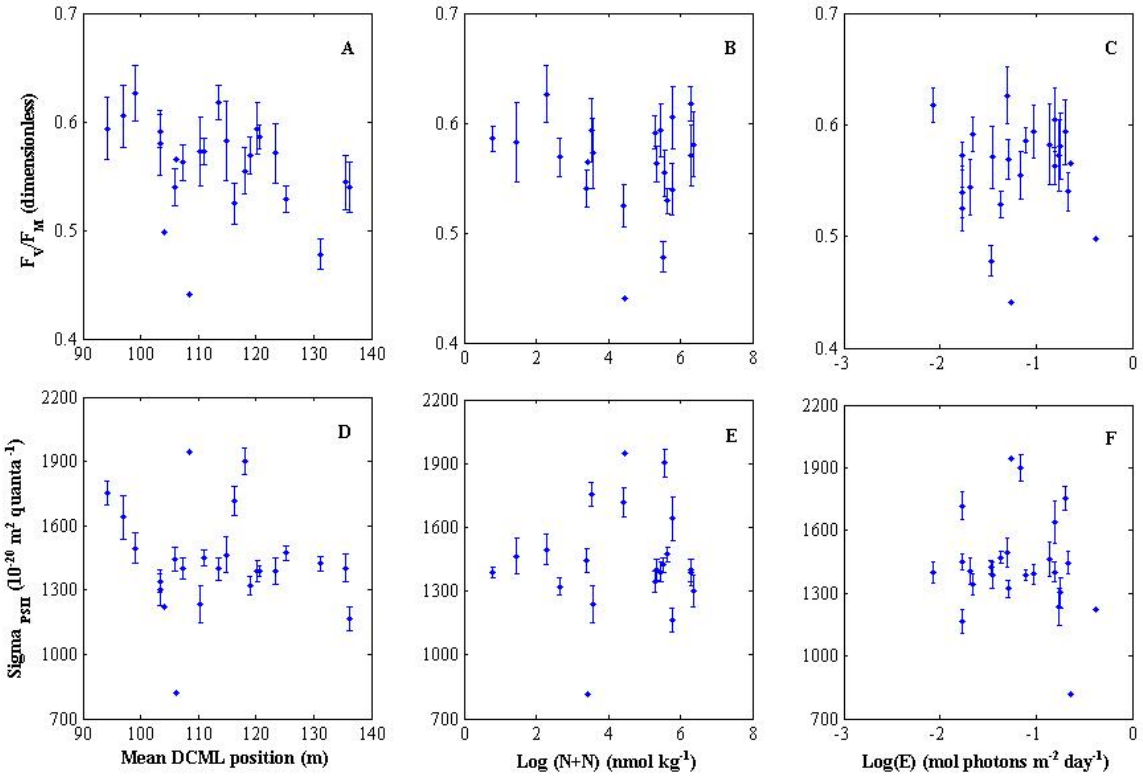
A
B
C
D
E
F
$F_V/F_M$ (dimensionless)
$Sigma_{PSII}$ ($10^{-20}$ m$^2$ quanta$^{-1}$)
Mean DCML position (m)
Log (N+N) (nmol kg$^{-1}$)
Log(E) (mol photons m$^{-2}$ day$^{-1}$)

Figure 4.10

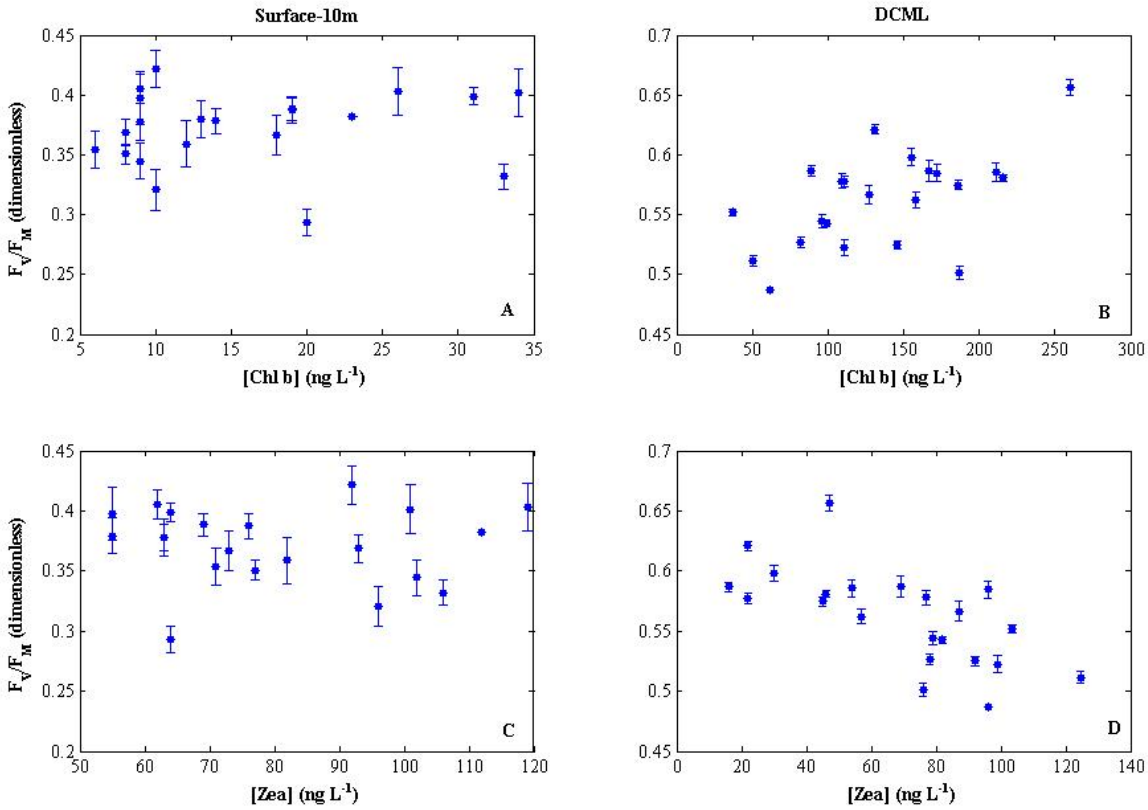
Surface-10m
DCML
$F_V/F_M$ (dimensionless)
[Chl b] (ng $L^{-1}$)
[Zea] (ng $L^{-1}$)
A
B
C
D

# 5. Summary of findings, concluding remarks and future prospective

## 5.1 Summary of findings

This investigation was aimed to understand mechanisms controlling biological variability, and in particular PP variability, across different temporal and vertical scales in the NPSG. Associated with this general aim, specific questions were formulated:

*1. What is the relationship between large-scale climate phenomena and PP patterns at Sta. ALOHA?* It appears that a unique relationship between PP and large-scale climate phenomena does not exit at Sta. ALOHA and, in turn, in the NPSG. Even though PP increased during two separate ENSO events, different temporal and vertical PP dynamics were observed. During the 1991-1994 ENSO, the increased PP in the upper euphotic zone was related to increased stratification, while a decrease in stability of the upper water column during the 1997-1998 ENSO and PDO reversal led to an increase in PP through out the entire euphotic zone.

*2. What is the relationship between gross and net PP at Sta. ALOHA?* The GPP:NPP ratio was vertically and, to some extent temporally, variable at Sta. ALOHA. The ratio was greater at the surface and decreased with depth; it peaked during fall and reached a minimum during winter.

*3. What is the photosynthetic activity and efficiency at Sta. ALOHA?* Photosynthetic efficiency was low at the surface and increased with depth. These vertical patterns indicated photosynthetic stress conditions in the surface photoautotrophic population, with higher photosynthetic efficiency in assemblages of

the lower euphotic zone. These results further indicated that at Sta. ALOHA surface photosynthetic activity is controlled by chronic nutrient limitation, while higher photosynthetic efficiency in the lower euphotic zone appears sensitive to community structure changes.

In addition to these specific findings, other significant results were obtained by the present investigation. A significant floristic shift in photoautotrophic community structure has occurred at Sta. ALOHA during the last two decades. Decreasing *Prochlorococcus* spp. cell concentrations and increasing picoeukaryotes and prymnesiophytes abundances were related to the physical-chemical changes that occurred at Sta. ALOHA due to the large-scale interactions during the ENSO and PDO variations. Furthermore, the comparison between the derived light-driven photoautotrophic respiration and total community respiration (TCR) indicated that photoautotrophic respiration could account for approximately 50-70% of the TCR in the higher euphotic zone. The high vertical resolution of FRRF measurements also allowed observing variations and features in photosynthetic activity (such as the transition around the MLD and the activity increase through the water column) not achievable with standard PP technique. Finally, FRRF was found feasible to assess PP in these oligotrophic waters across a range of vertical (10-20m) and temporal (months) scales.

### 5.2 An emerging view of the NPSG

This investigation has provided further evidence in support of the current view of the NPSG as a more productive and variable ecosystem than previously

considered. In addition, these analyses presented some insights towards the elucidation of the emerging paradigm regarding the environmental control of high biological variability (PP) in the NPSG. PP increased approximately 50% at Sta. ALOHA during the last two decades, and it has not shown a decreasing trend in the last 5 years. If PP dynamics at Sta. ALOHA are considered representative of PP variations for the majority of the NPSG, these results indicate that the role of the NPSG in the marine (and global) C-cycle needs to be re-considered in terms of absolute gross C-fixation. The absolute variability (i.e. standard deviation) in PP is currently 20-25% of the mean value; this variability is greater than earlier estimates (15%). Furthermore, the step increase in PP revealed the dynamic and variable behavior of this ecosystem in relation to perturbations. The relatively rapid increase in photosynthetic activity through the water column following a perturbation also supports the variable nature of this ecosystem.

In addition to supporting the NPSG current view, this investigation has also refined some earlier conceptions of this ecosystem processes and provided some new prospective regarding such processes. The vertical difference in photosynthetic activity, and relative controlling factors, has added a new prospective to the previously proposed two-layer model for this oligotrophic ocean (Coale and Bruland 1987, Small *et al.* 1987, Knauer *et al.* 1990, Harrison *et al.* 1992). If photosynthetic activity is considered to be related to other major biogeochemical processes in this ecosystem (i.e. recycling, export), these results have added a more precise vertical definition of the two-layer model for the NPSG. The MLD appears to be the physical limit to distinguish between the top layer (characterized by low photosynthetic

efficiency, high recycling rates and low export) and the bottom layer (where high photosynthetic efficiency, low recycling rate and high export dominate). If vertical photosynthetic variations are considered, the idealized two-layer model can be further refined to a four-layer model (Fig. 5.1). During normal condition (i.e. physical and chemical environment approximate the long-term mean), photosynthetic efficiency is low in the mixed-layer due to chronic nutrient limitation. The MLD represents a physical transition to higher photosynthetic efficiency within a region where light is decreasing and nutrients are low, but the associated nutrient flux becomes higher due to the proximity of the top of the nutricline. This chemical feature marks the physical transition to a region where the maximum in photosynthetic efficiency is found. Here the upward flux of nutrients is the greatest in the euphotic zone and it is likely to control the efficiency maximum. Finally, the decrease of light to a critical threshold level (to a first approximation 1%) represents the transition to a region of low photosynthetic efficiency because light is limiting the uptake of the available nutrients. These idealized vertical patterns in photosynthetic efficiency based on these research observations reflect the relative interaction between nutrient vs. light availability in controlling photosynthetic processes and their efficiency.

Extending this refined vertical biogeochemical model to ecological dynamics, the upper and lower euphotic zone may also differ in terms of resilience (i.e. the time required for community or system to return to a former state after being displaced by a perturbation) and resistance (i.e. the time before a change of the anomaly sign after the perturbation has occurred). Variations in PP at Sta. ALOHA can be related to the changes in the ecosystem state, defined here as principal biogeochemical

characteristics (i.e. mean and variance of PP, photoautotrophic group abundance, nutrient concentrations) of a system at any given time. Overall, the ecosystem reached two different states following the physical perturbations during ENSO and PDO. If the system is considered vertically, the upper euphotic zone appeared able to return to a former state following perturbation (1991-1994 ENSO and PDO positive index), while the lower euphotic zone was less resilient to perturbation (in this case the onset of the 1997-1998 ENSO and reversal of the PDO). Although these definitions of resilience and resistance do not adhere to a derivation based on a community matrix (Laws 2003), they provide a suitable proxy in the case of the present dataset. If the sign of the PP anomaly is used as a proxy for the state of the NPSG, following the 1991-1994 ENSO, the resilience of the NPSG was approximately two years; following the 1997-1998 ENSO event the resilience of the system increased to greater than 5 years. The resistance of the NPSG ecosystem demonstrated apparent depth-dependence; the upper euphotic zone demonstrated relatively low resilience and resistance, requiring only ~2 years to recover from the physical perturbations brought on by the combined ocean-atmosphere interactions during ENSO and PDO. In contrast, the lower euphotic zone demonstrated greater resilience and resistance than the upper euphotic zone. Such results support the hypothesis that the upper euphotic zone is more prone to perturbation, but also demonstrates faster recovery and return of ecosystem properties to an initial condition.

The new insights into NPSG ecosystem processes highlighted by the present research consist of (i) the role of community structure in influencing PP dynamics and (ii) the contribution of photoautotrophs respiration processes to the TCR.

According to these results, variations in the community structure in the NPSG can significantly control PP changes. At the physiological level, the observed variability in PSII photosynthetic efficiency in the DCML appears related to the relative contribution of prochlorophytes vs. cyanobacteria to the photoautotrophic community structure. The underlying environmental factors controlling the abundance of these groups can then significantly influence photosynthetic processes and, in turn, PP in this region of the water column. Considering larger temporal and vertical scales, floristic shifts in the NPSG photoautotrophic community could as well be responsible for significant PP variations in this ecosystem over decadal scales. The relative increase of picoeukaryotes and prymnesiophytes relative to *Prochlorococcus* spp. was related to the observed PP rise during the last decade. Another novel insight into NPSG ecosystem processes is the potential significant role of photoautotrophs activity in influencing the system metabolic balance. Even though the empirical and theoretical derivation used here for photoautotrophs respiration relies on some untested assumptions, the contribution of photoautotrophic respiration to the TCR was between 50-70% in the higher euphotic zone. This investigation suggests that the background metabolic state of the NPSG may be controlled by the activities of photoautotrophs.

### 5.3 Primary Productivity methods

In this investigation, PP derivation has been based on $^{14}C$ and FRRF measurements. Such measurements were limited in space and time, and also presented some technical limitations (Suggett *et al.* 2004, Corno *et al.* 2006). Therefore, the present understanding and interpretations of PP variations and

dynamics in the NPSG could be missing important events and trends. In particular, information may be missed regarding the role of (i) intermittency in the biological pump, (ii) mesoscale events in influencing the metabolic balance of this system, (iii) blooms in uncoupling respiration and production (iv) PP dynamics during large scale perturbations and (v) near inertial oscillations in controlling PP changes in the lower euphotic zone. The PP response in relation to these bio-physical forcings spans different temporal (daily to years) and vertical scales. In order to properly determine such response, the use of different PP techniques needs to be invoked. The integration of different PP methods will allow bridging some of the PP scales in relation to those of environmental forcings. In particular, the use of surface moorings equipped with $O_2$ sensors would allow studies of the temporal role of the biological pump. Previous studies have already demonstrated the feasibility of such measurements in detecting sudden GPP changes in the NPSG (Emerson *et al.* 2002). The use of triple oxygen coupled with $O_2$/Ar measurements represents a feasible approach to determine the background metabolic balance of the system by determining the GPP and net community respiration (NCR). These methods would be able to detect sudden changes in GPP and NCR, as their integration time consists of two weeks. The major limitation of the approach is the vertical resolution. An ideal study would then be to contemporaneously use the triple oxygen, $O_2$/Ar, $^{18}O$, $^{14}C$ and continuous vertical FRRF profiles during approximately 4 weeks period at a pre-established location (i.e. Sta. ALOHA). This temporal resolution will allow two full cycles for the triple oxygen and $O_2$/Ar measurements, with a full monthly cycle of near-inertial oscillation. This study should be conducted during summer and fall in order to

increase the probability of detecting blooms and mesoscale events, respectively. The high vertical resolution given by continuous FRRF measurements would provide indications of possible PP hot spots in the water column and PP changes due to the near oscillation forcings. Finally, a comparison (*in situ* and *in vitro*) between the different techniques would also be achieved by this study so as to further constrain the PP components (from GPP to NPP) each method is measuring.

This research has focused on FRRF to determine photoautotrophic activity, based on Chl *a* fluorescence transients from PSII reaction centers. However, the restricted FRRF spectral resolution (i.e. selectively targeting Chl *a* fluorescence emission wavelengths) may have not properly assessed the photoautotrophic activity due to influence of accessory pigments on energy transfer towards PSII. Two possible avenues can be proposed to better determine photoautotrophic activity in this ecosystem by active fluorescence. The first technical solution would be to selectively measure active fluorescence transients for different wavelengths in relation to the fluorescence exication/emission for the different pigments (i.e. targeted energy excitation/emission for Chl *b, c*…). The second possibility is represented by correcting the excitation energy of FRRF to the *in situ* light field to adjust the measured fluorescence transients to real environmental conditions. In this way, photosynthetic activity would be better constrained to actual *in situ* light and pigments conditions.

The time series analysis of PP at Sta. ALOHA allowed determining temporal trends in relation to large scale perturbations. However, the trends' characteristics (shape and magnitude) were a function of the frequency of *in situ* PP measurements at

Sta. ALOHA. In order to better determine the temporal evolution of PP variations during large scale perturbations, higher frequency sampling is required. The integration between self-powered mooring $O_2$ measurements, different *in situ* PP measurements and time series satellites images of Chl *a*, which can be used as a proxy for PP variations based on predictive models (Behrenfeld and Falkowski 1997), represents a possible methodological and practical solution to determine higher frequency PP variations across different spatial and temporal scales.

**5.4 Scientific implications**

Marine photosynthesis and photoautotrophic activity still remain poorly understood for *in situ* populations across different temporal and spatial scales. The present results provide new information regarding *in situ* marine photosynthetic dynamics in an oligotrophic ocean. The substrate limitation appears to control both the probability of light harvesting ($\sigma_{PSII}$) and efficiency of light utilization in PSII ($F_V/F_M$), implying an energetic limitation in the first step of energy flow through this ecosystem. Furthermore, the lack of a seasonal cycle in surface photosynthetic quantum yield (ΦC) but the observed significant ΦC temporal variability imply that (i) the interaction between different environmental factors, and not mainly light, are controlling surface ΦC variations and (ii) model parameterizations of ΦC should take into account the non-linearity of such variations. If these results are considered indicative of other oligotrophic regions, the development of PP models may require more non-linear parameterization between photosynthetic parameters and environmental factors than present attempts (Ondrusek *et al.* 2001).

The observed increase in PP in the NPSG over nearly two decades has important biogeochemical implications for this ecosystem. Firstly, given the current PP in the NPSG, this ecosystem could account up to 30 and 20 % of the marine and global PP, respectively. Consequently, the NPSG may play a primary role in the global C-cycle in terms of gross C-fixation, and it needs to be considered a significant global source of fixed solar energy. The observed PP increase at Sta. ALOHA without an appreciable change in major inorganic nutrient reservoir may indicate that the organic nutrient pool could support a fraction of the PP energy requirements. If so, this observation implies an ecological selection against photoautotrophs that can supply their energetic requirements by utilizing some fraction of the organic pool. Furthermore, the enhanced PP has important implications regarding NPSG trophic dynamics. Both lower and higher trophic level would be influenced by the higher availability of fixed energy. If DOM production is considered a function of PP (Baines and Pace 1991), bacterial activity would be enhanced with possible consequences for the metabolic status of the system. The greater PP may also affect the recruitment and survival of larval stages for different crustacean and fish species, with implications for food web production and fishery yields. The significant change in community structure also has potential implications for the food quality and, in turn, larvae fitness. Finally, the PP increase has also important consequences for the surface ocean-lower atmosphere interactions, in particular by influencing the $CO_2$ flux. If the requirement for inorganic C becomes large enough due to the PP increase, surface waters may become $CO_2$ under-saturated and a net $CO_2$ flux may be induced from the atmosphere to the ocean. This possible scenario has important implications

for the role of the NPSG in influencing the atmospheric $CO_2$ concentrations and, in turn, the earth climate.

The observed relationship between GPP and NPP at Sta. ALOHA presents important biogeochemical implications regarding the NPSG ecosystem efficiency. First, if light-driven photoautotrophic respiration is approximately 50-70% of the overall total community respiration at the surface, variations in physiological status could contribute significantly to the regulation of $O_2$ and $CO_2$ fluxes from and to the atmosphere. Furthermore, the increase in efficiency of carbon storage by photoautotrophs with depth also highlights the greater efficiency of this ecosystem in recycling biomass (in terms of C) at depth. Finally, these results may imply that variations in photoautotrophic respiration could play a major role for blooms formation by controlling the decoupling dynamics between respiration and photosynthesis.

The observed relationship between physical forcing (ENSO, PDO and mixing events) and PP variations indicates that physical disturbance can significantly affect NPSG ecosystem processes. The change in physical stability of the upper water column following a strong ENSO and PDO phase reversal has potentially significant biogeochemical implications for this ecosystem. The instability increase in the upper euphotic zone can influence the frequency of summer blooms by *Trichodesmium* spp. and diatoms containing $N_2$ fixing-endosymbionts, as these events require periods of strong stratification. The biogeochemical consequence would be a decrease in $N_2$-fixation activity and the availability of reduced N to the upper euphotic zone. Furthermore, considering the decreasing probability of summer diatom blooms, the

aperiodic burst in C-export due to these events may also decrease with implications for the role of NPSG in transferring energy (fixed C) to other trophic levels (particularly to the abyssal ecosystem) and C sequestration. The hypothesized $N_2$-fixation decrease by *Trichodesmium* spp. would also increase the importance of unicellular $N_2$-fixers organisms activity in providing a source of reduced N. Finally, by controlling the probability of blooms formation, the physical stability change would also indirectly affect the temporal metabolic balance dynamics of the NPSG by influencing the uncoupling between respiration and photosynthesis.

Understanding ecosystem resilience and resistance is crucial for defining the flexibility of the system in the face of abrupt environmental change. Considering the observed PP variations, the NPSG appears to be able to return to former equilibrium following ENSO events, while it is more likely to reach a new state when there is significant correlation between ENSO and PDO. This resilience change indicates that ecosystems will tend to evolve to the state most resilient to perturbation (Laws 2003). Such information needs to be considered when trying predicting future ecosystem change in relation to climate disturbance.

This investigation presents also some methodological implications. Firstly, from a modeling prospective, the role of community structure in influencing PP and photosynthetic activity should be included in PP modeling efforts. The non-linear behavior of ΦC and the empirical relationship between PP and ENSO-PDO should also be considered to better predict PP variations in the NPSG. Furthermore, from a field prospective, the integration between *in situ* FRRF and $^{14}C$ measurements may be a relatively cheap and practical solution to distinguish between GPP and NPP,

respectively. Finally, the ability of capturing PP changes in relation to large scale perturbations supports the need for long-term research in the marine realm, to better characterize and understand these systems behaviors in relation to natural and anthropogenic disturbances.

### 5.5 Conclusion and future prospective

According to the present research, the NPSG should be considered as a moderately productive and variable ecosystem. PP displays a dynamic behavior in response to physical perturbations across different temporal scales (decadal to monthly) and vertical scales (meters). How PP variability in the NPSG changes across different temporal, vertical and physiological scales? This research suggests that over intra-annual and decadal scales the PP variability appears related to environmental perturbations driven by ENSO and PDO (i.e. temporal scales ranging from 3-5 to 7-10 years). In addition, the intracellular variability in partitioning energy between anabolism and catabolism processes in photoautotrophs seems to vary in relation to season's development, as highlighted by the temporal variability in the GPP:NPP ratio. The higher frequency temporal variability (monthly) in photosynthetic efficiency appears likely linked (i) to aperiodic physical disturbances that would alter the nutrient environment in the upper euphotic zone and (ii) to temporal scales of community structure changes in the lower euphotic zone. Finally, the vertical variability in photosynthetic efficiency, and in turn PP, might vary in relation to the vertical scales of nutrients vs. light availability.

Even though this research provided some novel information regarding PP dynamics, PP patterns across different spatial and temporal scales in the NPSG have yet to be fully elucidated. In particular, the PP dynamics during blooms and the evolution of mesoscale events remains poorly understood, despite their biogechemical implications for this ecosystem processes in terms of energy storage and biological variability. The integration of different PP techniques, as described by the idealized study above, may represent a solution for addressing this question. Another important PP process to consider for future research is the relative contribution of abiotic processes to the total budget of fixed energy (abiotic plus biotic processes). The DOM generation by photo-degradation should be taken into consideration when trying to understand the efficiency of the NPSG in providing sources of fixed energy. This comparison (photodegradation vs. photosynthesis) would provide an indication of the energetic baseline in relation to variations in biotic PP. The role of other photo-driven auto and heterotrophic processes in the energy budget of this ecosystem needs also to be further constrained. Such information is needed to determine the key processes (and organisms) in controlling the metabolic balance of the NPSG. Finally, the role of inorganic vs. organic pool in influencing photosynthetic activity remains to be investigated. This future research has important physiological and biogeochemical implications as the role of organic compounds in providing an intracellular energy source and C-cycling would be assessed. The role of NPSG in the global C-cycle in terms of absolute gross C-fixation appears more significant than previously considered. This investigation has also highlighted the role of species succession in controlling ecosystem processes. In particular, community structure appears to play

an important role in influencing PP and photosynthetic processes variations in the NPSG across different temporal scales (decadal to monthly) and vertical scales (higher vs. lower euphotic zone). The efficiency of the NPSG in transferring energy to other trophic levels appears affected by photoautotrophic activity through its large contribution to TCR. Finally, the chronic substrate limitation of the NPSG is significantly affecting photosynthesis in the MLD.

The PP and community structure variations following physical perturbations (across large and small scales) stimulate intriguing questions for future research regarding the underlying ecological laws regulating the NPSG ecosystem processes. In particular, do the concomitant PP and community structure variations following perturbation maintain a thermodynamic equilibrium for the NPSG system? How do these variations influence the higher trophic behavior? Can these variations create temporal niches for evolutionary establishment of genes and subsequent metabolic processes? The challenge to answer such questions will provide a deeper understanding of natural processes in the NPSG ecosystem.

**5.6 Reference**

Baines, S. and Pace, M.L. 1991. The production of dissolved organic matter by phytoplankton and its importance to bacteria: patterns across marine and freshwater systems. *Limnol. Oceanogr.* **36:** 1078-1090

Behrenfeld, M.J. and Falkowski, P.G. 1997. Photosynthetic rates derived from satellite-based chlorophyll concentration. *Limnol. Oceanogr.* **42:** 1-20

Coale, K.H. and Bruland, K.W. 1987. Oceanic stratified euphotic zone as elucidated by $^{234}$Th:$^{238}$U disequilibria. *Limnol. Oceanogr.* **32:** 189-200

Corno, G., Letelier, R.M., Abbott, M.R. and Karl, D.M. 2006. Assessing the temporal variability of primary production in the North Pacific Subtropical Gyre: A comparison of Fast Repetition Rate Fluorometry and $^{14}$C measurements. J. Phyc. **42**: 51-60.

Emerson, S., Stump, C., Johnson, B. and D. Karl, D.M . 2002. Autonomous determination of oxygen and nitrogen concentrations in the Ocean. *Deep-Sea Res. I* 49: 941-952.

Harrison, W.G., Harris, L.R., Karl, D.M., Knauer, G.A. and Redalje, D.G. 1992. Nitrogen dynamics at the VERTEX time-series site. *Deep-Sea Res. I* **39** : 1535-1552.

Karl, D.M. 1999. A sea of Change: Biogeochemical Variability in the North Pacific Subtropical Gyre. *Ecosystems* **2**: 181-214.

Karl, D.M., Bidigare, R.R. and Letelier, R.M. 2002. Sustained and Aperiodic Variability in Organic Matter Production and Phototrophic Microbial Community Structure in the North Pacific Subtropical Gyre. In: P. J. le B. Williams, D. R. Thomas and C. S. Reynolds, Eds., Phytoplankton Productivity and Carbon Assimilation in Marine and Freshwater Ecosystems, Blackwell Publishers, London, 222-264.

Karl, D.M., Dore, D.V., Hebel, R.M., Letelier, R.M. and Tupas, L.M. 1996. Seasonal and interannual variability in primary productivity and particle flux at Station ALOHA. *Dee- Sea Res. II* **43**: 539-568.

Karl, D.M., Letelier, R.M., Hebel, D., Tupas, L., Dore, J., Christian, J. and Winn, C. 1995. Ecosystem changes in the North Pacific subtropical gyre attributed to the 1991-92 El-Niño. *Nature* **373**: 230-4.

Knauer, G.A., Redalje, D.G., Harrison, W.G. and Karl, D.M. 1990. New production at the VERTEX time-series site. *Deep-Sea Res. I* **37**: 1121-1134.

Laws, E.A. 2003. Partitioning of microbial biomass in pelagic aquatic communities: maximum resiliency as a food web organizing construct. *Aquatic Micr. Ecol.* **32** :1-10.

Letelier, R.M., Dore, J.E., Winn, C.D. and Karl, D.M. 1996. Seasonal and interannual variations in autotrophic carbon assimilation at Station ALOHA. *Deep-Sea Res. II* **43:** 467-490.

Maranon, E., Behrenfeld, M.J., Gonzalez, N., Mourino, B. and Zubkov, M.V. 2003. High variability of primary production in oligotrophic waters of the Atlantic Ocean: uncoupling from phytoplankton biomass and size structure. *Mar. Ecol. Prog. Ser.* **257**: 1-11.

Ondrusek, M.E., Bidigare, R., Waters, K. and Karl, D.M. 2001. A predictive model for estimating rates of primary production in the subtropical North Pacific Ocean. *Deep-sea Res. II* **48:** 1837-1863.

Small, L.F., Knauer, G.A. and Tuel, M.D. 1987. The role of sinking fecal pellets in stratified euphotic zone. *Deep-Sea Res. I* **34**: 1705-1712.

Steinberg, D.K., Carlson, C.A., Bates, N.R., Johnson, R.J., Micheals, A.F. and Knap, A.H. 2001. Overview of the US JGOFS Bermuda Atlantic time-series study

(BATS): a decade-scale look at ocean biology and biogeochemistry. *Deep-Sea Res. II* **48**: 1405-1447.

Suggett, D.J., MacIntyre, H.L.and Geider, R.J. 2004. Evaluation of biophysical and optical determinations of light absorption by photosystem II in phytoplankton. *Limnol. Oceanogr. Meth.* **2**: 316-332.

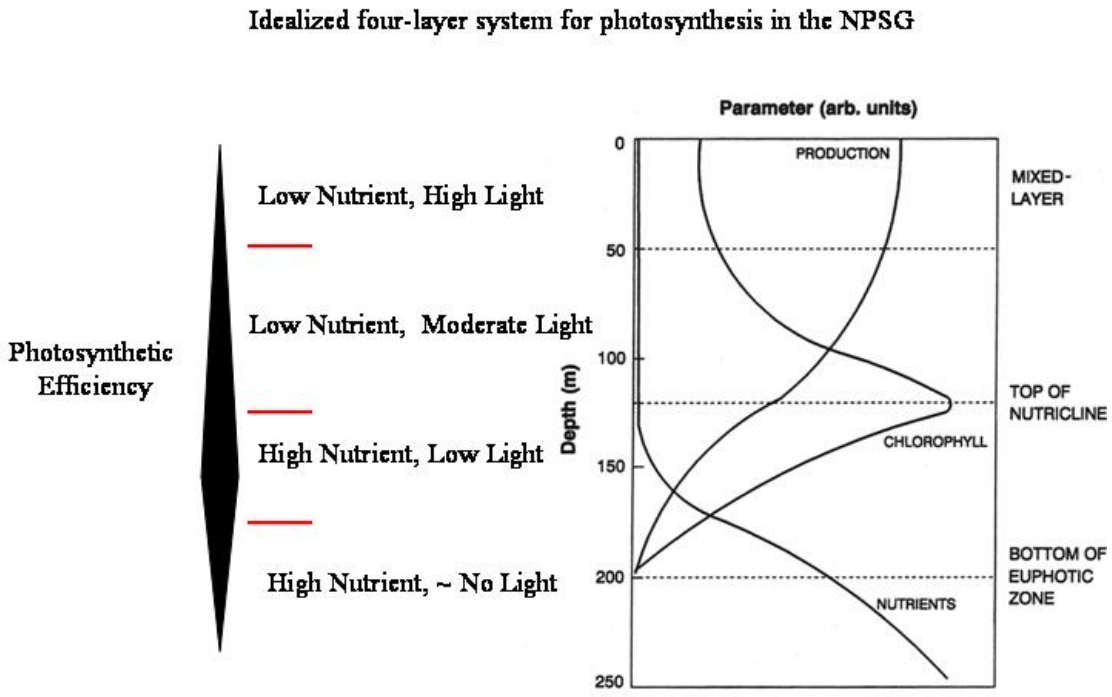


Figure 5.1. Conceptualized model of the four-layer system in the NPSG. The red horizontal lines represent the idealized vertical transition between the four regions characterized by different photosynthetic efficiency.